

OCEAN HEAT TRANSPORT IN A SIMPLE OCEAN DATA ASSIMILATION
(SODA): STRUCTURE, MECHANISMS, AND IMPACTS ON CLIMATE

A Dissertation

by

YANGXING ZHENG

Submitted to the Office of Graduate Studies of
Texas A&M University
in partial fulfillment of the requirements of the degree of

DOCTOR OF PHILOSOPHY

August 2007

Major Subject: Atmospheric Sciences

OCEAN HEAT TRANSPORT IN A SIMPLE OCEAN DATA ASSIMILATION
(SODA): STRUCTURE, MECHANISMS AND IMPACTS ON CLIMATE

A Dissertation

by

YANGXING ZHENG

Submitted to the Office of Graduate Studies of
Texas A&M University
in partial fulfillment of the requirements of the degree of

DOCTOR OF PHILOSOPHY

Approved by:

Co-Chairs of Committee,	Benjamin S. Giese
	Gerald R. North
Committee Members,	Ping Chang
	Fuqing Zhang
Head of Department,	Richard E. Orville

August 2007

Major Subject: Atmospheric Sciences

ABSTRACT

Ocean Heat Transport in A Simple Ocean Data Assimilation (SODA): Structure,
Mechanisms, and Impacts on Climate.

(August 2007)

Yangxing Zheng, B.S., Ocean University of China;

M.S., Institute of Atmospheric Sciences, Chinese Academy of Sciences, China;

M.S., Stony Brook University

Co-Chairs of Advisory Committee: Dr. Benjamin S. Giese
Dr. Gerald R. North

A Simple Ocean Data Assimilation (SODA) reanalysis is used to investigate the trend and variability of global ocean heat transport for the period 1958-2004. The forecast model utilizes Parallel Ocean Program (POP) physics, with an average 0.4° (lon) x 0.25° (lat) x 40-level resolution, and is forced with ERA-40 atmospheric reanalysis from 1958 to 2001. The reanalysis is updated in a second run which is forced with QuickSCAT wind stress from 2000 to 2004. SODA uses a sequential estimation algorithm, with observations from the historical archive of hydrographic profiles supplemented by ship intake measurements, moored hydrographic observations and remotely sensed sea surface temperature.

The results suggest that the interannual to decadal variability of ocean heat transport (OHT) is primarily controlled by the strength of the meridional overturning circulation (MOC), particularly in the Atlantic Ocean. The role of variation of temperature on variability of meridional OHT increases in the northern North Atlantic Ocean. Results

from an analysis of the vertical structure of OHT show that most change of OHT in the oceans occurs in the upper 1000m.

A heat budget analysis for the North Atlantic Ocean suggests that the long-term change of surface heat flux is principally balanced by the convergence of OHT as compared to change in the heat storage. The linear change in heat storage rate is only about one third as large as the convergence of OHT.

Enhanced subtropical cells (STCs), largely affected by strengthened equatorial upwelling processes, are responsible for an intensified northward OHT in the north tropical Atlantic Ocean and a weakened northward OHT in the south tropical Atlantic Ocean. Convergence of flow due to a northward shift of the atmospheric circulation in the mid-latitude Atlantic reinforces the MOCs, which contribute to a positive trend of OHT. Finally, in the northern North Atlantic Ocean, a small increase in meridional OHT and a slight weakening of MOC are detected. The weakening in the northern North Atlantic MOC mainly arises from a freshening in the Labrador Sea and slowdown of the overflows from the Nordic Seas into the northern North Atlantic Ocean.

ACKNOWLEDGEMENTS

I am grateful to my advisor, Dr. Benjamin Giese, for his patience and assistance in the work presented here, for his generous support that allows me to complete this research. I also greatly thank Dr. Gerald R. North as my co-chair and for his encouragement.

I would also like to thank the other committee members, Dr. Ping Chang, and Dr. Fuqing Zhang, for reading this dissertation and their invaluable suggestions and discussions. I greatly thank Dr. Achim Stössel for productive suggestions on the ocean circulation, particularly on the thermohaline circulation.

Dr. Link Ji and Dr. Seidel also helped me a lot in various ways, especially in ferret scripts. I am grateful to Dr. Alejandro Orsi for discussion in ocean circulation issue. I also thank my colleagues Xiuquan Wan, Caihong Wen, Jen-Shan Hsieh, etc.

Last and foremost, I am deeply indebted to my parents for their unconditional love, support and encouragement. Without their love, it would not have been possible for me to finish this work.

TABLE OF CONTENTS

	Page
ABSTRACT.....	iii
ACKNOWLEDGEMENTS.....	v
TABLE OF CONTENTS.....	vi
LIST OF FIGURES.....	ix
LIST OF TABLES.....	xiv
CHAPTER	
I INTRODUCTION.....	1
1.1 Importance of Ocean Heat Transport.....	1
1.2 Previous Studies.....	3
1.2.1 Long-term Mean.....	3
1.2.2 Seasonal Variability.....	6
1.2.3 Interannual-decadal Variability.....	7
1.3 Mechanisms of Temperature Change.....	10
1.4 Ocean Heat Budget.....	11
1.5 Unresolved Problems.....	13
1.5.1 Long-term Mean.....	13
1.5.2 Mechanisms of Variability and Trend.....	15
1.5.3 Impacts of Ocean Heat Transport on Climate.....	17
1.6 Overview.....	18
II METHODOLOGY.....	19
2.1 Methods of Estimating Heat Transport.....	19
2.2 SODA.....	21
2.2.1 Model Description.....	21
2.2.2 Observed Data Employed in SODA.....	22
2.3 Data Archives.....	24
III OCEAN HEAT TRANSPORT IN SODA.....	27
3.1 Spatial Structure of Mean Heat Transport and Its Trend.....	27

CHAPTER	Page
3.1.1 x-y Structure.....	27
3.1.2 y-z Structure.....	33
a. OHT in Density Layers.....	33
b. OHT in the Mixed Layer of Tropical Atlantic Ocean.....	42
3.2 Characteristics of Heat Transport Variability.....	43
3.3 Components of OHT.....	48
3.3.1 Contributions from Components.....	48
a. Contributions to Mean OHT.....	48
b. Contributions to Variability of OHT.....	49
3.3.2 Factors Affecting OHT.....	54
a. Contributions to Mean OHT.....	55
b. Contributions to Variability of OHT.....	58
 IV THE NORTH ATLANTIC OCEAN HEAT BUDGET.....	 60
4.1 Changes in Ocean Heat Content.....	60
4.2 Ocean Heat Budget.....	62
4.2.1 Heat Equation.....	62
4.2.2 Change in World Ocean Heat Storage Rate.....	62
4.2.3 Mean and Standard Deviation.....	64
4.2.4 Heat Budget in the North Atlantic Ocean.....	64
 V CLIMATE MECHANISMS FOR OCEAN HEAT TRANSPORT.....	 69
5.1 Background.....	69
5.2 Ocean Heat Transport and Ocean Circulation.....	72
5.2.1 Meridional OHT linked with MOC and Gyre.....	72
a. Strength of MOC and Gyre.....	74
b. OHT Response to MOC and Gyre.....	77
c. Phase Relationship between OHT and MOC.....	80
d. Evolution of the Atlantic MOC and OHT.....	80
e. Pseudo-heat function.....	85
5.2.2 NAO and SST in the North Atlantic Ocean.....	90
5.3 Possible Causes of the Atlantic MOC Changes.....	93
5.3.1 Causes of Weakening Atlantic MOC.....	95
a. Spatial Pattern of Surface Properties.....	95
b. Temporal Characteristics.....	100
c. The Roles of the Overflows.....	106
5.3.2 Causes of Strengthening MOC at Low-mid Latitudes.....	112
5.4 Discussion.....	116

CHAPTER	Page
VI SUMMARY AND DISCUSSION.....	121
6.1 Summary.....	121
6.2 Discussion.....	124
REFERENCES.....	127
VITA.....	137

LIST OF FIGURES

FIGURE	Page
1.1 World ocean heat transport in PW from the NCEP-derived and ECMWF-derived products compared to the results from the HADCM3 (years 81-120) and CSM (years 250-299) coupled models, along with those from Macdonald and Wunsch (1996) at $24^{\circ}N$ and $30^{\circ}S$, and at $24^{\circ}N$. From Trenberth and Caron 2001.....	2
1.2 An ocean heat budget showing the roles that heat advection by ocean currents plays in the anthropogenic warming of the world's oceans. From Barnett et al., 2005.....	14
2.1 Meridional heat transport in PW across $40^{\circ}N$ in the Atlantic Ocean based on monthly datasets (black) and 5-day datasets (red) for (a) total value and (b) mean-removed anomalies.....	25
3.1 Long-term mean and standard deviation (in parentheses) of oceanic heat transport in PW ($1PW = 10^{15} W$) across sections and (b) trend of oceanic heat transport in $PW \cdot decade^{-1}$ for the period 1958-2001 in SODA-1.4.2.....	29
3.2 Same as Fig. 3.1 except for SODA-1.4.0.....	31
3.3 Time-mean of zonal-averaged meridional currents in $cm \cdot s^{-1}$ (shaded) and density class σ_{θ} in $kg \cdot m^{-3}$ (contours) in the Atlantic Ocean. The vertical structure of the ocean is identified by a variety of density classes.....	35
3.4 Map of the mean and standard deviation (in parentheses) of global ocean heat transport in PW using a reference temperature of $0^{\circ}C$ in the different density layers.....	37
3.5 Heat transport in PW using a reference temperature of $0^{\circ}C$ in the mixed layer (red), shallow layer (bright green), intermediate layer (blue) and deep layer (turquoise) for the (a) Atlantic, (b) Pacific, and (c) Indian Oceans. The total heat transport is denoted with a black curve.....	39
3.6 Time series of normalized meridional heat transport and zonal-averaged zonal wind stress at $10^{\circ}N$ in the mixed layer of the Atlantic Ocean. The sign of τ_x has been reversed to ease comparison with heat transport.....	44

FIGURE	Page
3.7 The correlation between meridional heat transport and zonal-averaged zonal wind stress in the mixed layer of the Atlantic Ocean.....	45
3.8 Latitude-time evolution of meridional heat transport anomalies in PW in the Atlantic (top), Pacific (middle), and Indian (bottom) Oceans derived from the reanalysis for the period 1958-2004.....	46
3.9 Contributions in percentage from $\bar{V}\bar{T}$ (blue), and $V'T'$ (red) to total mean meridional heat transport in the (a) Atlantic, (b) Pacific, and (c) Indian Oceans for SODA-1.4.2 (left) and SODA-1.4.0 (right). Contributions to zonal heat transports in the ITF and in the Southern Ocean are shown in (d)...	50
3.10 Anomalies of total meridional heat transport in PW at $30^\circ N$ in the Atlantic Ocean (black) from SODA-1.4.2. Three contributing components are shown: red shows the contribution from $V'\bar{T}$; green indicates the contribution from $\bar{V}T'$; blue shows the contribution from $V'T'$	51
3.11 Contributions in percentage of $V'\bar{T}$, $\bar{V}T'$, and $V'T'$ to total meridional heat transport anomalies VT in the (a) Atlantic, (b) Pacific, and (c) Indian Oceans for SODA-1.4.2 and SODA-1.4.0. Contributions to zonal heat transports in the ITF and in the Southern Ocean are in the bottom panel.....	53
3.12 Mean (left) and linear change (right) in the total meridional heat transport transport (black) of heat due to Ekman currents (red) and geostrophic currents (green) and the residual (blue) over the (a) Atlantic, (b) Pacific, and (c) Indian Ocean for the period 1958-2001.....	56
3.13 Contribution in percentage from geostrophic (blue), Ekman currents (red), and the residual term (yellow) to total mean meridional heat transport in the (a) Atlantic, and (b) Pacific Oceans for SODA-1.4.2 (left) and SODA-1.4.0 (right).....	57
3.14 Contribution in percentage from geostrophic (blue), Ekman currents (red), and the residual term (yellow) to the interannual-decadal variability of meridional heat transport in the (a) Atlantic, and (b) Pacific Oceans for SODA-1.4.2 (left) and SODA-1.4.0 (right).....	59
4.1 Time series and the corresponding trend of world ocean heat content integrated from surface to bottom (10^{22} J) for the period 1958 – 2004 from (a) SODA-1.4.2 and (b) from Levitus et al. (2005).....	61

FIGURE	Page
4.2 Time series of world ocean heat storage rate ($W \cdot m^{-2}$) for the period 1958 – 2003 from SODA-1.4.2.....	63
4.3 Mean and standard deviation in PW of the mean divergence of heat transport (adv) and mean heat storage rate (st) in regions of world oceans from SODA-1.4.2 based on the period 1958-2001. Surface heat flux (shf) is calculated as a residual of the other terms.....	65
4.4 Heat content ($10^{22} J$) in the region north of $26.75^{\circ} N$ in the North Atlantic Ocean for the period 1958 -2003.....	66
4.5 Time series of convergence of heat transport (black), heat storage rate (red), and surface heat flux (green) in $W \cdot m^{-2}$ and their corresponding trends in $W \cdot m^{-2} \cdot decade^{-1}$ in the North Atlantic Ocean.....	67
5.1 The Great Ocean Conveyor Belt. It consists of an interconnected network of warm surface currents (in orange) and cold deep water currents (shown in blue). Source: Intergovernmental Panel on Climate Change (IPCC), “Climate Change 2001: The Scientific Basis”.....	73
5.2 Nordic Seas Overflow and Inflow Systems. Arrows on the map indicate the main overflow (blue) and compensating inflow (red) branches. On the schematic section to the right, temperature in $^{\circ}C$ and volume transport in Sv ($1 Sv = 10^6 m^3 \cdot s^{-1}$) are approximate values. DS, Denmark Strait; FBC, Faroe Bank Channel. Source: Hansen et al. 2004.....	73
5.3 Mean gyre circulations in Sv of the (a) Atlantic and (b) Pacific Oceans, and mean meridional overturning circulations of the (c) Atlantic and (d) Pacific Oceans.....	75
5.4 Meridional heat transport response to strength of MOC and gyre circulation in the Atlantic and Pacific Oceans.....	78
5.5 Normalized ocean heat transport (black), local MOC (red) and gyre circulation (green) strength at $30^{\circ} N$ in the Atlantic Ocean Normalized values are obtained using the anomalies divided by their standard deviation...	81
5.6 Temporal evolution of anomalous strength of (a) the Atlantic MOC and (b) meridional heat transport for the period 1958-2004.....	82
5.7 Same as Fig. 5.6 except for the period 1968-2004.....	84

FIGURE	Page
5.8 Mean (a) and standard deviation (b) in PW of the Atlantic MOC pseudo-heat function.....	86
5.9 Same as Fig.5.8 except for the Indo-Pacific Ocean.....	89
5.10 Time series of the NAO index (black) and the normalized SST (red) averaged over ($50^{\circ}N - 66^{\circ}N$) in the northern North Atlantic for the period 1958-2004.....	92
5.11 (a) Mean and (b) difference of the Atlantic MOC between (1981-2001) and (1958-1980).....	94
5.12 Linear change in zonal wind stress, SST, surface density and surface salinity of the North Atlantic Ocean for the period 1958-2004.....	96
5.13 Same as Fig. 5.12 except for boreal winter case.....	99
5.14 Evolution of anomalous zonal wind stress τ_x in $\text{dynes}\cdot\text{cm}^{-2}$, SST in $^{\circ}\text{C}$, surface density ρ in $\text{kg}\cdot\text{m}^{-3}$, and surface salinity (in $\text{g}\cdot\text{kg}^{-1}$) of the North Atlantic Ocean for the period 1958-2004 averaged from $50^{\circ}N - 62^{\circ}N$	101
5.15 Same as Fig. 5.14 except for boreal winter case.....	103
5.16 Temporal evolution of anomalous density averaged from $50^{\circ}N - 62^{\circ}N$ of the North Atlantic Ocean is calculated three ways. The left hand panel uses climatological SST and the right hand panel uses climatological salinity. The central panel uses time dependence (actual) temperature and salinity.....	105
5.17 Two main overflows across the Greenland-Scotland Ridge and their spreading pathways to the Labrador Sea (heavy dashed lines) (from Dickson et al., 2002).....	107
5.18 Meridional current and temperature across the Denmark Strait at $66.25^{\circ}N$ (a) and Faroe Bank Channel at $60.75^{\circ}N$ (b) for the period 1958-2004.....	109
5.19 Volume flux of overflow through DS (a), the FBC (b), and sum of DS and FBC (c).....	110
5.20 Mean and difference of the Atlantic wind stress, curl of wind stress, and gyre strength for the period 1958-2001.....	113

FIGURE	Page
5.21 Mean (a) and difference (b) in the wind stress over the Atlantic Ocean for the period 1958-2001. The difference between the period 1981-2001 and 1958-1980 is shown in (c). The implied meridional shift (in degree) is displayed in (d) along with its linear trend in red. There is a linear northward shift of $0.39^{\circ} \cdot decade^{-1}$, so there is a total northward shift of 1.56° for the period 1958-2001.	115
5.22 Schematic map of mechanisms of changes in the meridional heat transport in the Atlantic Ocean for the period 1958-2004. Red (blue) arrows denote the increase (decrease) of meridional heat transport with respect to its prevalent mean transport.....	120

LIST OF TABLES

TABLE	Page
1.1 Ocean heat transport in previous studies.....	5
5.1 Volume flux of the overflow across the Denmark Strait and the Faroe Bank Channel.....	112

CHAPTER I

INTRODUCTION

1.1 Importance of Ocean Heat Transport

It has long been known that the sun distributes energy unequally over the globe. Absorbed incoming shortwave radiation is not locally compensated by outgoing longwave radiation. Despite a surplus in the tropics and a deficit at high latitudes, the temperature meridional gradient is relatively constant. Therefore, heat must be transported poleward from the tropics on a global scale. Conduction of heat by the solid earth is negligible, so both the atmospheric and oceanic circulations play an important role in the redistribution of heat from low latitudes to high latitudes.

The importance of oceanic heat transport relative to atmospheric component has prompted several studies of poleward heat transport. Early studies (e.g., Sverdrup et al. 1942; Vonder Haar and Oort 1973; Newell et al. 1974; Hastenrath 1980, 1982; Newell and Chiu 1981; Talley 1983; Carissimo et al. 1985; Hsiung 1985; Trenberth and Solomon 1994) found that the ocean contribution to heat transport is comparable to that of the atmosphere.

This dissertation follows the style and format of *Journal of Climate*.

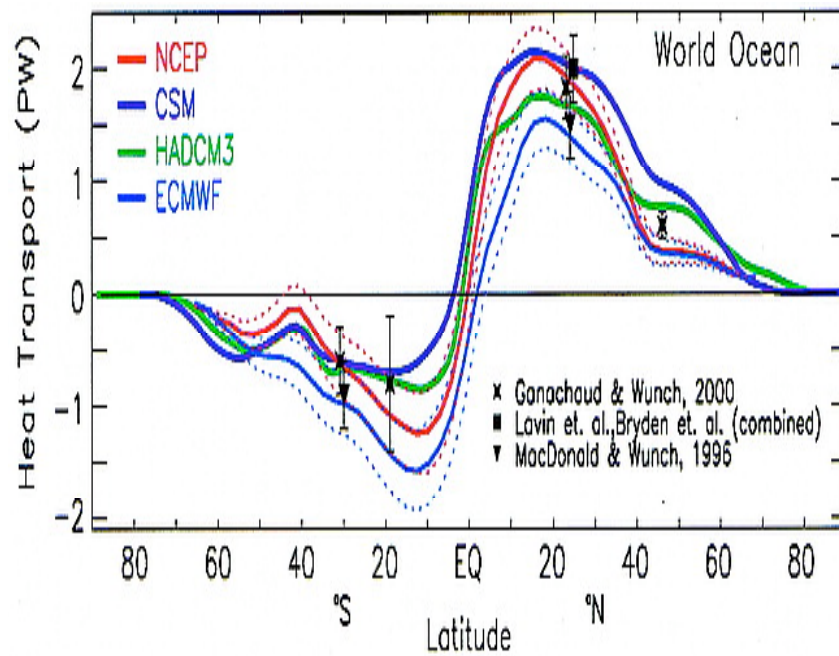


Fig. 1.1 World ocean heat transport in PW from the NCEP-derived and ECMWF-derived products compared to the results from the HADCM3 (years 81-120) and CSM (years 250-299) coupled models, along with those from Macdonald and Wunsch (1996) at $24^{\circ}N$ and $30^{\circ}S$, and at $24^{\circ}N$ (the combined Lavin et al. 1998 and Bryden et al. 1991 and from Ganachaud and Wunsch 2000) (from Trenberth and Caron 2001).

In a recent work, Trenberth and Caron (2001) find that the overall Northern

Hemisphere atmospheric heat transport is much larger than ocean transport, hence reducing the oceanic fraction. Fig. 1.1 shows world ocean heat transport derived from ocean stand-alone models and atmosphere-ocean coupled models. It is apparent that both in the Northern and Southern Hemisphere, the direction of heat transport in the world ocean is from low latitudes to high latitudes. However, using in situ oceanic measurements, Wunsch (2005) shows that the Northern Hemisphere oceans and atmosphere carry comparable poleward heat fluxes to about $28^{\circ}N$ where the oceanic poleward flux falls rapidly as heat is lost to the atmosphere. He also argues that an atmospheric radiative forcing change of about $9W \cdot m^{-2}$ would be required if the oceanic heat transport of $0.5 PW$ ($1PW = 10^{15}W$) is removed. This effect on climate is larger than what is expected from doubled atmospheric CO_2 .

1.2 Previous Studies

1.2.1 Long-term Mean

The fact that the oceans transport heat poleward is a fundamental mechanism of the climate system. Ocean heat transport has been computed as the difference between directly calculated atmospheric heat transport and satellite measurements of net radiation at the top of the atmosphere (Trenberth and Caron 2001). However, heat transport in individual oceans (i.e., Atlantic, Pacific and Indian Oceans) is more difficult to directly estimate due to a scarcity of ocean measurements. As more hydrographic datasets

become available during the World Ocean Circulation Experiment (WOCE), direct estimate of individual ocean basin heat transport became possible, particularly in the Atlantic Ocean. For example, Ganachaud and Wunsch (2002) use hydrographic sections in combination with a geostrophic inverse model to provide a mean value of global and individual ocean heat transport with self-consistent error bars.

Table 1.1 contains all available published estimates of heat transport in the global oceans. Both in the South Atlantic and North Atlantic, the direction of heat transports are well determined and are northward. In the North Pacific, most heat transport estimates show a northward flux of heat. It is hard to determine the dominant direction of meridional heat transport in the South Pacific based on just two locations. However, consensus on the direction of ocean heat transport in the South Pacific is still not reached among different studies. For example, Trenberth and Caron (2001) suggest the southward zonal annual mean heat transport based on the surface fluxes for Feb 1985-Apr 1989, while Ganachaud and Wunsch (2000) indicate northward heat transport in two locations based on high-quality hydrographic datasets in section P21E and P6 from the WOCE program. Heat transport in the Indian Ocean is southward (e.g., Macdonald 1998; Ganachaud and Wunsch 2000; Trenberth and Caron 2001; Talley 2003). Since observational datasets of the Atlantic Ocean are more abundant than the other two oceans basins, heat transports across specified sections there are more common. Even in the same locations, for example at $24^{\circ}N$, $36^{\circ}N$ and $24^{\circ}S$, estimates of the magnitude of heat transport vary. These estimates, made with the different datasets, and with different computation methods, suggest that there is robust variability

Table 1.1 Ocean heat transport in the previous studies.

Section	Heat Transport	References
Atlantic 59N	0.70 PW	Talley 2003
Atlantic 53N	0.62 PW	Talley 2003
Atlantic 47N	0.60 PW	Ganachaud and Wunsch 2000
Atlantic 45N	0.62 PW	Talley 2003
	0.65 PW	Macdonald 1998
Atlantic 36N	0.86 PW	Talley 2003
	1.01 PW	Macdonald 1998
	1.20 PW	Sato and Rossby 2000
Atlantic 32N	1.38 PW	Rago and Rossby 1987
Atlantic 26.5N	1.11 to 1.77 PW	Fillenbaum et al. 1997
	0.87 to 1.55 PW	Molinari et al. 1990
Atlantic 24N	1.28 PW	Talley 2003
	1.07 PW	Macdonald 1998
	1.20 PW	Hall and Bryden 1982
	1.27, 1.2, 1.33 PW	Lavin et al. 1998
Atlantic 8N	0.73 PW	Talley 2003
	1.39 PW	Macdonald 1998
	1.1 PW	Friedrichs and Hall 1993
Atlantic 4.5S	1.0 PW	Ganachaud and Wunsch 2003
Atlantic 11S	0.89 PW	Macdonald 1998
	0.48 to 0.53 PW	Holfort and Siedler 2001
	0.5 to 1.3 PW	Ganachaud and Wunsch 2003
Atlantic 16S	0.16 PW	Talley 2003
	0.59 PW	Holfort and Siedler 2001
	0.62, 1.3 PW	Bryan 1962
Atlantic 19S	0.57 to 0.97 PW	Ganachaud and Wunsch 2003
Atlantic 24S	0.37 PW	Talley 2003
	0.33 PW	Macdonald 1998
	0.33 PW	Holfort and Siedler 2001
	0.31 PW	Bryan 1962
Atlantic 30S	0.2 to 0.5 PW	Ganachaud and Wunsch 2003
Atlantic 32S	0.23 PW	Talley 2003
	0.49 PW	Macdonald 1998
	0.25 PW	Rintoul 1991
	0.28 PW	Sloyan and Rintoul 2001a
Atlantic 40S	0.37 PW	Holfort and Siedler 2001
Atlantic 45S	0.54 to 0.78 PW	Ganachaud and Wunsch 2003
Pacific 47N	0.01 PW	Talley 2003
	0.45 PW	Macdonald 1998
Pacific 35N	0.77 PW	Talley 2003
Pacific 24N	0.81 PW	Talley 2003
	0.44 PW	Macdonald 1998
Pacific 10N	1.25 PW	Talley 2003
	0.44 PW	Macdonald 1998
	0.70 PW	Wijffels et al. 1996
Pacific 28S	-0.43 PW	Talley 2003 (with ITF)
Pacific 43S	0.05 PW	Talley 2003
	0.26 PW	Macdonald 1998
Indian 32S	-0.59 PW	Talley 2003
	-1.3 PW	Macdonald 1998
	-0.87 PW	Sloyan and Rintoul 2001a
	-0.42 PW	Robbins and Toole 1997
	-1.5PW	Ganachaud and Wunsch 2000

of ocean heat transport on a wide range of time scales.

1.2.2 Seasonal Variability

Although the sign and magnitude of the time-mean ocean heat transport has been reasonably addressed, uncertainties still exist. It is important to consider the time-dependent ocean heat transport. A number of papers describe the seasonal variability of meridional oceanic heat transport. For example, Oort and Vonder Haar (1976) investigate the annual cycle of air-sea heat balance over the Northern Hemisphere and find that the inferred oceanic heat transports undergo large seasonal variations, especially in the tropics. Lamb (1981) makes an indirect estimate of the annual variation of Atlantic Ocean heat transport obtained based on observed air-sea exchange and subsurface temperature datasets and suggests that the heat flux is northward with the possible exception of southward flux during November-December. Hsiung et al. (1987) investigate the annual variation of heat transport north of $20^{\circ}S$ for both the Pacific and Indian Oceans using a method similar to Lamb's. They argue that north of $20^{\circ}N$ in the Pacific Ocean heat flux is mostly northward with a maximum in September and transport between $20^{\circ}S$ and $20^{\circ}N$ is evenly divided between northward (with a March maximum at $10^{\circ}N$) and southward (with an August maximum at $10^{\circ}S$), while in the Indian Ocean the transport is mostly southward except during January-February when a small northward transport appears north of $5^{\circ}S$. Jayne and Marotzke (2001) review the dynamics of global ocean heat transport variability on timescales from monthly to

interannual and describe heat transport variability in a state-of-the-art, high-resolution ocean general circulation model. They suggest that strong seasonal variability of world ocean heat transport is concentrated within 20° of the equator with a fluctuation of $\pm 3PW$. Jayne and Marotzke (2001) further argue that seasonal variability is mostly attributed to wind-induced current fluctuations in which the time-varying wind drives Ekman layer mass transports that are compensated by depth-independent return flows. Recently, Wang and Carton (2002) describe the seasonal heat budget of the North Pacific and North Atlantic Oceans using a 49-year analysis based on data assimilation. They demonstrate that wind-driven transport plays a more important role in the annual cycle of heat transport in the North Pacific Ocean than in the North Atlantic Ocean, while seasonally varying geostrophic currents and seasonal diabatic effects are more important in the North Atlantic Ocean.

1.2.3 Interannual-decadal Variability

Interannual-decadal variability of ocean heat transport in the Atlantic Ocean can be linked to the meridional overturning circulation (MOC). In a recent report Bryden et al. (2005) describe a slowing of the Atlantic Ocean's MOC at $25^\circ N$ causing a decrease of the northward heat transport by 30% over the past 50 years. Although this weakening MOC is debated, it is an important issue. Because there is heat exchange between the ocean and the atmosphere, a disruption or collapse of MOC is likely to impact the global climate. Thus the possibility of a weakening or even a collapse of the MOC may have a

profound consequence on society.

The role of horizontal ocean gyre circulation variability in heat transport on interannual-decadal variability is still not well addressed, even in the Atlantic and Pacific Oceans. It is speculated that gyre circulation is less important than the MOC in generating mean meridional oceanic heat transport because the horizontal temperature difference between poleward warm water mass (i.e., western side) and equatorward cold water mass (i.e., eastern side) across a latitude line is generally much smaller than the vertical temperature difference between the warm surface water mass and cold return water mass at depth. Since the strength of gyre circulation is comparable to that of the MOC. This suggests that MOC is more effective at transporting heat poleward. However, it does not necessarily mean that the interannual-decadal variability of ocean heat transport is largely induced by the MOC change rather than by gyre circulation variation. The relative importance of how gyre circulation and MOC affect meridional oceanic heat transport is needed.

The processes that govern interannual to decadal variability of the global oceanic heat transport have been examined in recent years. Dong and Sutton (2001, 2003) diagnose the variability of the Atlantic meridional ocean heat transport on interannual to decadal timescales using a coupled ocean-atmosphere general circulation model. They show that interannual variability in Atlantic oceanic heat transport is primarily controlled by wind-driven Ekman fluctuations, while decadal and multidecadal variability is dominated by the fluctuation of the Thermohaline Circulation (THC), which is driven by convective process in the Greenland-Iceland-Norwegian (GIN) sea and wind stress curl.

These findings agree well with Klinger and Marotzke's (2000) key points about variability on interannual timescales in the subtropical oceans and Hakkinen's (1999) and Eden and Willebrand's (2001) notion that variability in the Atlantic Ocean on decadal time scales is associated with variations in the THC. Using a UK Met Office coupled climate model, HadCM3, Shaffrey and Sutton (2003) demonstrate that Ekman processes associated with the North Atlantic Oscillation (NAO) dominate interannual variability of the Atlantic Ocean heat transport in the northern midlatitudes. In the tropics, oceanic adjustment to coastal upwelling induced along the Venezuelan coast by a strengthening of the easterly trade winds regulates the variation of interannual heat transport.

More recently, Drijfhout and Hazeleger (2006) diagnosed anthropogenic change of the Atlantic meridional oceanic heat transport from an ensemble of 62 simulations for the period 1940-2080, as well as its possible relation to changes in the Atlantic MOC and the gyre circulation. They point out that internal variability (relative to anthropogenic change) in the Atlantic oceanic heat transport is closely linked to MOC variability, while anthropogenic change in the Atlantic oceanic heat transport is not coincident with a forced decrease in the MOC. They further argue that this happens due to the compensating effect in heat transport by the baroclinic gyre and by the MOC. Wunsch and Heimbach (in preparation) describe changes in the North Atlantic meridional overturning circulation and associated heat fluxes at $26^{\circ}N$ as well as the counterpart in the North Pacific Ocean using a global one-degree model constrained by least-squares to a multiplicity of datasets for the period 1993-2004. No significant trend

in meridional heat flux in the North Atlantic or in the North Pacific is found, yet large month-to-month variability implies an oceanic system noisiness that can lead to aliasing errors in the estimation of heat and mass flux just over one single cross section.

1.3 Mechanisms of Temperature Change

Since the ocean provides the basis for seasonal and longer time scale climate forecasting, in which sea surface temperature (SST) is the key variable, knowledge of SST is essential for the study of atmosphere-ocean interaction. Many previous studies discuss the dynamical processes that govern the generation and decay of SST anomalies over the tropical/subtropical Atlantic and Pacific Ocean. There are two possibilities. One is that ocean mean currents advect anomalous temperature ($\bar{v}T'$) and another whereby anomalous currents advect the mean temperature ($v'\bar{T}$). Gu and Philander (1997) argue that the prolonged persistence of unusually warm conditions over the tropical Pacific during the early 1990s arose as a result of an influx of water with anomalous temperatures advected by the mean currents from higher latitudes (the $\bar{v}T'$ process). Chang et al. (1997, 2001) provide a similar scenario, so-called wind evaporation SST feedback (WES) in the study of tropical Atlantic climate variability. Using the Lamont Ocean GCM coupled to a simple atmospheric mixed layer model, Seager et al. (2001) posit that changes in the oceanic meridional heat transport in the tropical Atlantic Ocean are also dominated by the same process. They further show that changes in oceanic heat

transport are largely in phase with the changes in surface heat fluxes and SST. In contrast, Schott et al. (2004) provide evidence that wind-driven Subtropical Cells (STC) (a $v' \bar{T}$ process) is more important than advection of subducted temperature anomalies by the mean STC currents in forming equatorial SST anomalies. Joyce et al. (2004) propose that the time-dependent oceanic flow is capable of providing a significant contribution to the damping of the ubiquitous SST dipole in tropical Atlantic Ocean variability. Much of the work on the tropical Atlantic Ocean variability relies on simple coupled models which are different from complex Ocean GCMs combined with abundant observations such as the one used in the present study.

1.4 Ocean Heat Budget

Global ocean heat content change over the last fifty years has been systematically studied by Levitus et al. (2000, 2005) who find that ocean heat content has increased $14.5 \times 10^{22} J$, equivalent to a mean temperature increase of $0.037^\circ C$. This requires a global heating rate of $0.20 W \cdot m^{-2}$. Many studies (e.g., Stott et al. 2000; Barnett et al. 2001, 2005; Levitus et al. 2001; Reichert et al. 2002; Gregory et al. 2004; Hansen et al. 2005) suggest that the observed increase in oceanic heat content is largely due to the increase of anthropogenic gases in Earth's atmosphere. Can this change of heat content affect ocean heat transport? For example, Rahmstorf (1995) suggests a collapse of the deep overturning circulation could be triggered by reducing convection in high latitude due to global warming.

The rate of change of ocean heat content (i.e., heat storage rate) may be essential to atmosphere-ocean interaction in the climate system. Heat content is related to heat flux by the equation:

$$\frac{\partial HC}{\partial t} + \nabla \cdot (VT) = Q \quad (1.1)$$

where $HC = \iiint \rho C_p T dx dy dz$ is ocean heat content, $VT = \iiint \rho C_p v T dx dy dz$ is heat transport, and Q is surface heat flux. Vertically integrated heat transport due to diffusive processes (particularly for vertical mixing) is small compared to other terms. It is important to note that an anomaly in storage rate rather than in heat content (or SSTs) is indicative of the change of magnitude of the surface heat fluxes. Eq. (1.1) also shows that the divergence of ocean heat transport is also related to surface heat flux. The roles of heat storage rate and divergence of ocean heat transport in altering the mean and time-varying surface heat flux need further investigation. Shaffrey and Sutton (2004) argue that on interannual time scales variability of heat storage rate plays a role in the heat budget of the upper ocean. As a result, the connection between surface heat flux and oceanic heat transport is less direct. On decadal and longer time scales, changes in heat storage rate are likely to be less important. Jayne and Marotzke (2001) analyze the ocean heat budget in a state-of-the-art, high-resolution ocean general circulation model and find that the divergence of the time-evolving heat transport is largely balanced by changes in heat storage rate, while the mean advective heat transport divergence is largely determined by the mean surface heat flux. This implies that heat storage rate is not important in causing the change in time-mean surface heat flux. However, Barnett et

al. (2005) analyze the role of mean heat transport by ocean currents as a residual term obtained from heat storage rate and net oceanic surface heat flux in the Parallel Climate Model (PCM) and conclude that the changes in heat advection with the combination of surface forcing give an overall warming pattern. Fig. 1.2 is a reproduction of Fig. 4 in Barnett et al.(2005). It is obvious that the contribution of mean heat storage rate to net surface heat flux is larger than that of heat advection by ocean currents for all individual basins. In a study of tropical Atlantic variability, Chang et al. (2001) propose that the change in ocean heat transport counteracts the effect of surface heat fluxes in an upper-ocean heat budget analysis, and they hypothesize that ocean heat transport must be phase shifted relative to surface heat fluxes and/or SSTs for the system to oscillate. Due to the sparsely observed datasets in the global ocean, the large uncertainty of surface flux datasets, and poor simulation of real ocean circulation, the role of oceanic heat transport and of the rate of change of oceanic heat content in the climate system is still poorly understood.

1.5 Unresolved Problems

1.5.1 Long-term Mean

Previous studies of ocean heat transport have been limited by short duration (in the case of observational studies) or by being unconstrained by the observations (in the case of modeling studies). As Wunsch and Heimbach (in preparation) emphasize, strong

month-to-month variability, regarded as an oceanic system noisiness for large time

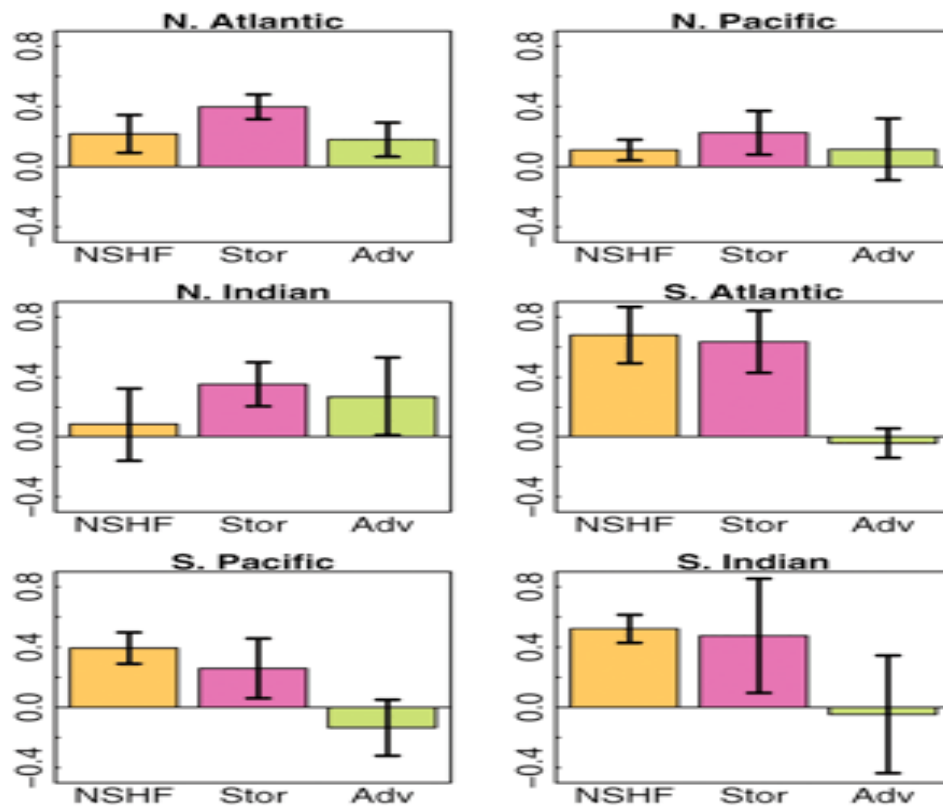


Fig. 1.2 An ocean heat budget showing the roles that heat advection by ocean currents plays in the anthropogenic warming of the world's oceans. From Barnett et al., 2005.

scales, can lead to aliasing errors in the estimation of heat and mass flux just over one single cross section. Robust interannual-decadal variability of ocean heat transport and its trend (if it exists) require long datasets to estimate the mean heat transport. In this study, a recently completed reanalysis called SODA is used to estimate the mean value of oceanic heat transport.

1.5.2 Mechanisms of Variability and Trend

It is believed that the mean meridional heat transport in the oceans is mostly produced by the MOC as mentioned above. One goal of this work is to describe the relationships between the meridional heat transport and strength of the MOC. Does a stronger MOC necessarily mean stronger meridional heat transport and vice versa? Based on work by Bryden et al. (2005), a slowing in the Atlantic Ocean's MOC at $25^{\circ}N$ implies a decrease of northward heat transport. But does a weaker MOC necessarily mean a weaker meridional heat transport? Using the concept of heat function to identify the contribution to the heat transport by different components of the MOC, Boccaletti et al. (2005) argue that a decrease in deep overturning circulation alone does not imply a significant reduction of the Atlantic and global oceanic heat transport because of the large contribution by the shallow circulation to the global heat transport in their model. However, Bryan (1962) provides evidence that the deep MOC in the Atlantic dominates the oceanic heat transport. As we know heat transport also depends on the temperature difference between the surface poleward flow and equatorward return flow at depth. The

difficulty in determining how the temperature difference between the poleward flow and return flow is qualitatively and quantitatively affected by a strengthening or weakening of MOCs in the real ocean makes this issue unresolved.

The horizontal and vertical resolution of the model Boccaletti et al. (2005) used is relatively coarse (2.8° (lon) \times 2.8° (lat) \times 15 levels) so that some small scale processes may not be well represented and eddy effects on heat transport may not be resolved. In addition to understanding how the mean state of oceanic heat transport is determined by different components of ocean circulation, it is also important to know what processes dominate the interannual-decadal variability of oceanic heat transport. Do different mechanisms control the variability in the tropics, midlatitude, and high latitude regions? The causes of this variability will be explored by a heat decomposition analysis since we have high-resolution datasets, including current velocity (not just geostrophic velocity), temperature, and in situ density of seawater. The result of this analysis will address the questions described in the above subsection. We demonstrate that variation of ocean circulation contributes predominantly to interannual-decadal variability of ocean heat transport. There are two aspects to the ocean circulation: a wind-driven circulation and a buoyancy-driven MOC. Ocean circulation is nonlinear and complex, and wind-driven circulation and buoyancy-driven MOC is closely linked, hence it is difficult to differentiate these two branches of ocean circulation. However, the different components of ocean circulation, associated with different underlying mechanisms, may be responsible for variability of oceanic heat transport on several time scales. In this study, we will explore the vertical structure of the mean and variability of ocean heat transport,

particularly in the Atlantic Ocean.

1.5.3 Impacts of Ocean Heat Transport on Climate

Barnett et al. (2005) calculate mean heat transport by ocean currents as a residual term from heat storage rate and net oceanic surface heat flux and argue that the changes in heat advection with the combination of surface forcing give an overall warming pattern. The effects of time-varying heat transport on surface heat fluxes have also been studied by several authors (Shaffrey and Sutton 2004; Jayne and Marotzke 2001). Possible phase relationship between heat transport and net surface heat flux have also been addressed (Chang et al. 2001; Seager et al. 2001), particularly in the study of tropical Atlantic variability. This study follows the line of previous work. We examine how anomalies in oceanic heat transport and storage rate regulate net surface heat flux, an important driving force to atmospheric circulation. We also intend to look for any phase changes in oceanic heat transport and storage rate relative to the changes in surface heat flux. In contrast to Barnett et al. (2005), we directly calculate divergence of oceanic heat transport and heat storage rate directly from the reanalysis datasets and compute surface heat flux as a residual term. We avoid the uncertain calculation of surface heat flux using an empirical formula based on the atmospheric and ocean state variables, thus it only relies on the accuracy of ocean circulation and state variables which are greatly improved as constrained by abundant observations.

1.6 Overview

This study is organized as follows: Chapter II describes the model and methods for estimating oceanic meridional heat flux together with discussion of their advantages and disadvantages. In Chapter III, we investigate horizontal and vertical structure of mean state and interannual-decadal variability of oceanic heat transport. Trend of oceanic heat transport for period 1958-2001 is examined. Underlying mechanisms responsible for the trend and interannual-decadal variability of oceanic heat transport are explored. In Chapter IV we examine the roles of oceanic heat transport in the North Atlantic Ocean heat budget. Chapter V is aimed to explore the relative roles of gyre and MOC in oceanic heat transport, particularly in the Atlantic Ocean. We provide climate mechanisms to explain the origins of the recent trend of heat transport in the Atlantic Ocean. Chapter VI summarizes the major results.

CHAPTER II

METHODOLOGY

2.1 Methods of Estimating Heat Transport

Heat (or enthalpy, Warren 1999) transport in the ocean is much more difficult to determine than in the atmosphere. Because the most energetic scales of motion in the ocean are smaller than in the atmosphere by an order of magnitude, determining ocean heat transport requires high resolution spatial sampling. The difficulty of obtaining observed data of global coverage with sufficient resolution makes estimating global ocean heat transport from observations unrealistic. Thus we must resort to using models to estimate ocean heat transport.

There are at least three methods employed to estimate oceanic heat transport. In the residual method, ocean heat transport is computed as a residual of the atmospheric heat budget (assuming no change in the atmospheric heat content and no effects due to land). This method relies on an accurate radiative balance measured by satellites (e.g., the Earth Radiation Budget Experiment (ERBE)) and has been used in several studies (e.g., Vonder Haar and Oort 1973; Oort and Vonder Haar 1976; Trenberth and Solomon 1994; Keith 1995; Trenberth and Caron 2001).

In a second method, the direct method, ocean heat transport is obtained by evaluating

the integral $C_p \int_{-D}^0 dz \int_{west}^{east} \rho v T dx$ using hydrographic data. In this equation C_p is the seawater heat capacity under constant pressure, D is the depth of ocean, ρ is the in situ ocean water density, v is current velocity and T is temperature. Since v is in general unknown, it has to be estimated using a geostrophic approximation. Bryden and Hall (1980), Hall and Bryden (1982), Bryden, Longworth and Cunningham (2005) use the direct method to estimate meridional heat transport. This method can be further improved by using inverse ocean models, in which a dynamic constraint is used. This method was used by Roemmich (1980), Roemmich and Wunsch (1985), Macdonald and Wunsch (1996), Wunsch (1996), Ganachaud and Wunsch (2000, 2003). One complication of the direct method is that oceanic heat transport can be calculated across sections where the net mass flux may not be zero. These regions include Indonesian Throughflow region, the Southern Ocean.

The third method of estimating ocean heat transport is the surface flux method, in which the ocean-atmosphere exchange is inferred from bulk formulae using ship observations, surface properties of the ocean and atmosphere (e.g., Josey et al. 1999) or from the fields derived from model reanalyses. Uncertainty associated with these estimates using different datasets and different computation method makes it difficult to obtain a global estimate of the ocean heat transport.

All these methods have distinct advantages and disadvantages. Since the ocean heat transport estimated by the residual method is the difference between two large terms, its error can be large. Bulk formulae employ datasets from ships and buoys and rely largely

on local observations. Hence the error associated with its calculation can be large due to its empirical formulae. The direct method can only be applied to regions where oceanographic datasets are abundant and continuous measurements are available. Unfortunately, limited oceanographic datasets prevents making long-term mean estimates of heat transport using the direct method. The emergence of high resolution ocean models constrained by observations makes estimating heat transport accurately a possibility.

2.2 SODA

2.2.1 Model Description

A multi-year Simple Ocean Data Assimilation (SODA) reanalysis is employed in this study to explore the variability of oceanic heat transport and to identify the processes responsible for the characteristics of heat transport in the world's oceans. The forecast model utilizes Parallel Ocean Program (POP) physics and numerics (Smith et al. 1992), with an average 0.4° (lon) \times 0.25° (lat) \times 40-level resolution, forced by the ECMWF ERA-40 atmospheric reanalysis for the 44-year period from January 1, 1958 to December 31, 2001. We update the reanalysis in a second run which is forced by QuikSCAT wind stress from 2000 to 2004. The North Pole is displaced onto Canada which allows the inclusion of the Arctic Ocean. Bottom topography is obtained from the $1/30^\circ$ analysis of Smith and Sandwell (1997) with modifications for certain passages.

Surface heat flux is based on bulk formulae, which is relatively unimportant as a boundary condition because a large number of near-surface temperature observations are used to update mixed layer temperature. Surface freshwater flux for the period 1979-2001 is provided by the Global Precipitation Climatology Project (GPCP) monthly satellite-gauge merged product (Adler et al. 2003) combined with evaporation obtained from a bulk formula. For the period before 1979, a climatology based on GPCP is used. Vertical diffusion of momentum, heat, and salt is based on non-local KPP scheme and horizontal diffusion for subgrid-scale processes is based on a biharmonic mixing scheme.

The model is constrained by observed temperature and salinity using a sequential assimilation algorithm. The details of the assimilation method are described by Carton et al. (2000a), Carton and Giese (2007). The assimilation component combined with the forecast model is called SODA-1.4.2. A second experiment SODA-1.4.0 without assimilation component was also performed in order to explore the effects of observations on ocean heat transport.

2.2.2 Observed Data Employed in SODA

The observation set used in SODA is as complete as possible and includes the historical archive of hydrographic profiles supplemented by ship intake measurements, moored hydrographic observations, and remotely sensed SST. The basic subsurface temperature and salinity data sets consist of approximately 7×10^6 profiles, of which two

thirds have been obtained from the World Ocean Database (WOD) 2001 (Boyer et al. 2002; Stephens et al. 2001) with on-line updates through December 2004. This data set represents an increase of almost 1.7 million profiles relative to the WOD 1998 data used in many recent studies and has been extended by operational temperature profile observations from the National Oceanographic Data Center\NOAA temperature archive. The primary temperature profiling instrument prior to the late-1960s was the Mechanical Bathythermograph (MBT). MBTs are limited to depths shallower than 285 meters and therefore do not sample the main thermocline in many parts of the ocean. In the late-1960s, a new Extendible Bathythermograph (XBT) began to be used which obtains samples to a depth of 450 meters and below. A drop-rate correction (Stephens et al. 2001) is applied to the XBT data.

A large number of near-surface temperature data sets are obtained from bucket and ship-intake in situ observations and satellite remote sensing. The in situ observations are made at a nominal depth of 1 meter and serve as an estimate of mixed layer temperature. In SODA, we use the ungridded nighttime NOAA/NASA Advanced Very High Resolution Radiometer (AVHRR) Oceans Pathfinder SST, 'best' data at 0.5° resolution (Vazquez et al. 1995). These observations are available starting January, 1981 and average 25,000 observations per week. Mixed layer salinity observations, which average more than 10,000 per year, are available since 1960 (Bingham et al. 2002).

The salinity data counts are lower than the temperature data by a factor of 3-4 since salinity is not measured by the bathythermographs, but by several less common deeper profiling instruments. The number of salinity observations reduced dramatically after

1995 due to the delay in getting salinity observations into the data archives. Recently a new observing system, ARGO, has been deployed, allowing the near-realtime data profiles to 1000-2000 meters and resulting in an increase in temperature sampling at 1000 meters and salinity sampling at all depths.

2.3 Data Archives

In the present study, averages of model output variables such as temperature, salinity, and velocity are saved at five-day intervals. These average fields are then mapped onto a uniform global 0.5° (lon) x 0.5° (lat) x 40-level (vertical) grid using the horizontal grid Spherical Coordinate Remapping and Interpolation Package with second order conservative remapping (Jones 1999). The mapping shifts the locations of the temperature and horizontal velocity grids, which are offset in the model, to the same set of remapped gridpoint locations.

The transport of heat by mesoscale eddies in the ocean is suspected to be an important term for the time-mean (Jayne and Marotzke 2002) and time-varying oceanic heat transport (Roemmich and Gilson 2001). The eddy heat transport arises from the covariance of velocity and temperature fields in the ocean. There are at least three regions that eddy is actively important in ocean circulation. These three regions are the western boundary currents and its extension, the Antarctic Circumpolar Current, and the equatorial region. Jayne and Marotzke (2002) analyze the eddy heat transport in an ocean general circulation model and suggest that the eddy heat transport is found to be

strong in these regions and is largely confined to the upper 1000 m of the ocean. They also argue that eddy heat transport in the equatorial region is largely due to tropical instability waves, while in the western boundary currents and the Antarctic Circumpolar current, meandering of currents gives rise to strong eddy heat transport. Roemmich and Gilson (2001) study eddy heat transport at an average latitude of $22^{\circ}N$ in the North Pacific using high-resolution XBT transects and TOPEX/Poseidon altimetric data and find a northward eddy heat transport of $0.086 \pm 0.012PW$ with a considerable seasonal-interannual variability.

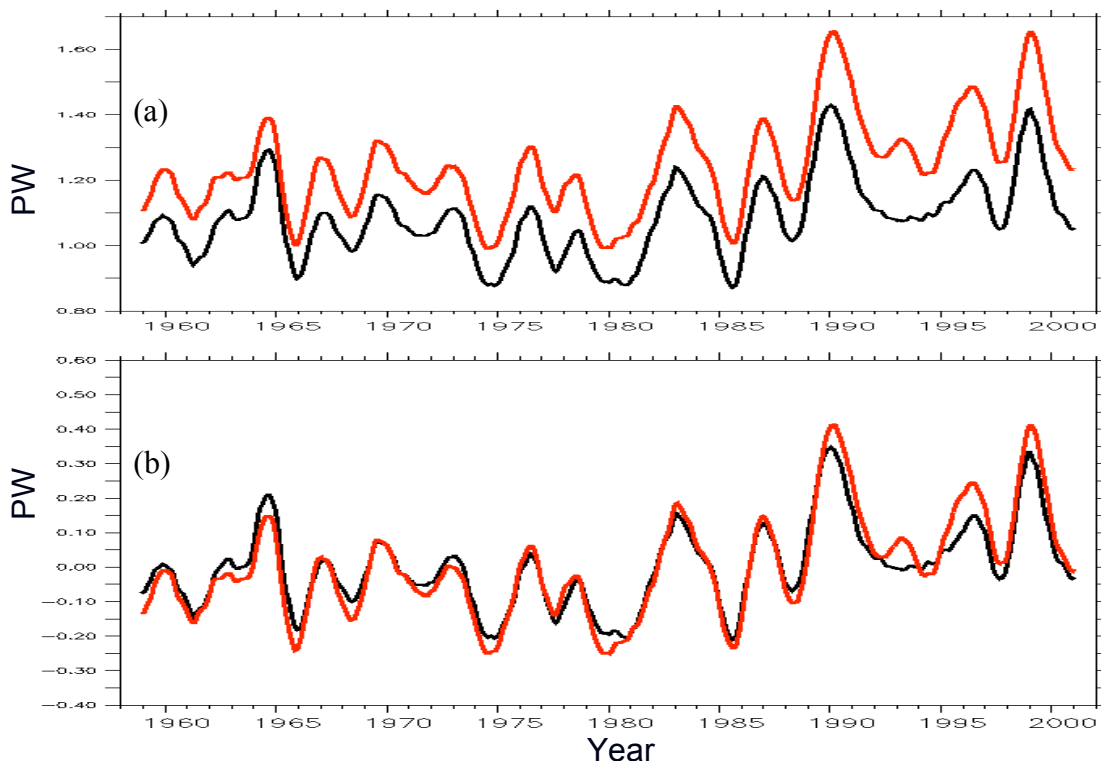


Fig. 2.1 Meridional heat transport in PW across $40^{\circ}N$ in the Atlantic Ocean based on monthly datasets (black) and 5-day datasets (red) for (a) total value and (b) mean-removed anomalies.

Since SODA is an eddy-permitting assimilating system and the resulting eddy heat transport is implicitly included as a part of total heat transport by ocean currents. Fig. 2.1 shows basin-scale meridional heat transport in PW across $40^\circ N$ in the Atlantic Ocean based on monthly and 5-day datasets for the total and mean-removed heat transport anomalies. Frequencies lower than the annual cycle are removed by using a Parzen window of 2 years for monthly datasets and 5-day datasets. The difference in mean heat transport calculated from 5-day datasets (the mean is $1.24 PW$) and from monthly datasets (the mean is $1.08 PW$) is $0.16 PW$, a 15% increase of northward heat transport induced by eddies. It is evident that eddies cause change in the mean heat transport in this study. However, one standard deviation of oceanic heat transport derived from 5-day is $0.147 PW$ and from monthly datasets is $0.120 PW$. Thus, eddy effect has little temporal variability relative to monthly datasets. Eddy effect on oceanic heat transport in the equatorial regions and Southern Ocean (not shown) is similar. Thus, oceanic heat transport derived from monthly values can be used to represent interannual-decadal variability, even in regions of strong eddy activity. Therefore, the monthly datasets are used for investigating interannual-decadal variability of oceanic heat transport whereas the 5-day data are used to calculate the mean heat transport. The underlying mechanism of why eddy effect on the interannual-decadal variability of oceanic heat transport is weak is not clear and is beyond the scope of present study.

CHAPTER III

OCEAN HEAT TRANSPORT IN SODA

3.1 Spatial Structure of Mean Heat Transport and Its Trend

3.1.1 x-y Structure

Because of limited spatial observations with short duration, early studies could not resolve variability and so focus on the long-term mean value of oceanic heat transport with error estimation (e.g., Hastenrath 1980, 1982; Hall and Bryden 1982; Talley 1983; Hsiung 1985). As more hydrographic datasets became available, especially during the World Ocean Circulation Experiment (WOCE), the direct method was used to estimate ocean heat transport across sections in ocean basins with greater accuracy (Ganachaud 1999; Ganachaud and Wunsch 2000, 2002).

Fig. 3.1a shows the long-term mean and standard deviation (in parentheses) of world ocean heat transport in PW across sections for the period 1958 – 2001 in SODA-1.4.2. Since the purpose of this study is to investigate the variability of ocean heat transport on time scales greater than one year, the standard deviation is calculated after the removal of high frequency variability (less than annual cycle). Northward mean heat transport in the Atlantic Ocean is consistent with results from many previous studies (refer to Table 1), with estimated heat transport values ranging from 0.38 to 1.24 PW with maximum

heat transport in the mid-latitudes. Further north, heat transport falls off rapidly because of cooler temperatures. In the Pacific Ocean, northward heat transport also dominates, though its magnitude is much smaller than that at the same latitude in the Atlantic Ocean. In the Pacific, the peak heat transport occurs in a narrow band centered on $20^{\circ}N$. It is not surprising to find that heat transport in the Southern Pacific sector is also northward. This is due to the fact that warm water in the Pacific is mainly transported to the Indian Ocean via the Indonesian Throughflow (ITF) (about $1.24 \pm 0.13 PW$ is transported), giving rise to a large southward heat transport in the Indian Ocean (Ganachaud and Wunsch, 2000). Heat transport is found to have strong variability at lower latitudes and small fluctuation at middle and high latitudes in the world oceans. Particularly, the strongest variability of heat transport in the tropical Pacific Ocean reflects active oceanic processes, and probably a strong response to atmospheric forcing. In the Southern Ocean, the small standard deviation of zonal heat transport reflects weak variability. The considerable large zonal heat transport of $2.2 PW$ south of Australia is due to the large contribution of about $1.3 PW$ of southward heat transport from the Indian Ocean.

Fig. 3.1b indicates the associated trend in $PW \cdot decade^{-1}$ for ocean heat transport shown in Fig. 3.1a. Large trends of heat transport are mostly found in the North Atlantic Ocean. For example, the trend of $0.058 PW \cdot decade^{-1}$ at the $30^{\circ}N$ in the Atlantic Ocean implies a $0.25 PW$ increase of heat transport from 1958 to 2001. This transport is much larger than its uncertainty of $0.15 PW$. No significant trend of meridional heat transport in the Indian Ocean is found. In the Southern Ocean, a $0.16 - 0.22 PW$ increase

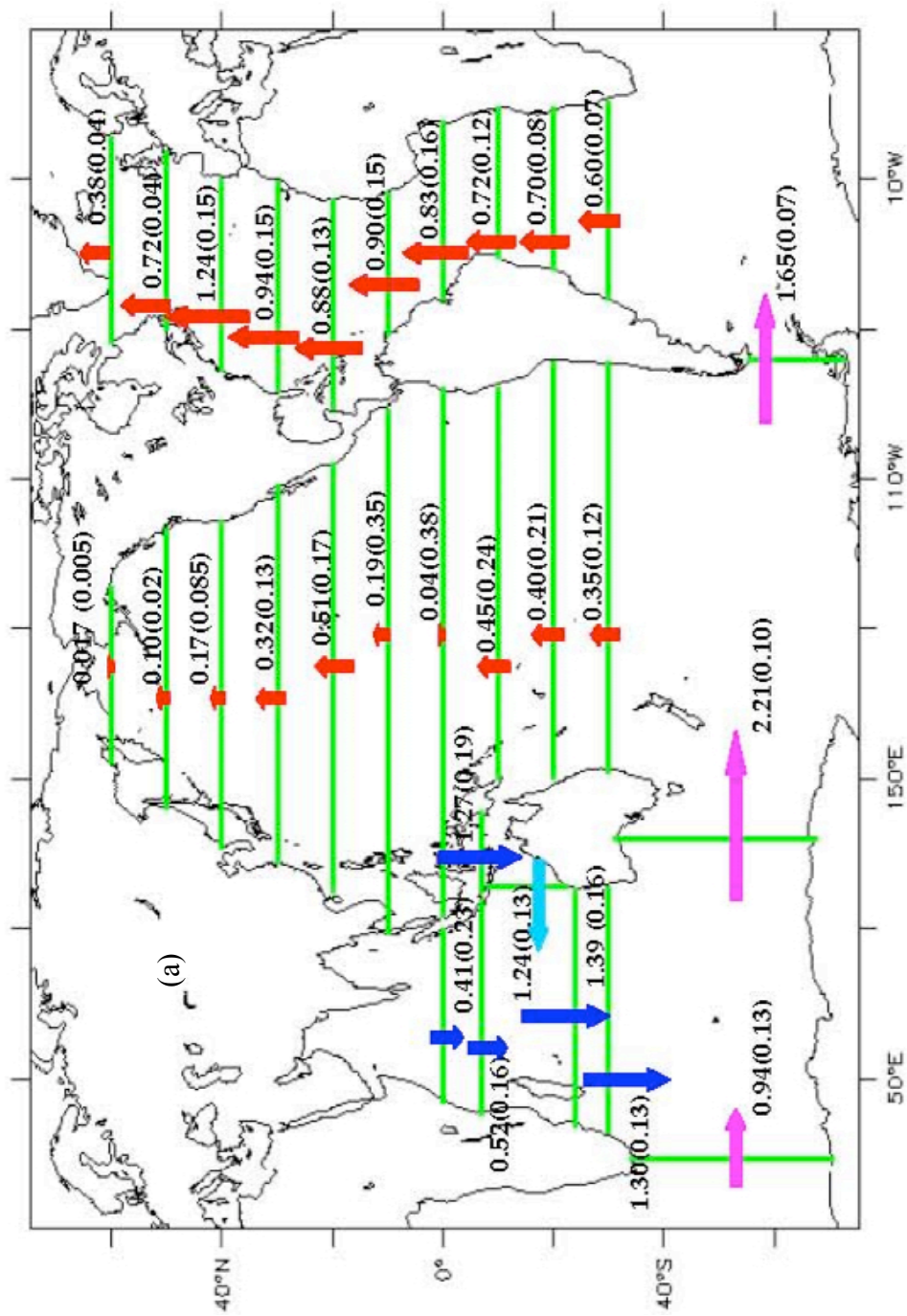


Fig. 3.1 (a) Long-term mean and standard deviation (in parentheses) of oceanic heat transport in PW ($1PW = 10^{15} W$) across sections and (b) trend of oceanic heat transport in $PW decade^{-1}$ across sections for the period 1958-2001 in SODA-1.4.2.

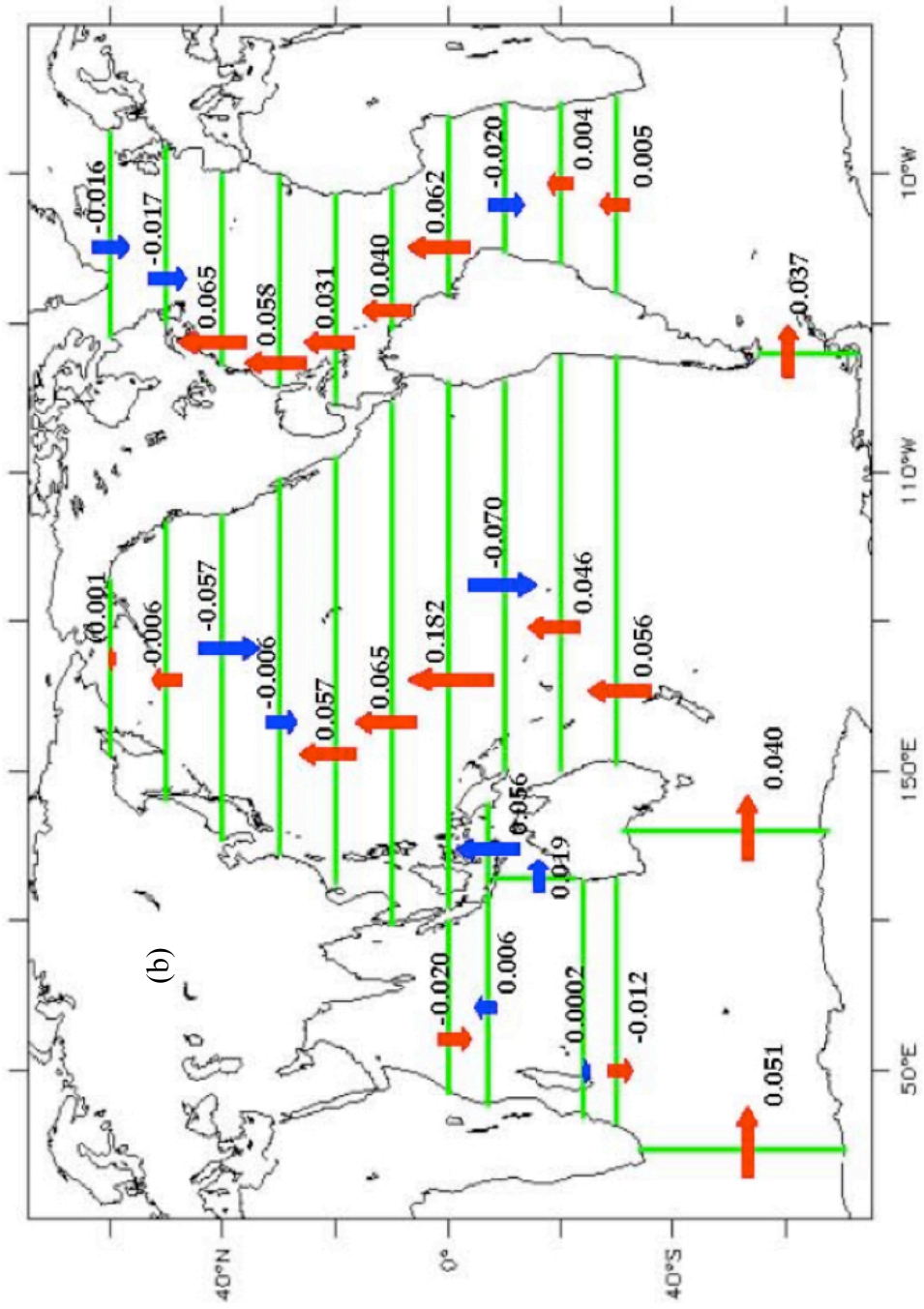


Fig. 3.1 (continued)

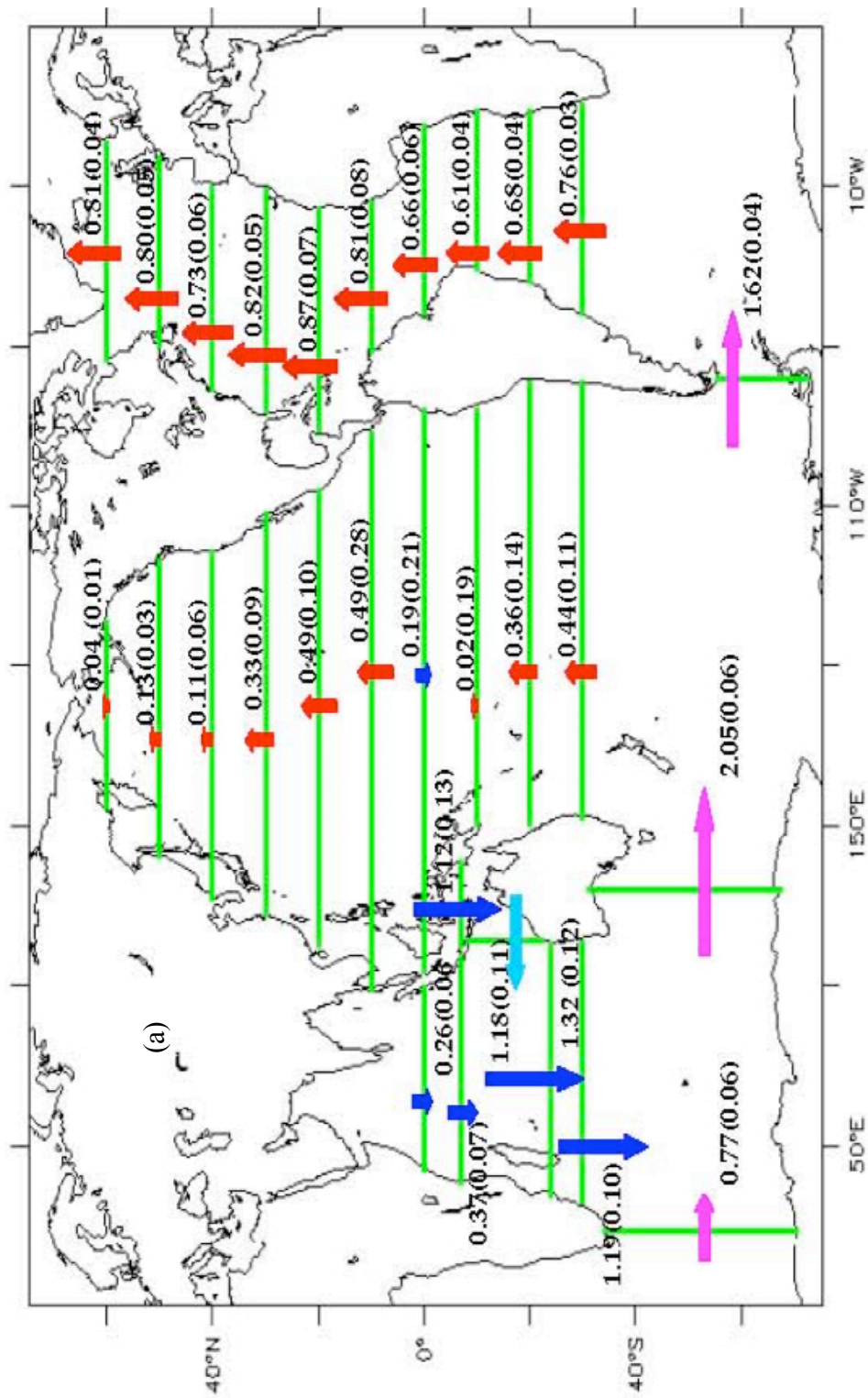


Fig. 3.2 Same as Fig. 3.1 except for SODA-1.4.0.

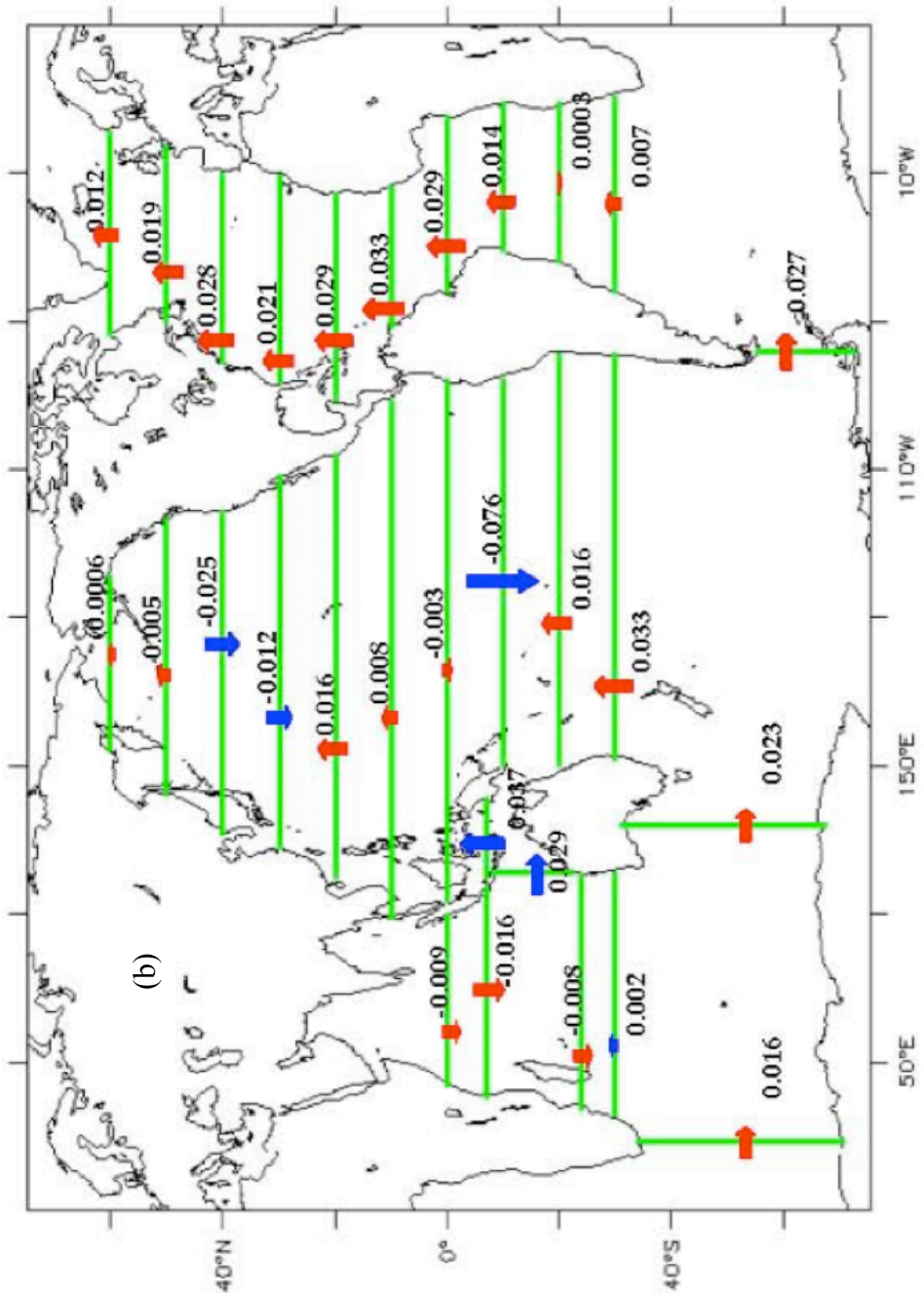


Fig. 3.2 (continued)

of zonal heat transport for the 44-year period is found.

In order to investigate the impact of observations from assimilation, we compare with oceanic heat transport in an ocean simulation without data assimilation. Fig. 3.2 shows the long-term mean and trend of oceanic heat transport derived from SODA-1.4.0. Heat transport in the three individual ocean basins is generally similar in structure to that in SODA-1.4.2. Northward transport of heat is prevalent in the Atlantic and Pacific Oceans and southward transport of heat is dominant in the Indian Ocean. The sign of the trend of heat transport is also similar in SODA-1.4.0 except in the high latitude of North Atlantic Ocean, where there is a convergence of heat transport in the region between $40^{\circ}N$ and $50^{\circ}N$ in SODA-1.4.2, while this signal is not present in SODA-1.4.0. This implies that inclusion of observations of temperature and salinity in the ocean may be important to constrain the change in heat transport. The influence of ocean observation upon heat transport will be discussed in section 3.2b where contributing processes for variability of heat transport are discussed.

3.1.2 y-z Structure

a. OHT in Density Layers

Ocean water masses are usually believed to flow along neutral surfaces identified by different density classes, especially below the mixed layer. In Ganachaud and Wunsch's (2000) study, water transport is calculated based on the different density classes bounded

by neutral surfaces across selected hydrographic sections. Heat transport is closely linked to movements of warm or cold water masses in different density classes. For example, in order to assess the shallow, intermediate and deep overturning components in the heat budget, the ocean heat transport in the Atlantic, Pacific, and Indian Oceans for different density classes are estimated using hydrographic datasets (Talley 2003).

In this study, a similar method is utilized to investigate contributions from different meridional overturning components. In order to estimate meridional heat transport in different components of MOC, density classes are needed to be defined to represent different layers of the overturning circulation. Fig. 3.3 illustrates the time-mean, zonal-averaged meridional currents and density class σ_θ in the Atlantic Ocean as a function of latitude and depth. The quantity σ_θ is defined as the difference between the in situ density of ocean water ρ in $kg \cdot m^{-3}$ and $1000 kg \cdot m^{-3}$. The ocean is categorized into four layers using density-based criterion: the mixed, shallow, intermediate, and deep layers. The mixed layer is defined to be the depth at which density differs by a density $\Delta\sigma_\theta = 0.125 kg \cdot m^{-3}$ from the surface. The shallow layer is identified by the density interval between the mixed layer and $\sigma_\theta \leq 27.3 kg \cdot m^{-3}$; the intermediate layer is denoted by $27.3 kg \cdot m^{-3} < \sigma_\theta \leq 27.72 kg \cdot m^{-3}$, and the deep layer is represented by $\sigma_\theta > 27.72 kg \cdot m^{-3}$. Many studies (Miller 1976; Levitus 1982; Spall 1991; Huang and Russell 1994) used $\Delta\sigma_\theta = 0.125 kg \cdot m^{-3}$ for the mixed layer depth definition because it corresponds to the water mass characteristics of Subtropical Mode Water in the North Atlantic Ocean as described by Levitus (1982). The definition of shallow, intermediate, and deep layer is similar to those used by Talley (2003) to describe the meridional

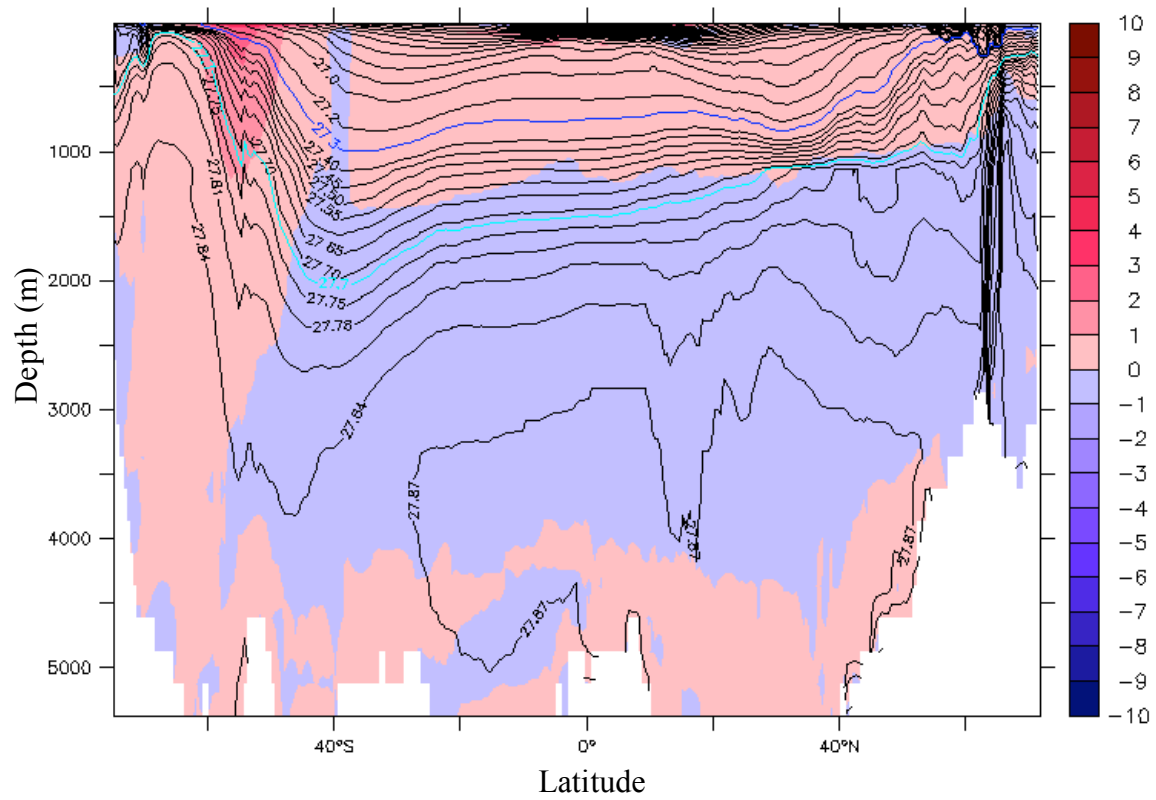


Fig. 3.3 Time-mean of zonal-averaged meridional currents in $cm \cdot s^{-1}$ (shaded) and density class σ_θ in $kg \cdot m^{-3}$ (contours) in the Atlantic Ocean. The vertical structure of the ocean is identified by a variety of density classes.

overturning transport in the North Atlantic at $24^{\circ}N$ and by Ganachaud and Wunsch (2000) to describe zonally integrated layer mass transport in the world ocean.

The transport in the different density layers is shown in Fig. 3.4. A reference temperature of $0^{\circ}C$ is used and the corresponding standard deviation is shown in parentheses. Heat transport in the mixed layer, as expected, is closely related to surface wind stress. In the Atlantic and Pacific Oceans, the direction of heat transport in the mixed layer is largely determined by the trade winds. There is a small mean transport of heat but with large variability in the mixed layer of equatorial Indian Ocean which is associated with the Indian and East Asian monsoons. In the region south of $7^{\circ}S$ in the Indian Ocean, heat transport in the mixed layer rises dramatically because a large volume of light warm water that comes from the western Pacific regions via the Indonesian Throughflow region. In the Southern Ocean, heat transport in the mixed layer is directly affected by the strong westerlies.

The direction of heat transport in the shallow layer is determined by the subtropical and subpolar gyre circulations, particularly in the Pacific Ocean. In the tropical Atlantic Ocean, the zonally averaged motion in the shallow layer is northward from $30^{\circ}S$ to $50^{\circ}N$ as illustrated in Fig. 3.3. This northward moving warm water gives rise to a northward heat transport in this layer. Particularly in the South Atlantic Ocean, convergence of heat from Drake Passage and $20^{\circ}E$ in the shallow layer reinforces northward transport of heat. Heat transport in the shallow layer of the ITF is the largest of the other three layers. This result is expected because the ITF itself is very shallow.

In the intermediate layer, heat transport is very small except in the Southern Ocean

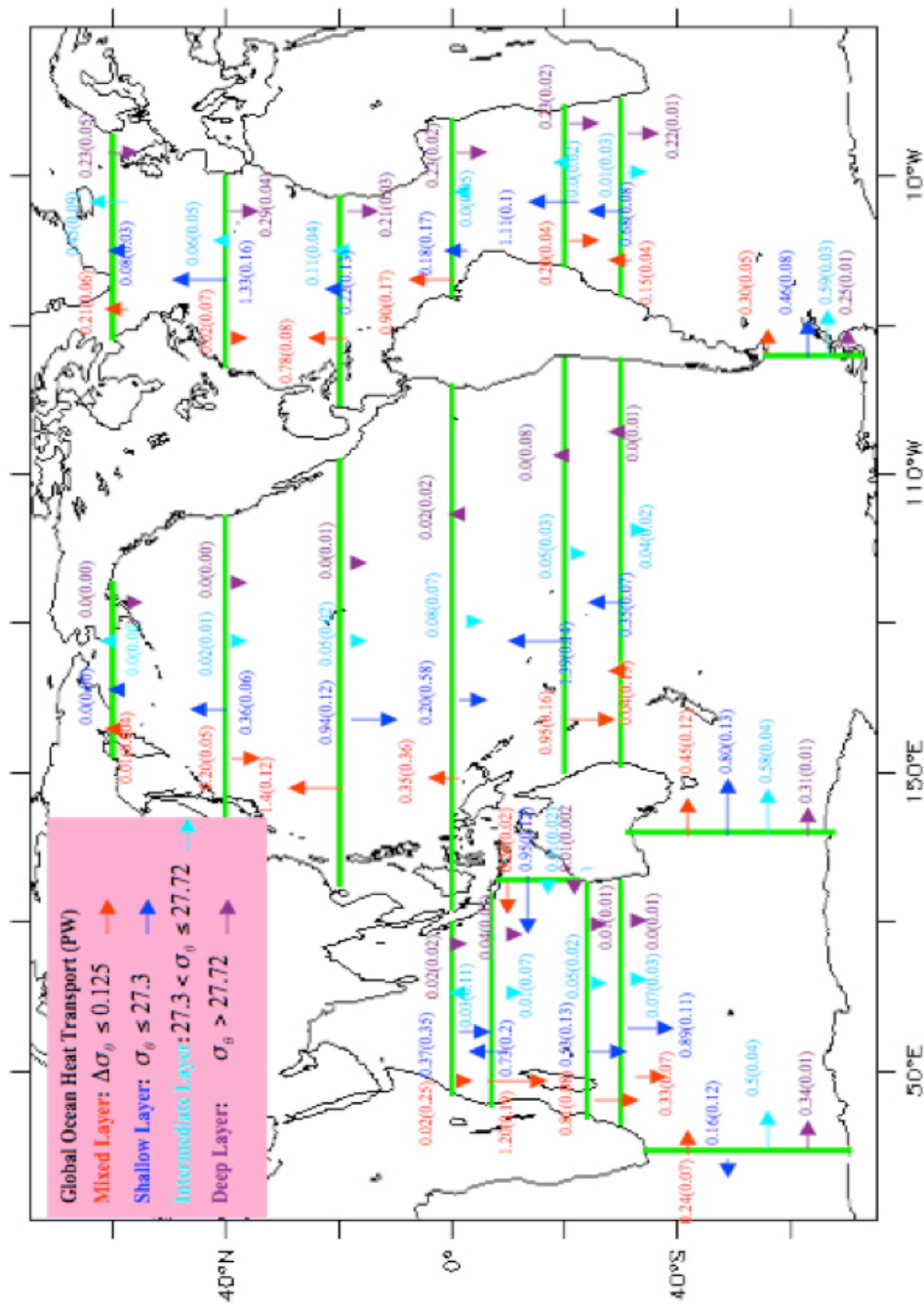


Fig. 3.4 Map of the mean and standard deviation (in parentheses) of global ocean heat transport in PW using a reference temperature of $0^\circ C$ in the different density layers.

where it circulates around Antarctica. In the deep layer, heat transport in the three ocean basins is southward. It has a very stable heat transport in an order of $0.2 - 0.3 PW$ in the Atlantic Ocean. In the Pacific and Indian Ocean, heat transport in the deep layer is very small with values between 0 and $0.02 PW$. In the Southern Ocean, zonal heat transports at $20^{\circ}E$, $130^{\circ}E$, and $70^{\circ}W$ at each layer have little variability except in the shallow layer of $20^{\circ}E$ and $130^{\circ}E$, where there is a critical change from $0.16 PW$ of westward transport at $20^{\circ}E$ to $0.80 PW$ of eastward transport at $130^{\circ}E$. This is primarily due to the large volume of warm water from the ITF in this layer and eddy transport of heat from the Indian Ocean into the South Atlantic Ocean.

In order to better understand the meridional structure of the heat transport in the three ocean basins, we examine the transport of heat at each layer as a function of latitude. Meridional heat transport in the mixed layer, shallow, intermediate, and deep layers for the Atlantic, Pacific, and Indian Oceans is presented in Fig. 3.5. Heat transport in the mixed layer is quasi-symmetric about the equator, reflecting the important influence of wind stress. The largest heat transport is centered in the region of $10^{\circ}S-10^{\circ}N$ in the Atlantic and Pacific Oceans, and at $10^{\circ}S$ in the Indian Ocean. Heat transport in the shallow layer is considerably different between the three ocean basins. In the Atlantic Ocean, heat transport in this layer is mostly northward with peak values centered at $5^{\circ}S$ and $36^{\circ}N$. The northward heat transport in this layer results from the northward movement of warm water at the thermocline surface by strong western boundary currents. Interestingly, heat transport in the shallow layer of the Pacific Ocean is nearly opposite in direction but the same magnitude to that in the mixed layer. Unlike

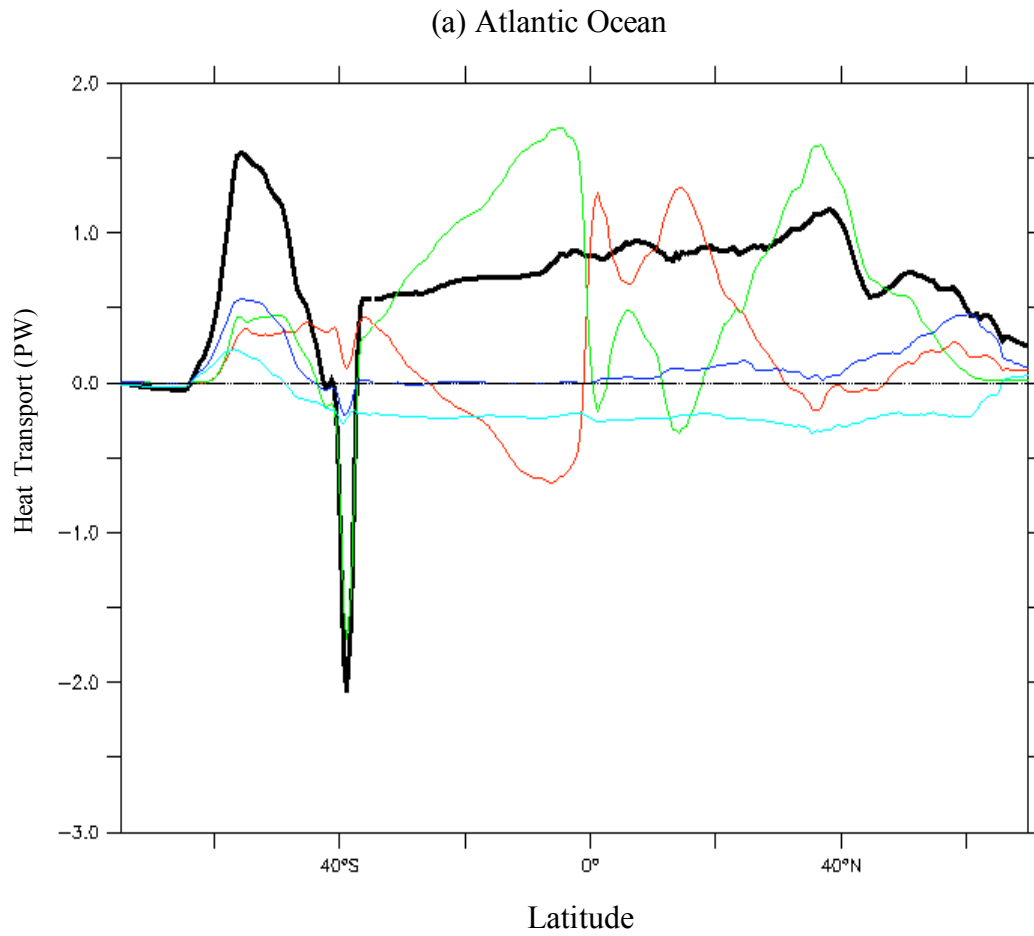


Fig. 3.5 Heat transport in PW using a reference temperature of 0°C in the mixed layer (red), shallow layer (bright green), intermediate layer (blue), and deep layer (turquoise) for the (a) Atlantic, (b) Pacific, and (c) Indian Oceans. The total heat transport is denoted with a black curve.

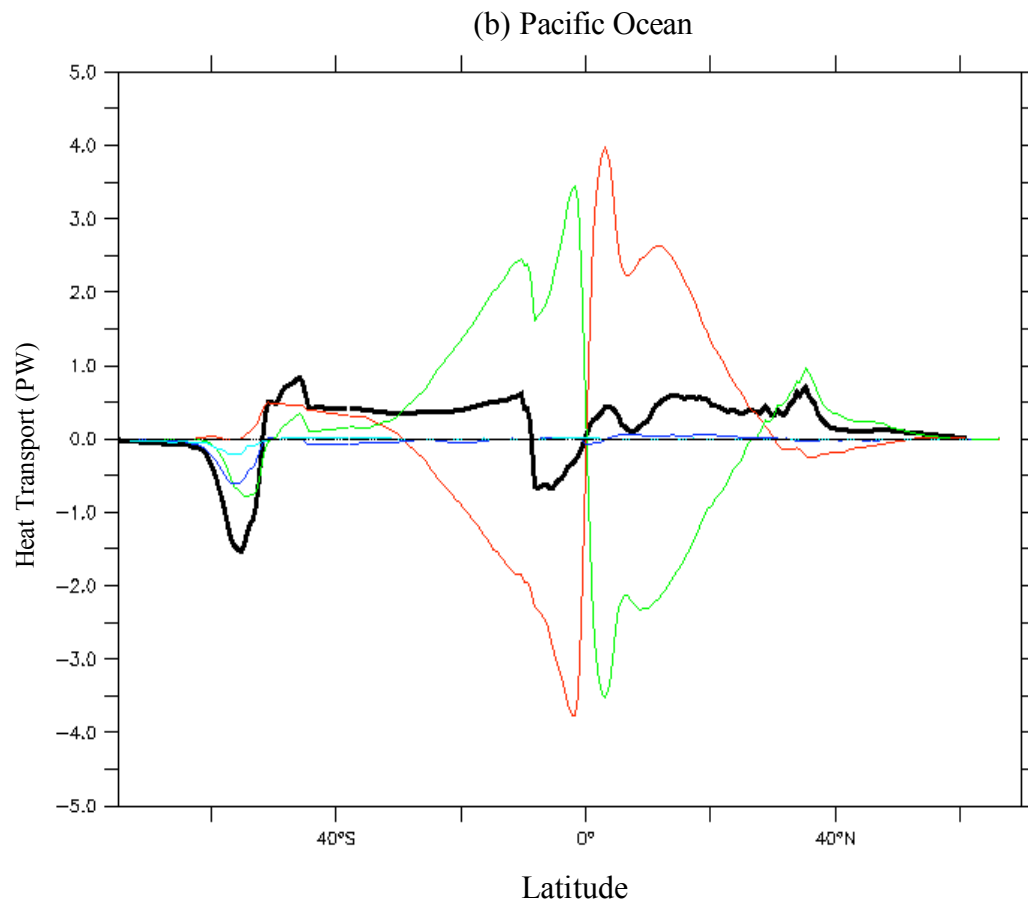


Fig. 3.5 (Continued)

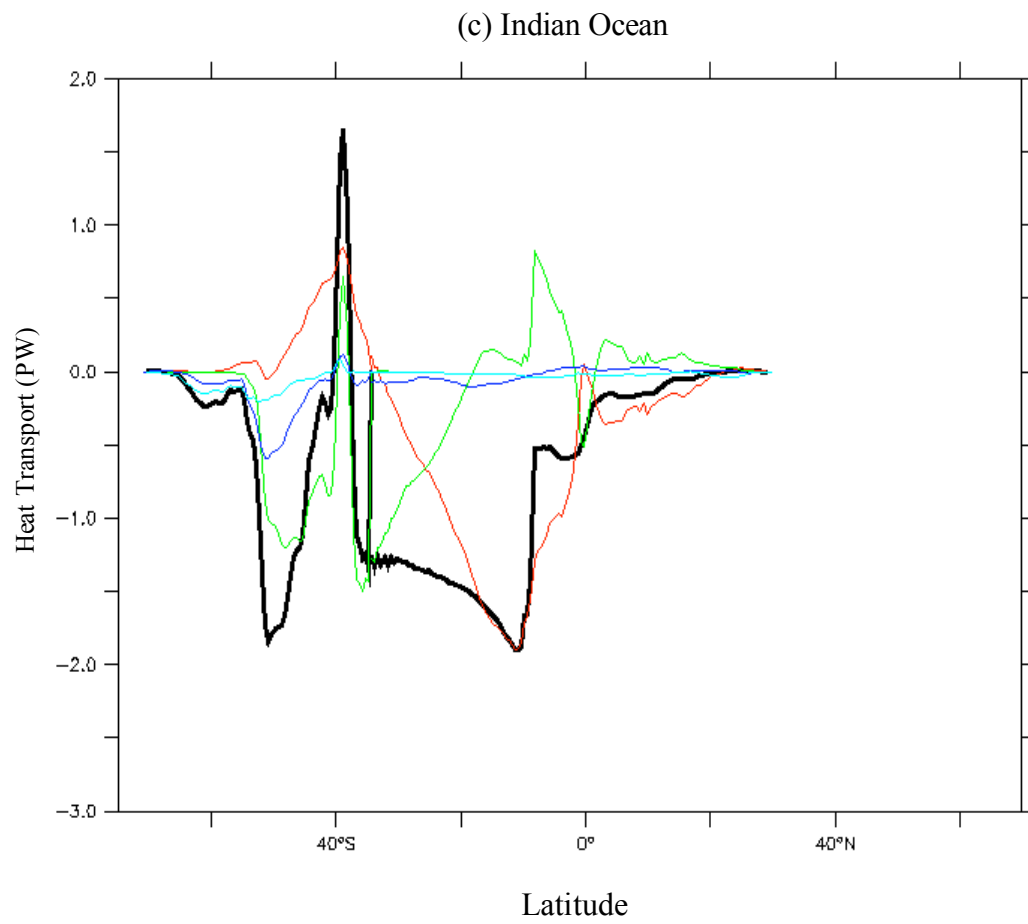


Fig. 3.5 (Continued)

the Atlantic where its peak transport occurs in the subtropical ocean, heat transport in the Pacific is strictly confined to the equatorial regions, and falls off sharply at higher latitude. This could also be due to the large warm water transport into the Indian Ocean through the ITF. The western boundary currents in the Pacific make the largest contribution to the total heat transport, though its magnitude is much smaller than that of the equatorial region. This phenomenon is the result of active processes equatorial dynamics in the Pacific Ocean. Heat transport in wedge-shape around $40^{\circ}S$ in the Atlantic and Indian Oceans can be owing to the influence of the strong eddies. Heat transport in the intermediate and deep layer is generally small as illustrated in Figs. 3.4. As a consequence the total heat transport in the ocean is largely from the contribution of mixed and shallow layer heat transports in the upper 1000m, especially in the tropical oceans. Heat transports in these two layers in the tropics largely counteract together to leaving a small residual heat transport in the ocean. In the extratropical regions, as the heat transport in the mixed layer gets small, heat transport in the shallow layer dominates.

b. OHT in the Mixed Layer of Tropical Atlantic Ocean

Now we turn our attention to ocean heat transport in the mixed layer. Heat transport in the mixed layer is important since it is the uppermost layer in the ocean that interacts with the overlying atmosphere. Many previous studies document the importance of heat transport in the Ekman layer and its contribution to variability of heat transport on the

interannual time scales (e.g., Levitus et al. 1987; Jayne and Marotzke 2001). Ekman flow dominates in the mixed layer, so it is natural to expect a relationship between heat transport in the mixed layer and Ekman current. The meridional Ekman V_{ek} transport in the mixed layer can be derived from the surface zonal wind stress τ_x :

$$V_{ek} = -\frac{\tau_x}{\rho f} \quad (3.1)$$

where ρ is the density of sea water and f is the Coriolis parameter.

Fig. 3.6 shows the normalized time series of meridional heat transport by the total currents and the negative of zonal-averaged zonal wind stress ($-\tau_x$) at $10^\circ N$ in the Atlantic mixed layer. It is apparent that total meridional heat transport in the Atlantic mixed layer is strongly correlated ($r = 0.95$) with local zonal stress. This high correlation between local zonal stress and total meridional heat transport in the mixed layer in the tropical Atlantic Ocean is not unique and can be applied to the entire tropical Atlantic Ocean. This can be seen in Fig. 3.7 though the correlation coefficient becomes relatively small at high latitude. A similar pattern exists in the Pacific and Indian Oceans (not shown).

3.2 Characteristics of Heat Transport Variability

Interannual-decadal variability of meridional ocean heat transport for the Atlantic, Pacific and Indian Oceans is shown in Fig. 3.8. Heat transport variability has a lot in common among three ocean basins. First, variability of oceanic heat transport for three

frequency spectrum of dominant variability between low and mid-latitudes to high ocean basins is highly dependent on latitude. There is a marked distinction in latitudes. At low latitudes, interannual variability dominates, whereas at the middle and high latitudes, decadal or multi-decadal variability is more pronounced. Second, interannual variability of oceanic heat transport at low latitudes is much stronger than at high latitudes. For instance, the interannual variation of ocean heat transport ranges from $-0.6 PW$ to $+0.6$

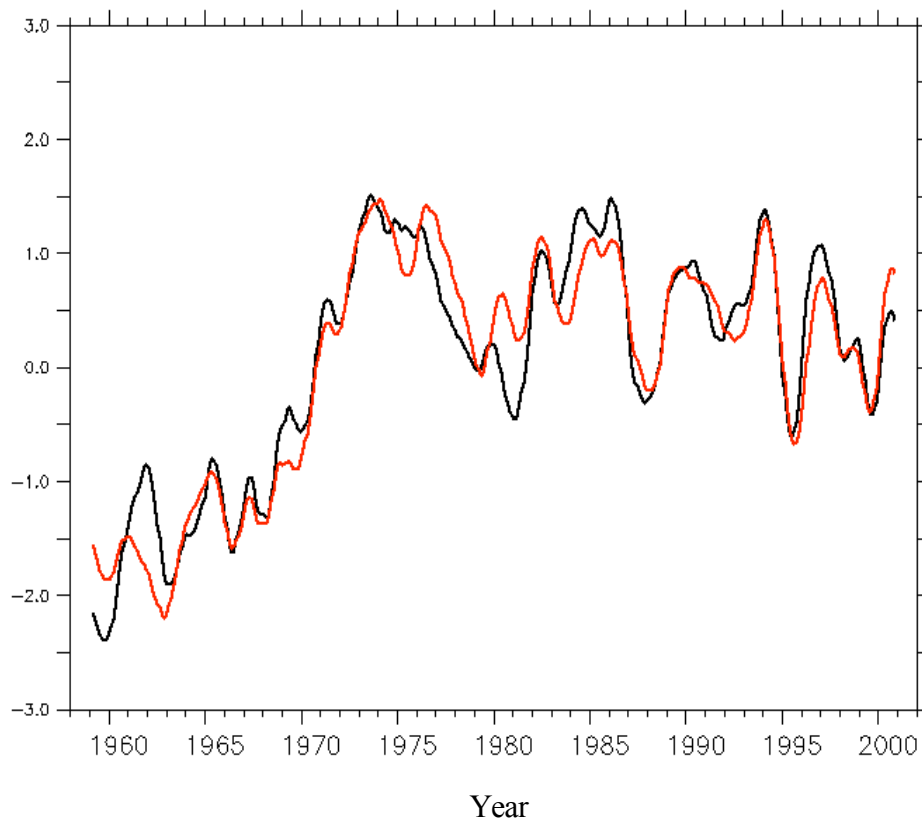


Fig. 3.6 Time series of normalized meridional heat transport (black) and zonal-averaged zonal wind stress (red) at $10^{\circ} N$ in the mixed layer of the Atlantic Ocean. The sign of τ_x has been reversed to ease comparison with heat transport.

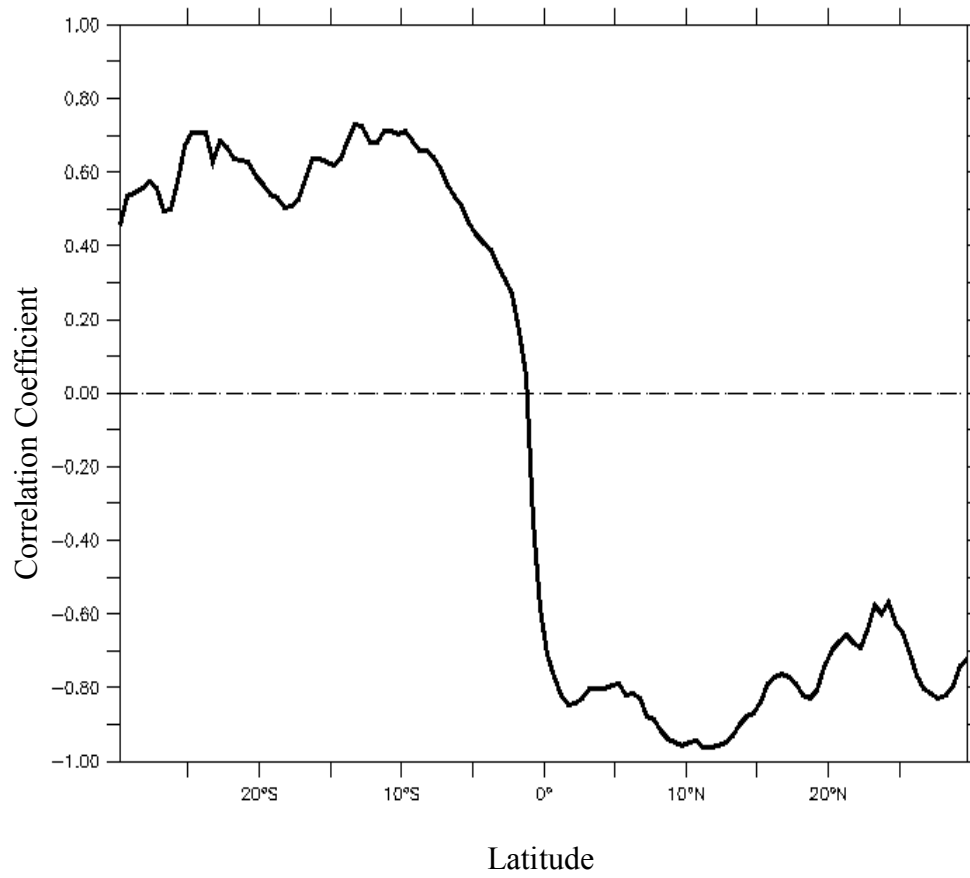


Fig. 3.7 The correlation between meridional heat transport and zonal-averaged zonal wind stress in the mixed layer of the Atlantic Ocean.

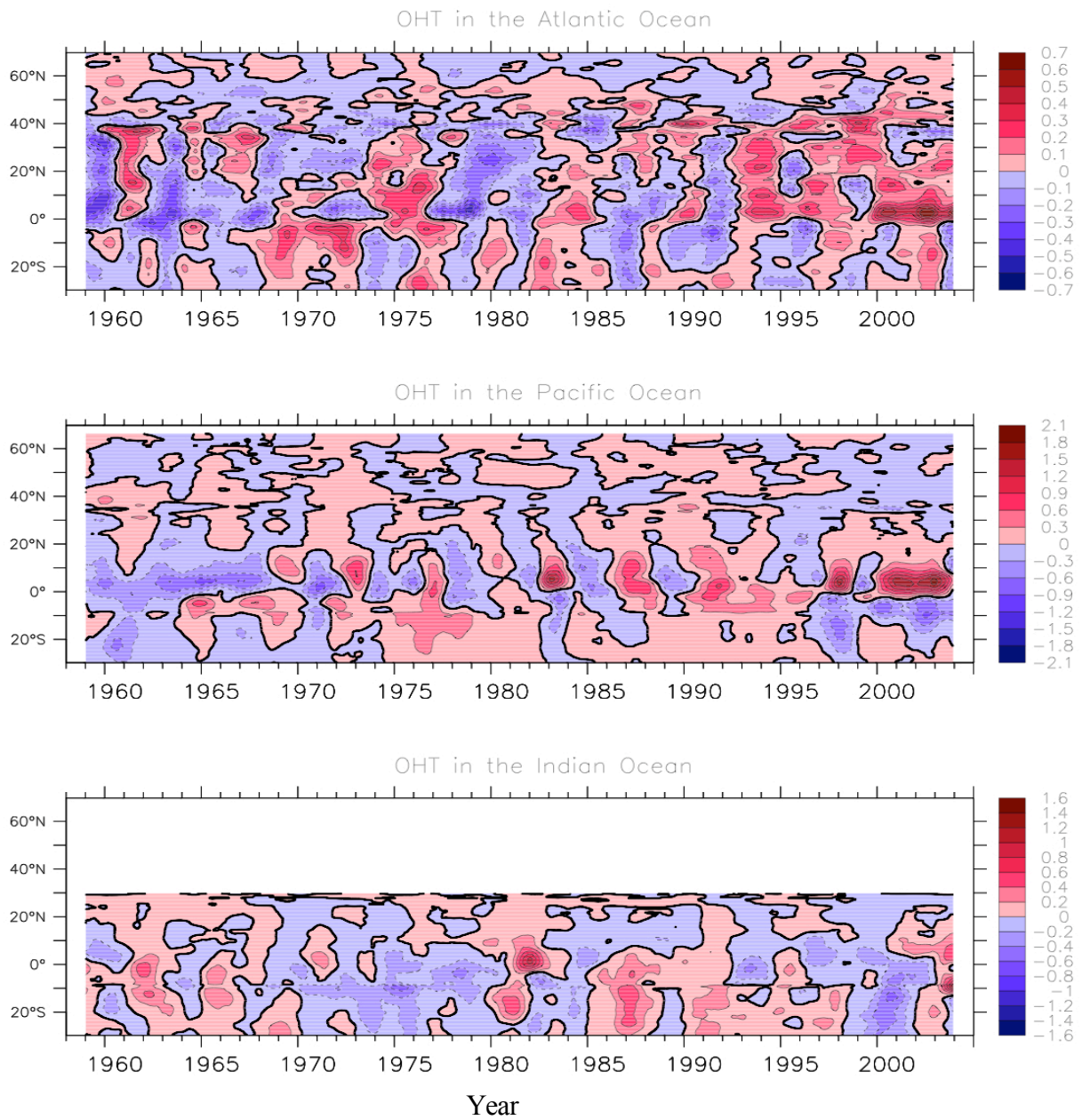


Fig. 3.8 Latitude-time evolution of meridional heat transport anomalies in PW in the Atlantic (top), Pacific (middle), and Indian (bottom) Oceans derived from the reanalysis for the period 1958-2004.

PW in the tropical Atlantic, whereas the decadal variation only varies from $-0.2 PW$ to $+0.2 PW$ in the North Atlantic. Similar behavior is found in the Pacific and Indian Oceans. The resemblance of latitude-dependence of variability of ocean heat transport among the three oceans reflects the coherence of ocean dynamics that is independent of the topography and basin shape but depends on latitudes (i.e., β effect).

It is also evident that there are different aspects of interannual-decadal variability of ocean heat transport among three ocean basins. First, by contrast, the discrepancy between interannual variability in tropical Pacific and decadal or longer variability in North Pacific is much larger than the counterpart of the Atlantic Ocean. In other words, the variability of oceanic heat transport in the Atlantic Ocean becomes weaker gradually. Note that the regions of robust interannual variability can be extended to $40^\circ N$ in the Atlantic Ocean, while in the Pacific Ocean, the strong interannual variability of ocean heat transport is very narrow ($10^\circ S-10^\circ N$) and centered on $5^\circ N$. This behavior in the Pacific might just be the strong El Nino Southern Oscillation (ENSO) signal. Note that the bar scaling for the Atlantic Ocean (top) is smaller than that for the Pacific Ocean (middle), indicating much stronger interannual variability of ocean heat transport in the equatorial Pacific than that in the equatorial Atlantic. The interannual-decadal variability of heat transport in the Indian Ocean is mostly in the south of equator ($30^\circ S-10^\circ N$). Heat transport in the ITF may play a role in the spatial pattern of the variability. For example, the 10-year lasting negative anomalies of the variability of heat transport in $14^\circ S-8^\circ S$ in the 1970's and positive anomalies for the period 1985-1998 are probably due to the anomalous ITF processes.

3.3 Components of OHT

Several mechanisms for heat transport variability have been proposed. Anomalies could arise from the mean advection of temperature anomalies (the $\bar{V}T'$ process)(e.g., Gu and Philander 1997; Change et al. 1997, 2001; Seager et al. 2001) or from anomalous advection of mean temperature (the $V'\bar{T}$ process) (e.g., Schott et al. 2004). In this section, the SODA reanalysis is used to explore the cause of mean heat transport and heat transport anomalies in the global oceans.

3.3.1 Contributions from Components

a. Contributions to Mean OHT

The mechanisms that control the mean heat transport can be illuminated by expanding the equation for heat transport:

$$\langle VT \rangle = \left\langle \left(\bar{V} + V' \right) \left(\bar{T} + T' \right) \right\rangle = \langle \bar{V} \bar{T} \rangle + \langle V' \bar{T} \rangle + \langle \bar{V} T' \rangle + \langle V' T' \rangle = \langle \bar{V} \bar{T} \rangle + \langle V' T' \rangle \quad (3.2)$$

where \bar{V} and \bar{T} are the monthly climatologies of velocity and temperature, and V' and T' are departures from the monthly climatology. Brackets, $\langle \rangle$, denote a long-term average.

Two terms make a contribution to the mean heat transport, which includes seasonal change $\bar{V}\bar{T}$ and the correlation in transient eddies $V'T'$.

Fig. 3.9 shows the fraction that $\bar{V}\bar{T}$ and $V'T'$ make to the total mean heat transport for SODA-1.4.2 and SODA-1.4.0. In both experiments the mean heat transport is predominantly induced by the product of the means. Transient eddy effects play an important role in the mean heat transport in the regions of active eddies, such as in the Gulf Stream extension region in the Atlantic and the Kuroshio extension region in the Pacific. This can be seen in Fig. 3.9 for SODA-1.4.2 where at $40^\circ N$ in the Atlantic eddies account for 40% of mean heat transport. In the Pacific Oceans eddies dominate. Large contribution by $V'T'$ is also present in the equatorial region of the Pacific. The equatorial Pacific has an active instability wave field, and observational studies (e.g., Wang and McPhaden 1999) and modeling studies (e.g., Bryden and Brady 1989; Jayne and Marotzke 2002) show that the instability wave activity can produce a significant contribution to the meridional flux of heat.

b. Contributions to Variability of OHT

To explore the mechanisms responsible for heat transport variability, it is useful to again decompose the heat transport equation. Anomalies of heat transport are generated by three terms:

$$(VT)^a = \left[\left(\bar{V} + V' \right) \left(\bar{T} + T' \right) \right]^a = \left(V' \bar{T} \right)^a + \left(\bar{V} T' \right)^a + \left(V' T' \right)^a \quad (3.3)$$

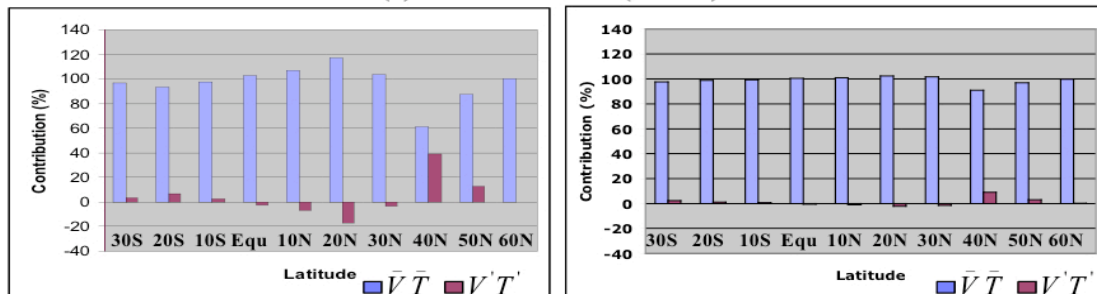
The bracket $()^a$ denotes an anomaly defined as a departure from the long-term mean.

Anomalies of total meridional heat transport in *PW* at $30^\circ N$ Atlantic Ocean are

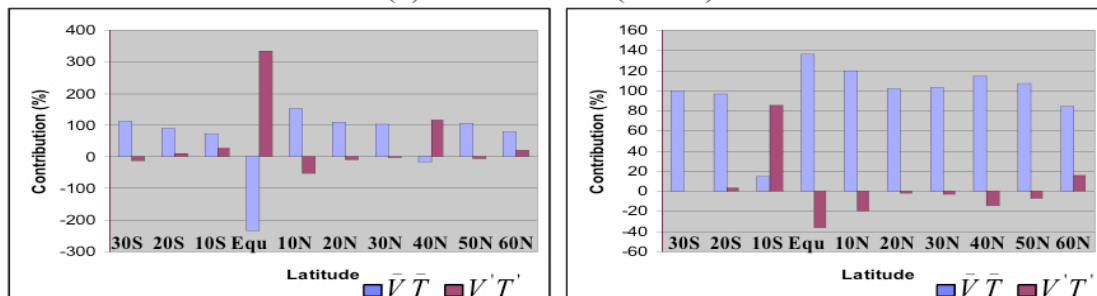
SODA-1.4.2

SODA-1.4.0

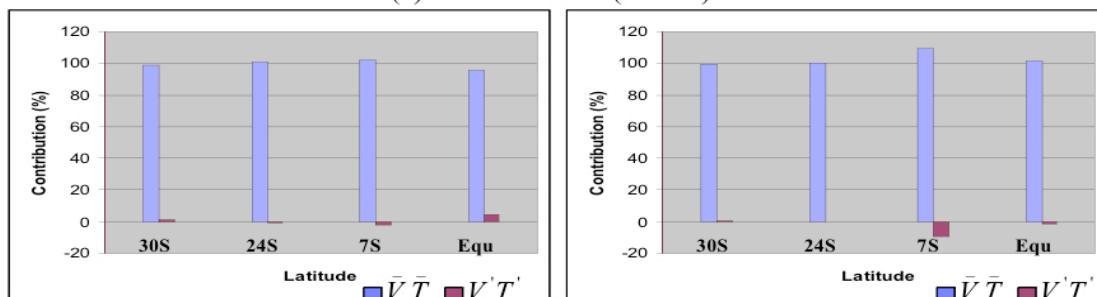
(a). Atlantic Ocean (0-5km)



(b). Pacific Ocean (0-5km)



(c). Indian Ocean (0-5km)



(d). Zonal Heat Transport (0-5km)

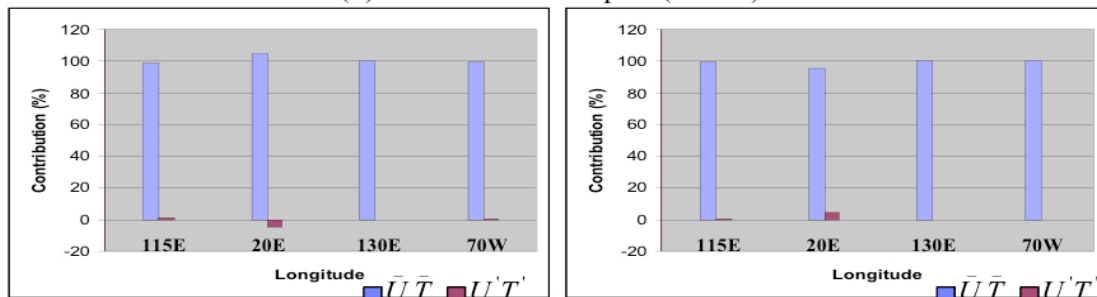


Fig. 3.9 Contributions in percentage from $\bar{V}\bar{T}$ (blue), and $V'T'$ (red) to total mean meridional heat transport in the (a) Atlantic, (b) Pacific, and (c) Indian Oceans for SODA-1.4.2 (left) and SODA-1.4.0 (right). Contributions to zonal heat transports in the ITF and in the Southern Ocean are shown in (d).

shown in Fig. 3.10 together with its three contributing components. $30^{\circ}N$ is chosen as being representative of an mid-ocean basin. The term $(V'\bar{T})^a$ contributes most to anomalies of total meridional heat transport. Next in importance is $(\bar{V}T')^a$, and variations of $(V'T')$ are very small. This implies that variability of total heat transport at $30^{\circ}N$ Atlantic Ocean is predominantly induced by change in ocean currents. Temperature change, at least in this region, is not the most important in generating variability of ocean heat transport.

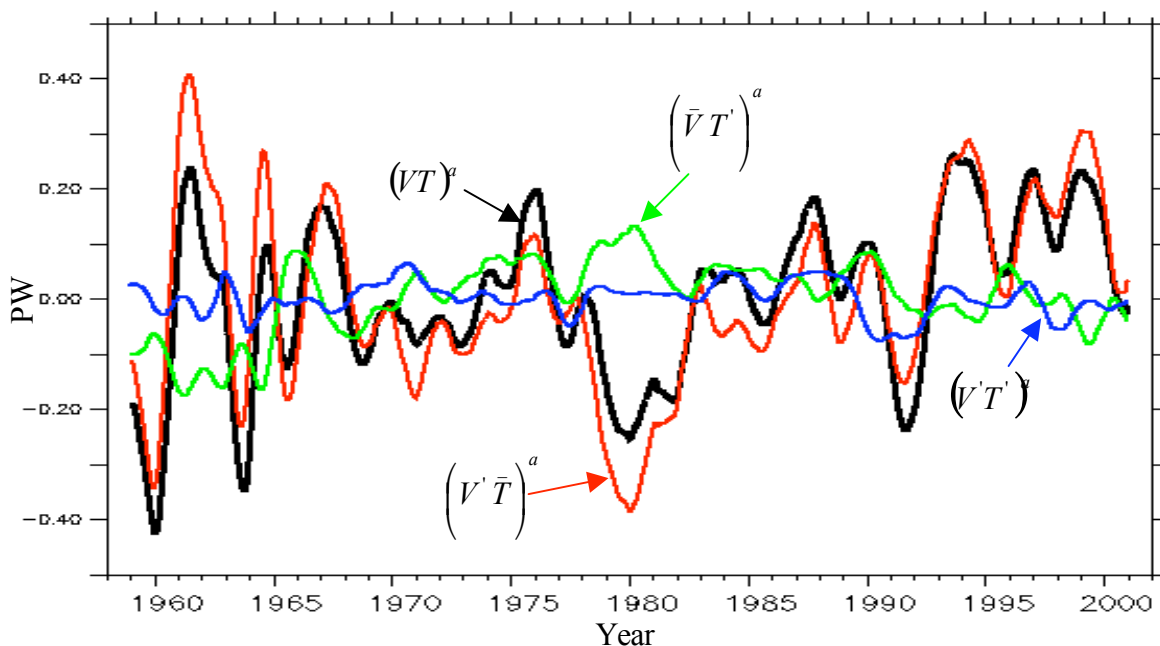


Fig. 3.10 Anomalies of total meridional heat transport in PW at $30^{\circ}N$ in the Atlantic Ocean (black) from SODA-1.4.2. Three contributing components are shown: red shows the contribution from $V'\bar{T}$; green indicates the contribution from $\bar{V}T'$; blue shows the contribution from $V'T'$.

In order to examine whether changes in current velocity is a universal factor in producing variability of ocean heat transport in the global oceans, we evaluate the contributions from the three terms to total heat transport variability at several locations. We calculate the percentage of variance explained by each of the three terms from Eq. 3.3 in 10° bins in each of the ocean basins. The contribution in percentage from $V'\bar{T}$, $\bar{V}T'$, and $V'T'$ to the total meridional heat transport anomalies is shown in Fig. 3.11 for the Atlantic, Pacific, and Indian Oceans. Results for both SODA-1.4.2 and SODA-1.4.0 are presented. The term $V'\bar{T}$ accounts for the greatest contribution to variability of the total meridional heat transport for most regions in the Atlantic, Pacific, and Indian Oceans in both SODA-1.4.2 and SODA-1.4.0. However there are some notable exceptions. The similarity between SODA-1.4.2 and SODA-1.4.0 suggests that intrinsic ocean dynamics (i.e., ocean circulation) that governs variability of meridional heat transport and that this variability is captured by the model without assimilation. Assimilation improves the estimates of ocean heat transport, however the assimilation model does not change the inherent processes responsible for variability of ocean heat transport. Exceptions to the dominance of $V'\bar{T}$ is evident. In the North Pacific and Atlantic Oceans $\bar{V}T'$ becomes important. For example, at $60^\circ N$ in the Atlantic $\bar{V}T'$ is more important than $V'\bar{T}$ in SODA-1.4.2. Hence, combined with measurements of temperature and salinity, an assimilation model can effectively correct a modeled ocean circulation into a more realistic one and thus improve modeled ocean circulation. Eddies

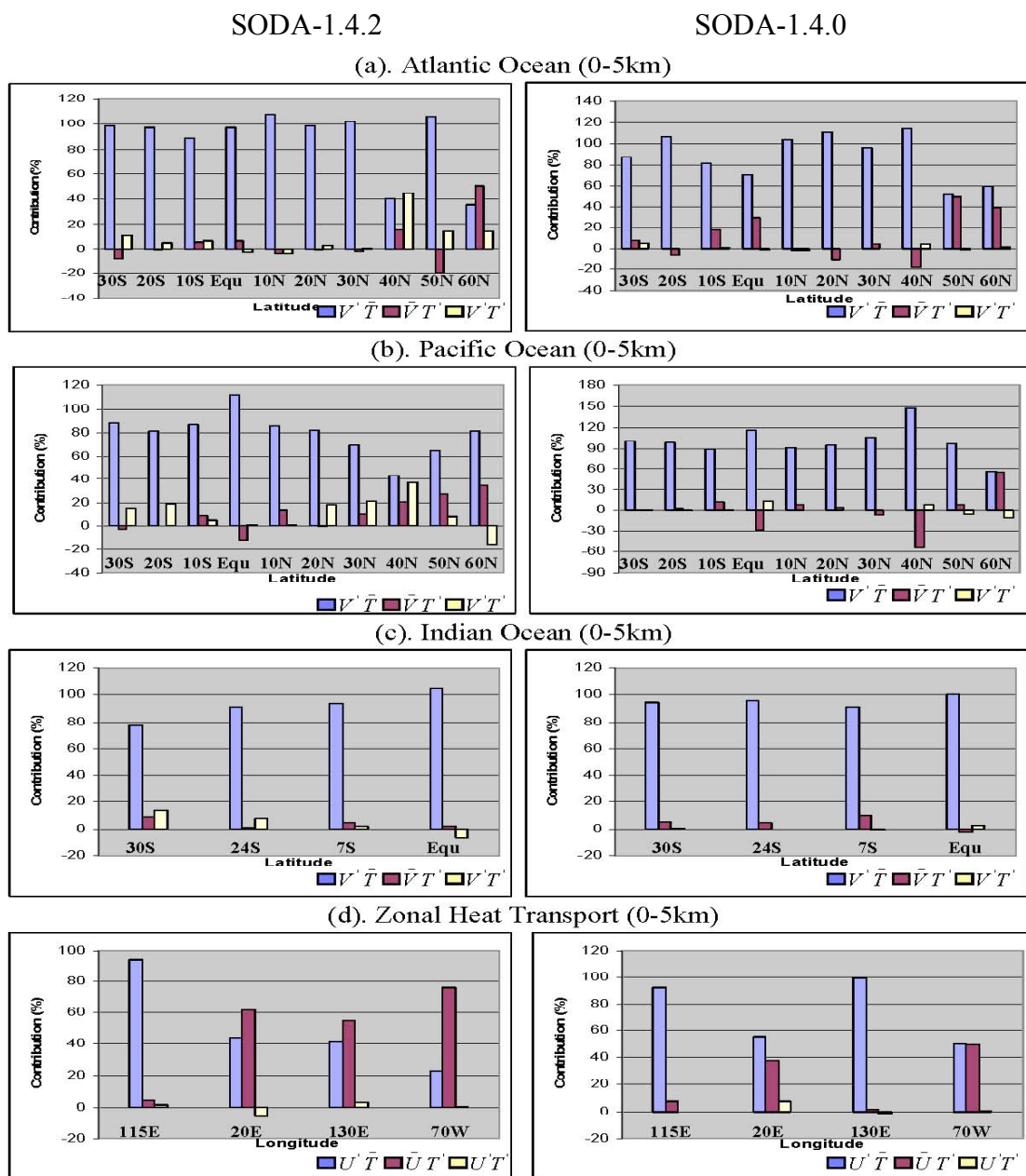


Fig. 3.11 Contributions in percentage of $V'\bar{T}$ (blue), $\bar{V}'T'$ (red), and $V'T'$ (yellow) to total meridional heat transport anomalies VT in the (a) Atlantic, (b) Pacific, and (c) Indian Oceans for SODA-1.4.2 (left) and SODA-1.4.0 (right). Contributions to zonal heat transports in the ITF and in the Southern Ocean are in the bottom panel.

become important in the regions of the Gulf Stream extension region in the Atlantic and the Kuroshio and Kuroshio extension region of the Pacific Ocean. The overall effect of ocean current velocity is the dominant factor that controls variability of meridional heat transport. Variability of zonal heat transport in the ITF ($115^{\circ}E$) is also predominantly controlled by the strength of currents. Because the ITF connects the tropical Pacific with the Indian Ocean, heat transport variability in these basins is determined by $V'T$, it is reasonable that heat transport variability between the basins is also determined by $V'T$. In contrast with the ITF, heat transport in the Southern Ocean has an important contribution from $\bar{V}T'$. In fact at $20^{\circ}E$, $130^{\circ}E$, and $70^{\circ}W$ $\bar{V}T'$ becomes the dominant term in SODA-1.4.2. The discrepancy in controlling the variability of zonal heat transport in the ITF and in the Southern Ocean suggests that there are different underlying mechanisms for the variability of heat transport in the ocean basins (i.e., the Atlantic, Pacific, and Indian Oceans) and in the Southern Ocean.

3.3.2 Factors Affecting OHT

It is clear that heat transport variability is determined by current variability. Further understanding can be gained by explaining the contribution from different current structures. Geostrophic flow results from the balance between the pressure gradient force and the Coriolis force and Ekman flow results from a balance between wind stress, friction and the Coriolis force. In addition to these horizontal currents, in certain regions

vertical motion in the ocean can be important. Several processes are responsible for vertical motion in the ocean. For example, buoyancy, upwelling (downwelling) due to divergence (convergence) of ocean water, convection and mixing can induce vertical motion.

a. Contributions to Mean OHT

The Ekman and geostrophic contributions to mean heat transport in the Atlantic, the Pacific and the Indian Oceans are shown in Fig. 3.12. The residual which represents the total minus the Ekman and geostrophic components is also shown. For the purpose of comparison, the total mean and linear change in heat transport are shown by a solid black curve. The total mean heat transport is primarily induced by Ekman currents and geostrophic currents. Interestingly, Ekman currents play a role in heat transport that is opposite to that of geostrophic currents. Value near $25^{\circ}N$ in the Atlantic Ocean is most likely due to the difficulties in the accurate estimate of geostrophic currents near the Gulf of Mexico. Similarly, the “spike” at $10^{\circ}N$ in the Pacific and Indian Oceans is probably due to the influence of the Indonesian archipelagoes that affects the estimate of geostrophic currents.

The partitioning method of mean heat transport described in section 3.1a does not differentiate between Ekman currents and geostrophic currents in the role of heat transport variability. The fractional contribution of geostrophic, Ekman flow, and the residual contributions to the mean heat transport in the Atlantic and Pacific Oceans are

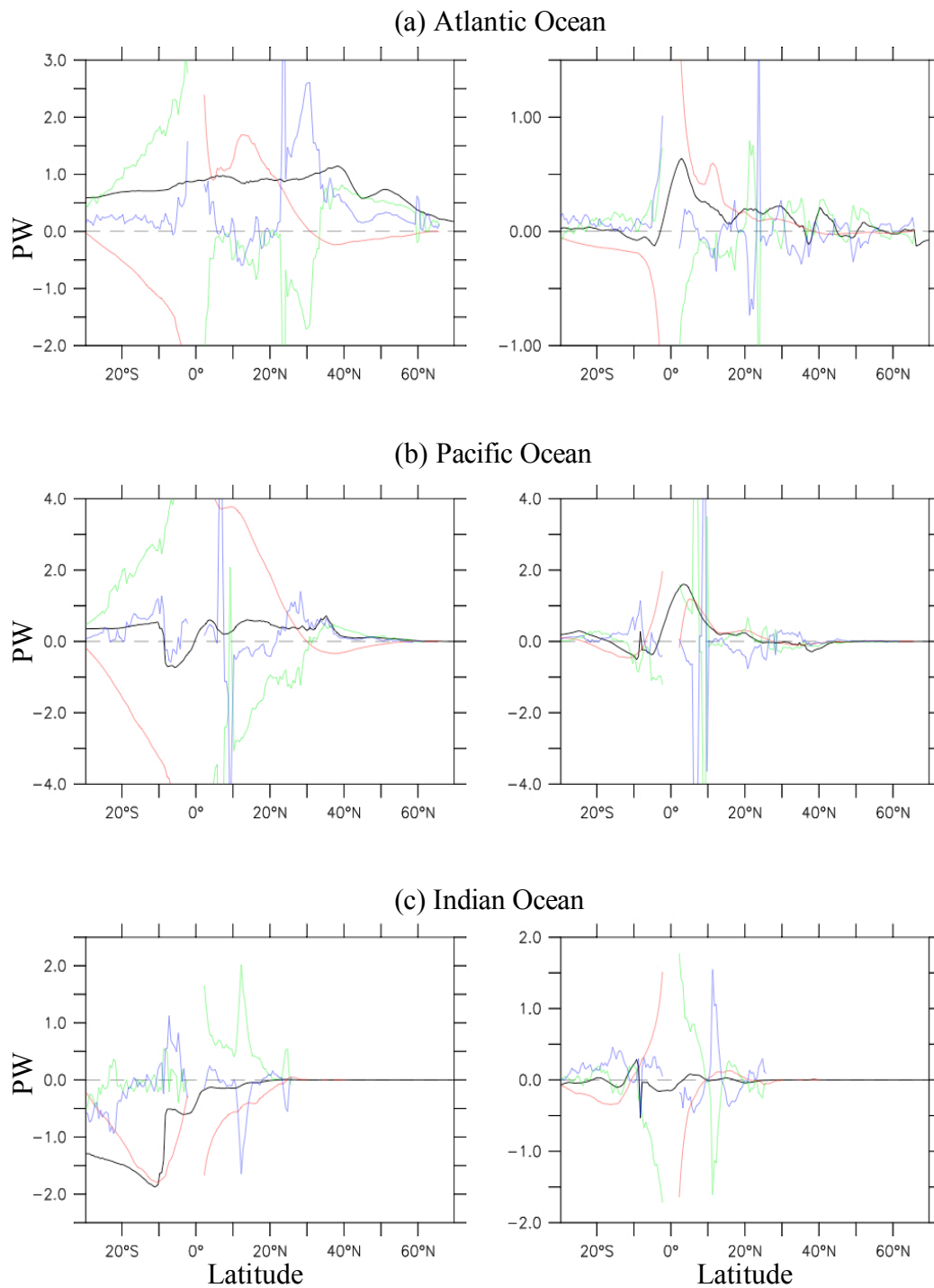


Fig. 3.12 Mean (left) and linear change (right) in the total meridional heat transport (black), transport of heat due to Ekman currents (red) and geostrophic currents (green) and the residual (blue) over the (a) Atlantic, (b) Pacific, and (c) Indian Oceans for the period 1958-2001.

shown in Fig. 3.13 for SODA-1.4.2 and SODA-1.4.0. In the tropical Atlantic and Pacific Oceans poleward heat transport by Ekman flow is largely compensated by equatorward heat transport induced by geostrophic flow. In the mid-to high latitudes poleward heat transport by geostrophic flow and the residual processes is generally compensated by equatorward heat transport due to Ekman processes. At high latitudes, the residual processes become more important. These features are present in both SODA-1.4.2 and SODA-1.4.0, which suggests that the mean heat transport is determined by the intrinsic oceanic dynamics.

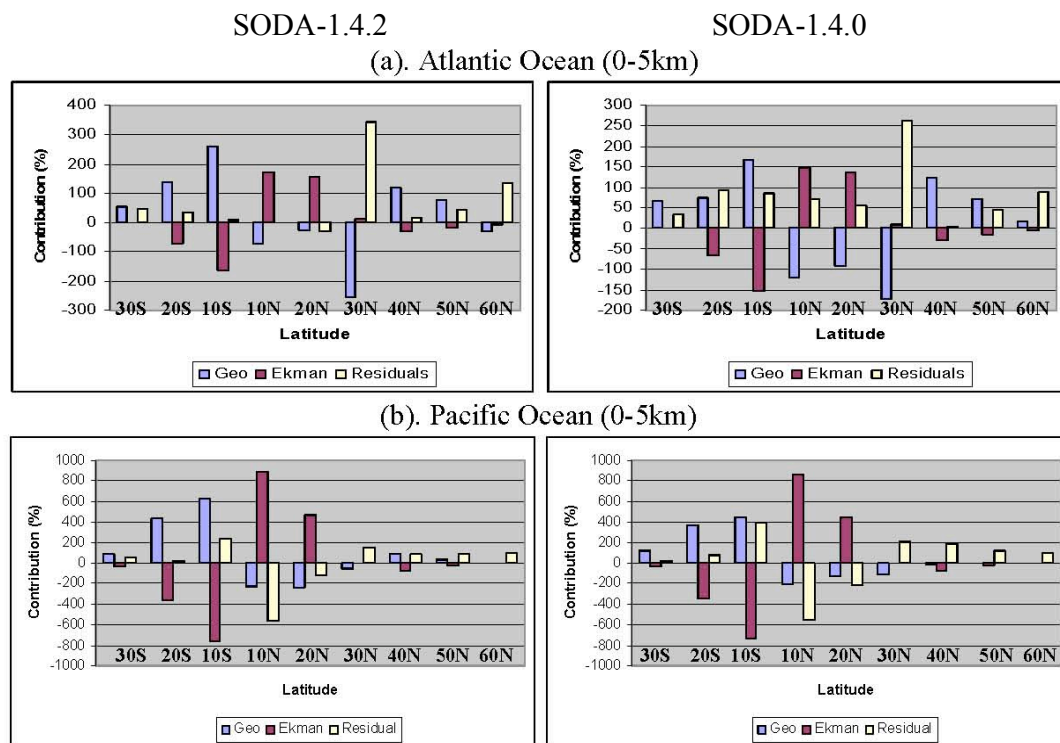


Fig. 3.13 Contribution in percentage from geostrophic (blue), Ekman currents (red), and the residual term (yellow) to total mean meridional heat transport in the (a) Atlantic, and (b) Pacific Oceans for SODA-1.4.2 (left) and SODA-1.4.0 (right).

b. Contributions to Variability of OHT

The same analysis can be applied to understand how geostrophic, Ekman flow and other processes make contributions to variability of heat transport. To this end, a contribution of heat transport due to these flows to the total varying heat transport is defined by replacing the components in Eqs. (3.3) by those due to geostrophic flow and Ekman flow, and residual processes. Fig. 3.14 shows the fractional contribution of geostrophic and Ekman flows, and the residual in percentage to the meridional heat transport on interannual-decadal time scales in the Atlantic and Pacific Oceans for SODA-1.4.2 and SODA-1.4.0. Role of geostrophy in variability of heat transport is more important in the South Atlantic and the South Pacific in both SODA-1.4.2 and SODA-1.4.0. In SODA-1.4.2, tropical Atlantic heat transport due to geostrophic and Ekman flows is pronounced in the south Atlantic, and geostrophic flow dominates variability of ocean heat transport. In the mid- and high latitudes, Ekman processes become less important and the residual and geostrophic flow dominate variability of ocean heat transport. Geostrophic flow is more important in SODA-1.4.2 than in SODA-1.4.0 in the tropical Atlantic.

Similar to the case in the Atlantic, the influence of geostrophic flow on varying heat transport in the tropical Pacific is enhanced by inclusion of observations, and the role of Ekman process reduces proportionally. Note that the residual is important in the North Atlantic and Pacific Oceans. The residual is complex and includes any dynamical forces other than geostrophic flow and Ekman flow. A change in buoyancy flux can explain

why the residual is important at high latitudes. It is possible that changes in western boundary currents, and strength of Gulf Stream in the Atlantic and of Kuroshio and its extension in the Pacific may explain why the residual is large in the assimilation run. ITF, an example of the influence of topography, can be a possible cause for why the residual is important in the Tropical Pacific ($10^{\circ} S - 20^{\circ} N$).

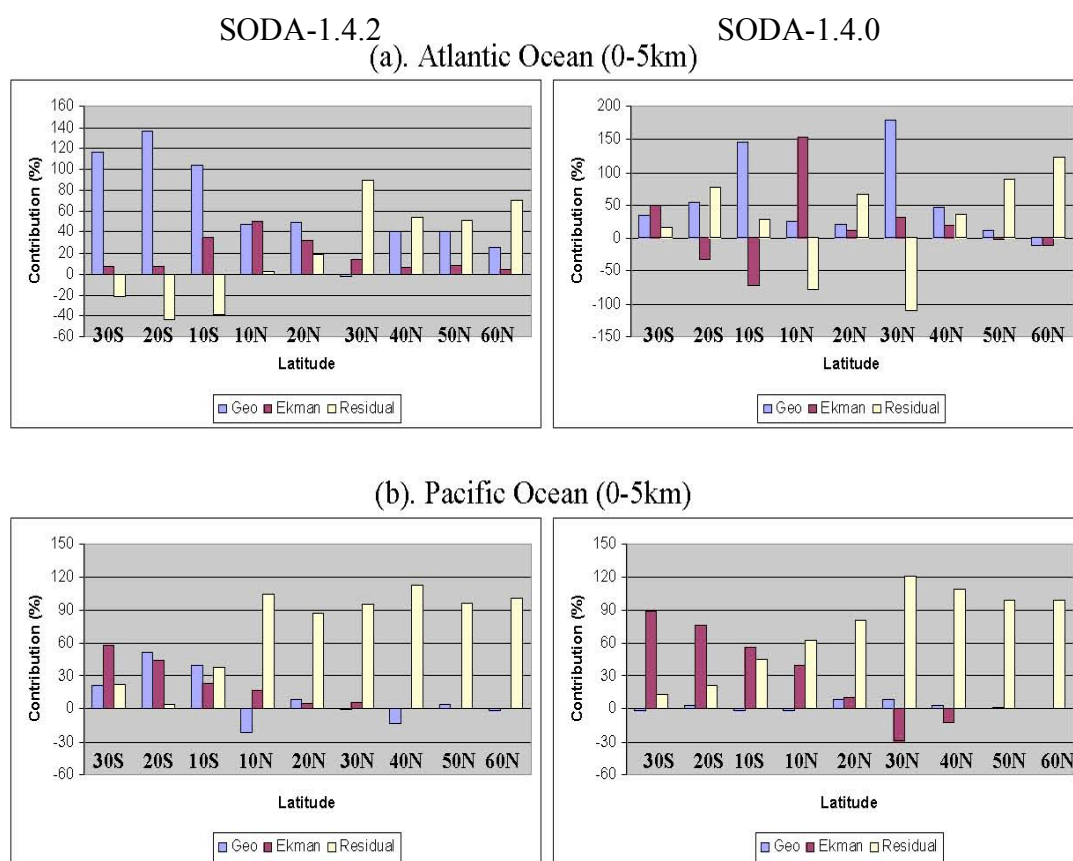


Fig. 3.14 Contribution in percentage from geostrophic (blue), and Ekman currents (red) and the residual term (yellow) to the interannual-decadal variability of meridional heat transport in the (a) Atlantic, and (b) Pacific Oceans for SODA-1.4.2 (left) and SODA-1.4.0 (right).

CHAPTER IV
THE NORTH ATLANTIC OCEAN HEAT BUDGET

4.1 Changes in Ocean Heat Content

A change in the meridional transport of heat can either warm the ocean or release heat out of the ocean into the atmosphere. Thus to understand the climate impact of heat transport variability it is important to account for changes in ocean heat content. A change in heat content for the upper 3000 m of world's ocean has been reported by Levitus et al. (2000, 2001, 2005) based on abundant ocean temperature records. Because SODA uses the same set of observations, but is constrained by ocean physics, SODA can also provide an estimate of variability of ocean heat. Heat content in the ocean is computed by

$$HC = \iiint \rho C_p T dx dy dz \quad (4.1)$$

World ocean heat content for the period 1958 -2004 is plotted in Fig. 4.1. There is an obvious increase over the 47 years period with a linear trend of $3.10 \times 10^{22} J \cdot decade^{-1}$. This trend represents a linear increase in heat content of about $14.9 \times 10^{22} J$, which corresponds to a mean heating rate of $0.19 W \cdot m^{-2}$ (per unit area of Earth's total surface area). This heating rate of change is consistent with the results of Levitus et al. (2005), which are reproduced in Fig. 4.1b.

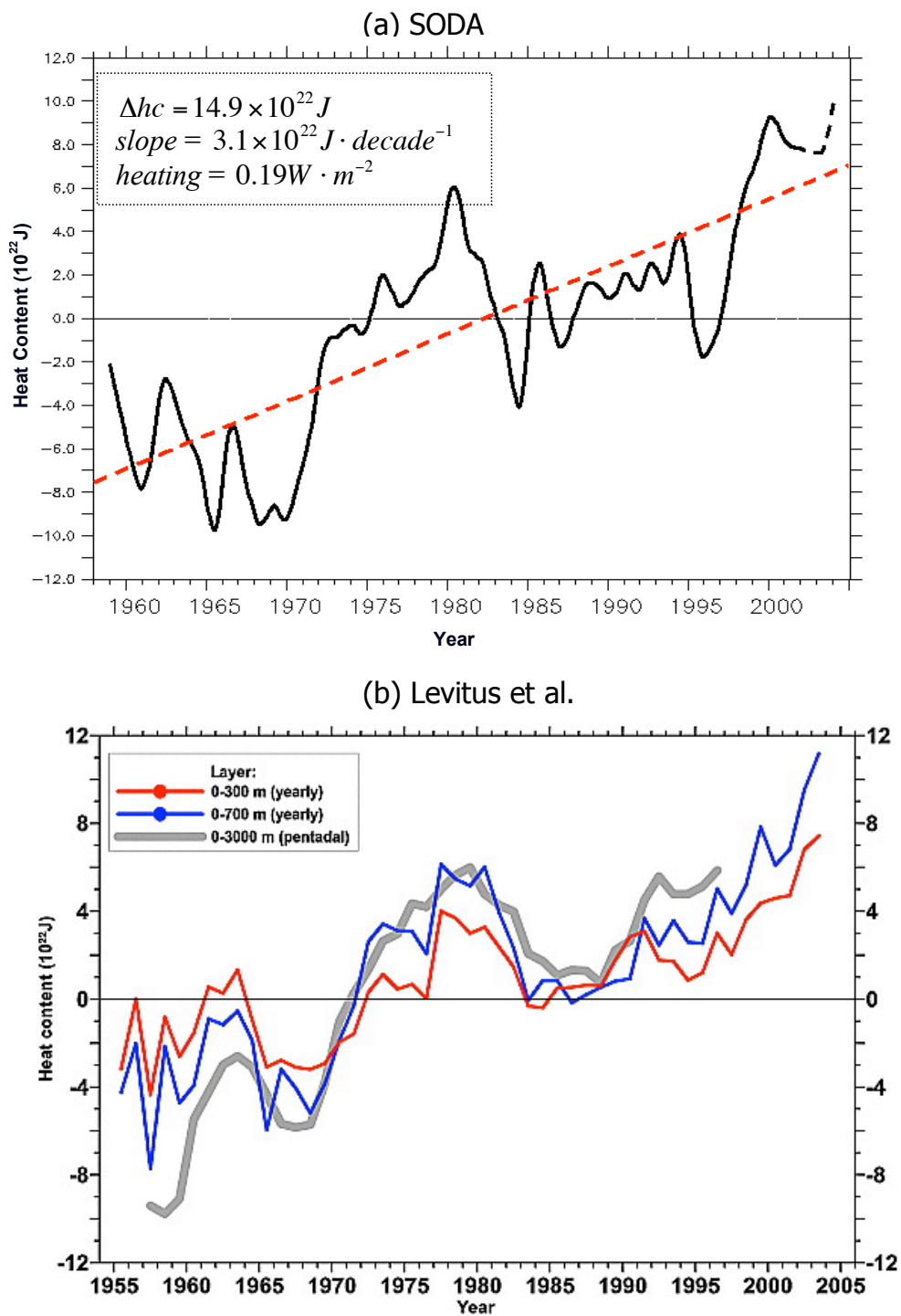


Fig. 4.1 Time series and the corresponding trend of world ocean heat content integrated from surface to bottom (10^{22} J) for the period 1958 – 2004 from (a) SODA-1.4.2 and (b) from Levitus et al. (2005).

4.2 Ocean Heat Budget

4.2.1 Heat Equation

The diffusion of heat in the oceans is generally believed to be small (e.g., Chirokova and Webster 2006); therefore the ocean heat budget can be represented by the equation

$$\frac{\partial HC}{\partial t} + \nabla \cdot (VT) = Q \quad (4.2)$$

where Q is the surface heat flux. The first term on the left hand side of Eq. (4.2) is the heat storage rate. Because of the high heat capacity of water, variability in heat storage rate may potentially play a role in climate change. The second term on the left hand side represents the divergence of heat transport by ocean currents. This term is determined by variability in either ocean currents or temperature fields or both. The ocean surface heat flux in this study is derived as a residual term in the Eq. (4.2).

4.2.2 Change in World Ocean Heat Storage Rate

The temporal variability of heat storage rate is needed to construct a heat budget. Fig. 4.2 shows the robust variability of world's ocean heat storage rate. There is a linear trend of $0.008W \cdot m^{-2} \cdot decade^{-1}$ in heat storage rate, though this change is not significant relative to the global ocean heat content. This linear trend explains 3.3% of the total variance and represents a 16% increase of heat storage rate from 1958 to 2003. Note that

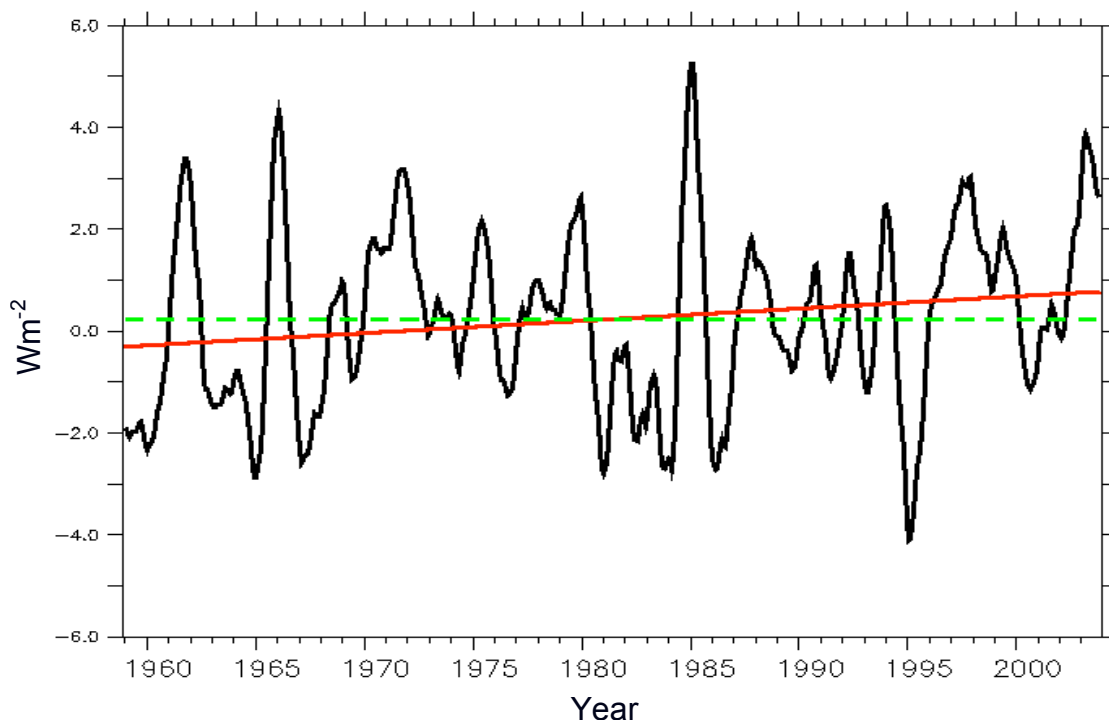


Fig. 4.2 Time series of world ocean heat storage rate ($W \cdot m^{-2}$) for the period 1958 – 2003 from SODA-1.4.2.

a mean heating rate of $0.236 W \cdot m^{-2}$ averaged over the four decades of SODA-1.4.2 is slightly different from that derived from the linear change of ocean heat content, which is $0.19 W \cdot m^{-2}$. The slight difference between the two can be explained by the fact that the linear change of global ocean heat content explains 66% of the total variance. The increase of heat storage rate in the global ocean would have warmed up the overlying atmosphere if the heat accumulated in the oceans during the warming period would be released.

4.2.3 Mean and Standard Deviation

Divergence of ocean heat transport is potentially important in ocean heat budget for regional climate. The mean and standard deviation of divergence of ocean heat transport, heat storage rate and implied net heat flux in each 10° bin of the global ocean is shown in Fig. 4.3. In all sections of the global oceans the heat storage rate is small, and as a consequence there is a balance between heat divergence and surface heat flux (i.e., $\nabla \cdot (VT) \approx Q$ in Eq. (4.2) since $\frac{\partial HC}{\partial t}$ is relatively small for long-term mean). However, heat storage rate does have robust variability which is comparable to that of the divergence of ocean heat transport. This suggests that at some time scales, heat storage rate plays an important role in the heat budget. This conclusion is supported in the Atlantic Ocean heat budget analysis in the following section.

4.2.4 Heat Budget in the North Atlantic Ocean

Since the Atlantic Ocean contributes most to the increase of world ocean heat content (Levitus et al. 2000, 005), we next focus on changes in heat content of the North Atlantic Ocean in SODA-1.4.2. Heat content in the region north of $26.75^\circ N$ of the North Atlantic Ocean for the period 1958-2003 is shown in Fig. 4.4. An increase of heat content, with a minimum during early 1963 to a maximum in late 1999, in the North Atlantic Ocean is clearly seen. Note that this increase is not continuous since there is no apparent trend during the period 1965-1995. However there appears a remarkable

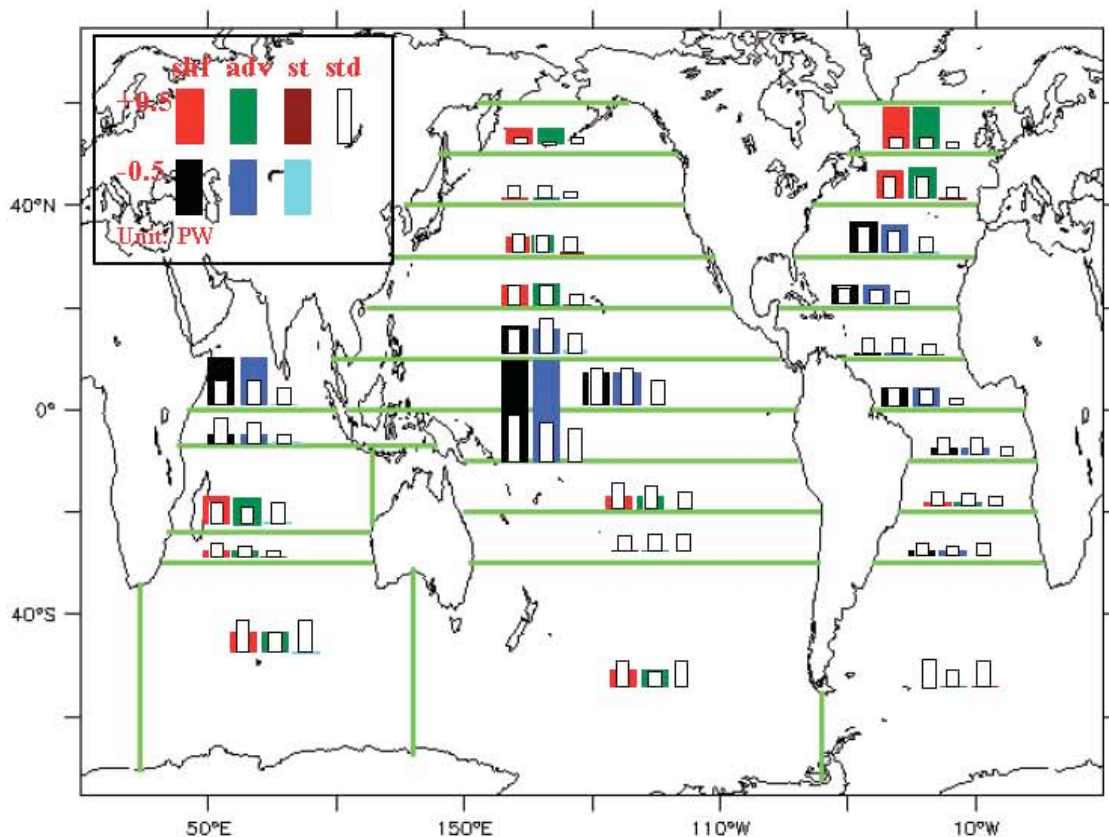


Fig. 4.3 Mean and standard deviation in PW of the mean divergence of heat transport (adv) and mean heat storage rate (st) in regions of world oceans from SODA-1.4.2 based on the period 1958-2001. Surface heat flux (shf) is calculated as a residual of the other terms.

increase for the period from 1995-2000. After 1999, a slight cooling of the North Atlantic Ocean occurs. Nevertheless, taken over the decades, the North Atlantic Ocean warmed at a rate of $0.51 \times 10^{22} J \cdot decade^{-1}$.

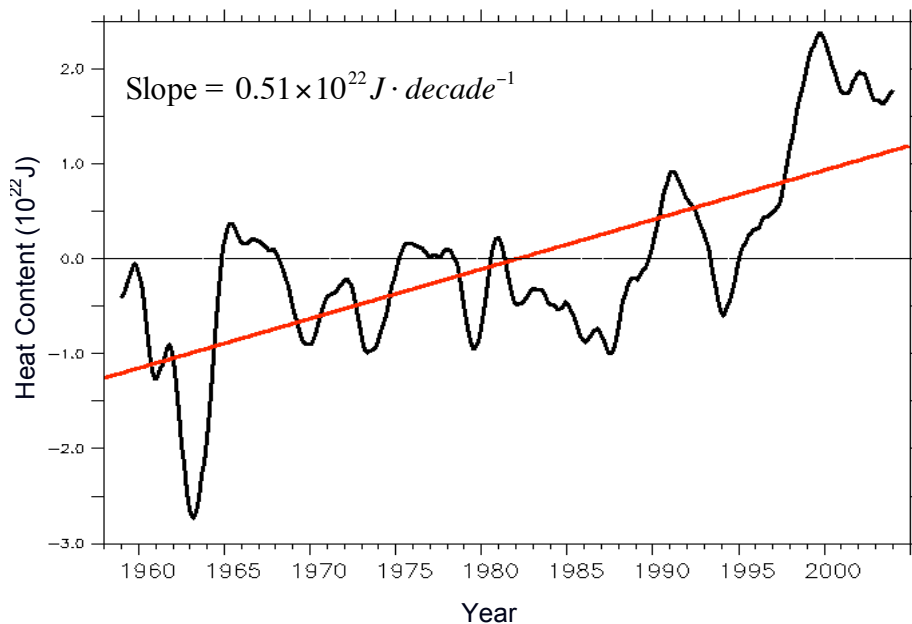


Fig. 4.4 Heat content (10^{22} J) in the region north of $26.75^{\circ}N$ in the North Atlantic Ocean for the period 1958 -2003.

Is warming of the North Atlantic Ocean critically important to change of heat exchange between the ocean and the atmosphere? Using the reanalysis allows us to directly evaluate the importance of the change of heat transport as compared to the increase of ocean heat content in air-sea exchange. The two terms on the left hand side of Eq. (4.2), averaged over the surface of North Atlantic Ocean are shown as time series in $W \cdot m^{-2}$ in Fig. 4.5 from 1958 to 2003. Also shown in Fig. 4.5 is the residual between the heat storage rate and convergence of heat transport, which is interpreted as the surface

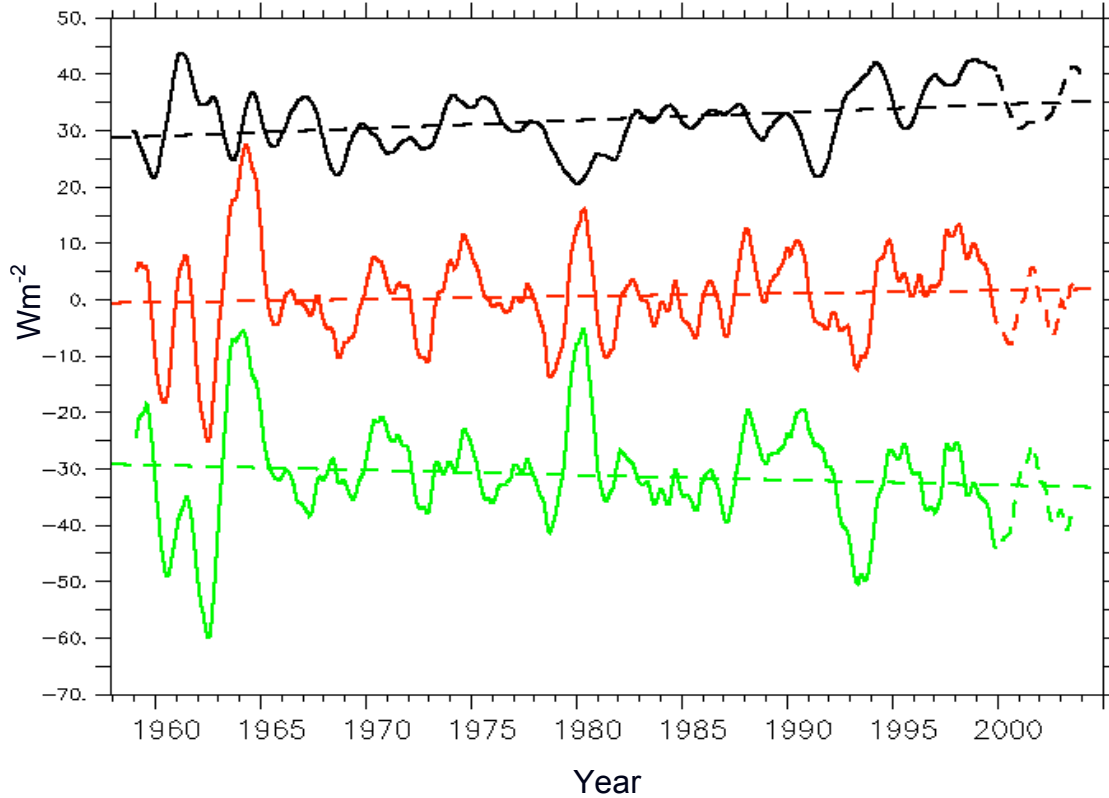


Fig. 4.5 Time series of convergence of heat transport (black), heat storage rate (red), and surface heat flux (green) in $W \cdot m^{-2}$ and its corresponding trends in $W \cdot m^{-2} \cdot decade^{-1}$ in the North Atlantic Ocean.

heat flux between the ocean and the atmosphere. These two terms are distinctively different from each other, and taken together describe an interesting feature of the North Atlantic Ocean heat budget. First, variability of heat storage rate is much larger than that of convergence of heat transport. There are prominent fluctuations of heat storage rate on

interannual time scales that are not nearly as large in the convergence of heat due to ocean currents. The implication of this is that on interannual time scales, variations in air-sea exchange of heat is largely determined by regional changes of heat content, which to some degree determines the persistence of sea surface temperature (SST) anomalies. One of the most intriguing features of the heat content record, however, is that the trend of heat storage rate is not large and is equivalent to a rate of $0.5W \cdot m^{-2} \cdot decade^{-1}$. In contrast, the convergence of heat transport by ocean currents has increased at a rate of $1.4W \cdot m^{-2} \cdot decade^{-1}$, a factor of 3 larger than the change in heat storage rate. To conserve heat, the change in heat storage rate and convergence of heat transport must be balanced by a surface heat flux into the atmosphere. Thus, the change in the implied surface heat flux into the overlying atmosphere is increasing at a rate of $0.9W \cdot m^{-2} \cdot decade^{-1}$. As discussed in Chapter III, it is the change in the strength of ocean circulation that leads to a change of heat transport, therefore the increased heat flux from the ocean into the atmosphere may come from a change in the Atlantic Ocean circulation if the divergence of heat transport is determined by the strength of ocean circulation.

CHAPTER V

CLIMATE MECHANISMS FOR OCEAN HEAT TRANSPORT

5.1 Background

The oceans play an important role in maintaining and regulating Earth's climate through the transport of heat from low latitudes to high latitudes. Thus a change in oceanic heat transport may induce climate change (Covey and Thompson 1989; Manabe and Stouffer 1995). Fluctuations in ocean heat transport can arise from two major sources: internal ocean processes and oceanic response to atmospheric fluctuations. An example of the latter is when ocean circulation changes in response to wind stress variations. In recent years, the impact of anthropogenic forcing has been drawn attention as a source of ocean heat transport variability, particularly in the Atlantic Ocean through change of the Atlantic MOC. In the region north of $30^{\circ}N$, the Atlantic MOC dominates global ocean heat transport (Ganachaud and Wunsch 2003). Observational studies of the Atlantic Ocean (Dickson et al. 1996; Curry and McCartney 2001) reveal that fluctuations in thermohaline circulation is a key to understanding climate change on decadal time scales, and these fluctuations arise in part from the response to the fluctuations in the North Atlantic Oscillation (NAO) (Walker 1924; Hurrell 1995). These conclusions are supported by modeling studies (Hakkinen 1999; Eden and Willebrand 2001; Dong and Sutton 2001).

Numerous modeling studies have identified mechanisms linking North Atlantic salinity distributions to changes in the strength of the Atlantic MOC (Rahmstorf 1996; Marotzke 2000; Wu et al. 2004). The predominant notion is that the Atlantic MOC will slow down in response to greenhouse warming. However, Wu et al. (2004) use an ensemble of four coupled model simulations with both natural and anthropogenic forcing to study change in the Atlantic MOC. Their model reproduces the high-latitude freshening, trace its source to the melting of Arctic sea ice and increased river runoff. Interestingly, they found a slightly enhanced MOC.

In fact, observations reveal that a large region of the North Atlantic Ocean has been growing fresher since the late 1960s when melting glaciers and increased precipitation due to the effect of greenhouse warming, have accelerated continental runoff into the Arctic and sub-Arctic seas. Over the same period, salinity records indicate that large pulses of extra sea ice and fresh water from the Arctic have flowed into the North Atlantic Ocean. Until recently, the actual amounts and rates of fresh water accumulation have not been explicitly known. Curry and Mauritzen (2005) report that changes in salinity in the high-latitude North Atlantic Ocean have not affected the Atlantic MOC yet. Despite the steadily declining salinity in the Nordic Seas Overflow Waters (NSOW), there are no sustained changes monitored in freshwater export to the subpolar region of the North Atlantic Ocean from the Nordic Seas. However, because of the long lead time for feedback in the climate system, continued freshening can affect the ocean conveyor in the next two centuries. Most recently, Peterson et al. (2006) suggest that freshwater may now be accumulating in the Arctic Ocean which will likely be exported southward

to the North Atlantic Ocean if and when the North Atlantic Oscillation (NAO) enters into a new positive phase. Latif et al. (2006) suggest that change in the thermohaline circulation during the last century was likely the result of natural multidecadal climate variability driven by low frequency variations of the NAO via changes in Labrador Sea convection.

Sinking of cold surface waters that become deep-water masses occurs in the subpolar regions of the Atlantic Ocean. In the North Atlantic, the major sinking of surface water is believed to occur in the Norwegian Sea. From there it flows as a subsurface current into the North Atlantic, where it becomes part of North Atlantic Deep Water (NADW). Another source of deep water is from the margins of the Irminger Sea off southeastern Greenland and Labrador Sea. In the Southern subpolar latitudes, the most significant area where deep-water masses form is the Weddell Sea, where rapid winter freezing produces salt-laden high-density water that sinks down the continental slope of Antarctica and becomes Antarctic Bottom Water (ABW), which is the densest water in the open ocean. On a broad scale, some surface water masses converge/diverge, which may cause downwelling/upwelling. This convergence occurs within the subtropical gyres that produce a low rate of downwelling in the Arctic and Antarctic Oceans. Sinking also occurs along the Antarctic convergence and produces the Antarctic Intermediate Water (AAIW) mass. A schematic map of the thermohaline circulation of the world ocean is presented in Fig. 5.1. In the northern North Atlantic there are two major ventilation areas, which feed the flow of deep dense waters (blue lines with arrows), one near the Labrador Sea and another in the Nordic Seas. These two regions of deep water formation

may have the greatest impact on the Atlantic MOC and variations of meridional heat transport. The small number of observations in the Southern Ocean diminishes the confidence of results from the region near the Weddell Sea, and so it is not included here. Cooling and ice formation near the Nordic Seas increase the density of surface waters sufficiently to cause them to sink. Cold, dense water from the Nordic seas flows over the Greenland-Scotland ridge into the Atlantic Ocean. A schematic diagram of the main overflow (blue arrow) and compensating inflow (red arrow) is presented in Fig. 5.2.

In this chapter, we further investigate the possible relationship between the change in the meridional heat transport and the strength of the Atlantic MOC using SODA-1.4.2. We provide a quantitative analysis in the change of the Atlantic MOC and its associated meridional heat transport for the period 1958 through 2004. Emphasis is placed upon the causes of change in the strength of the Atlantic MOC in terms of changes in the properties of the ocean surface and the atmosphere.

5.2 Ocean Heat Transport and Ocean Circulation

5.2.1 Meridional OHT Linked with MOC and Gyre

The discussion in section 3.2 of chapter III outlines the influence of ocean circulation on the interannual-decadal variability of ocean heat transport. There is a vast literature that describes the importance of MOC in generating low frequency variability of climate (e.g., Bryden et al. 2005). However, because of the long duration needed to clearly show

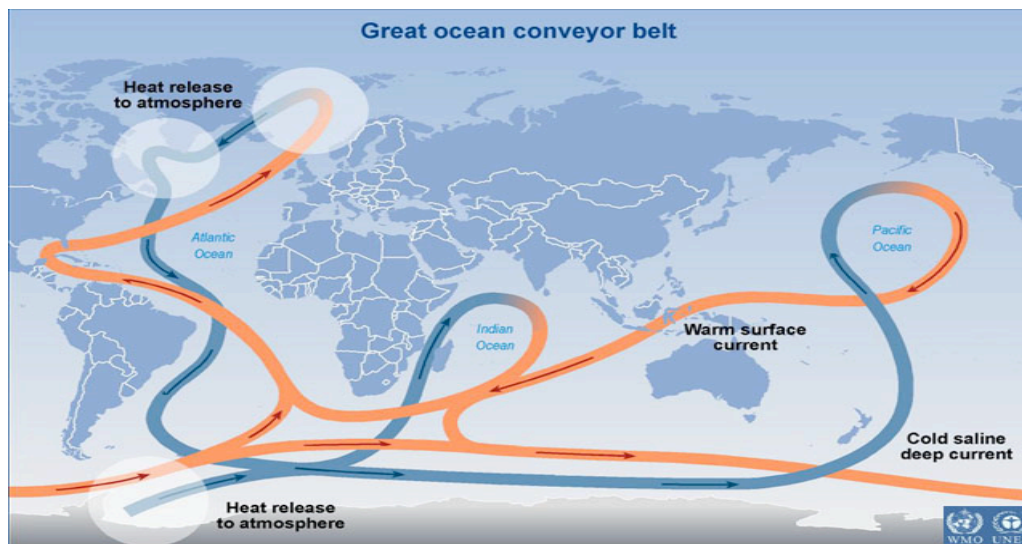


Fig. 5.1 The Great Ocean Conveyor Belt. It consists of an interconnected network of warm surface currents (in orange) and cold deep water currents (shown in blue). Source: Intergovernmental Panel on Climate Change (IPCC), “Climate Change 2001: The Scientific Basis”.

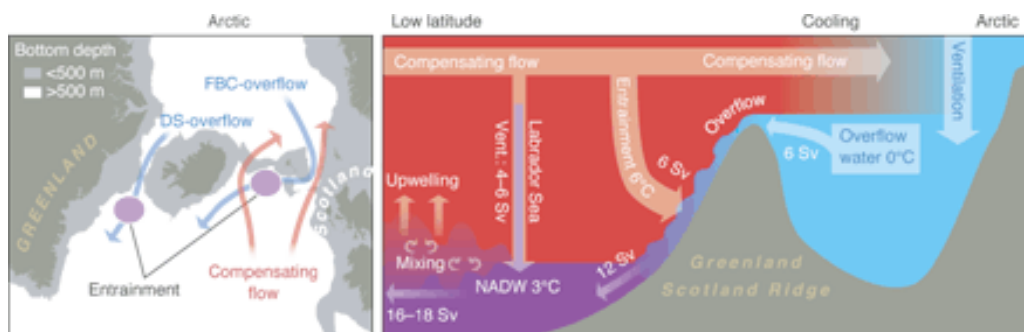


Fig. 5.2 Nordic Seas Overflow and Inflow Systems. Arrows on the map indicate the main overflow (blue) and compensating inflow (red) branches. On the schematic section to the right, temperature in $^{\circ}\text{C}$ and volume transport in Sv ($1 \text{ Sv} = 10^6 \text{ m}^3 \cdot \text{s}^{-1}$) are approximate values. DS, Denmark Strait; FBC, Faroe Bank Channel. Source: Hansen et al. 2004.

the link between MOC and climate, these connections have not been rigorously demonstrated. The analysis provides an opportunity to quantify the relationship between MOC and meridional heat transport.

a. Strength of MOC and Gyre

In order to determine how ocean heat transport responds to MOC and gyre circulation it is necessary to define the strength of MOC and the gyre circulation. It is usually difficult to quantify the strength of ocean circulation because of overlapping forcing mechanisms. For example, wind stress variability can contribute to changes both in MOC and the gyre circulation. In fact the circulations themselves overlap, making the definition of an index of circulation difficult. By confining attention to a limited domain, a unique index defined to depict strength of the ocean circulation is possible.

The conventional method for defining the strength of the ocean circulation is to first locate the maximum value of the streamfunction at any given latitude, and then to use the maximum value as an index of ocean circulation. One important assumption made in this definition is that the location of maximum streamfunction is not north-south shifted. A second assumption is that the representation of circulation strength be applied only to a limited area. This is necessary because any violation of assumption causes an aliasing of ocean circulation strength and affects the assessment.

The mean gyre circulation and MOC for the Atlantic and Pacific Oceans are shown in Fig. 5.3 by contouring the horizontal and meridional overturning streamfunctions. The

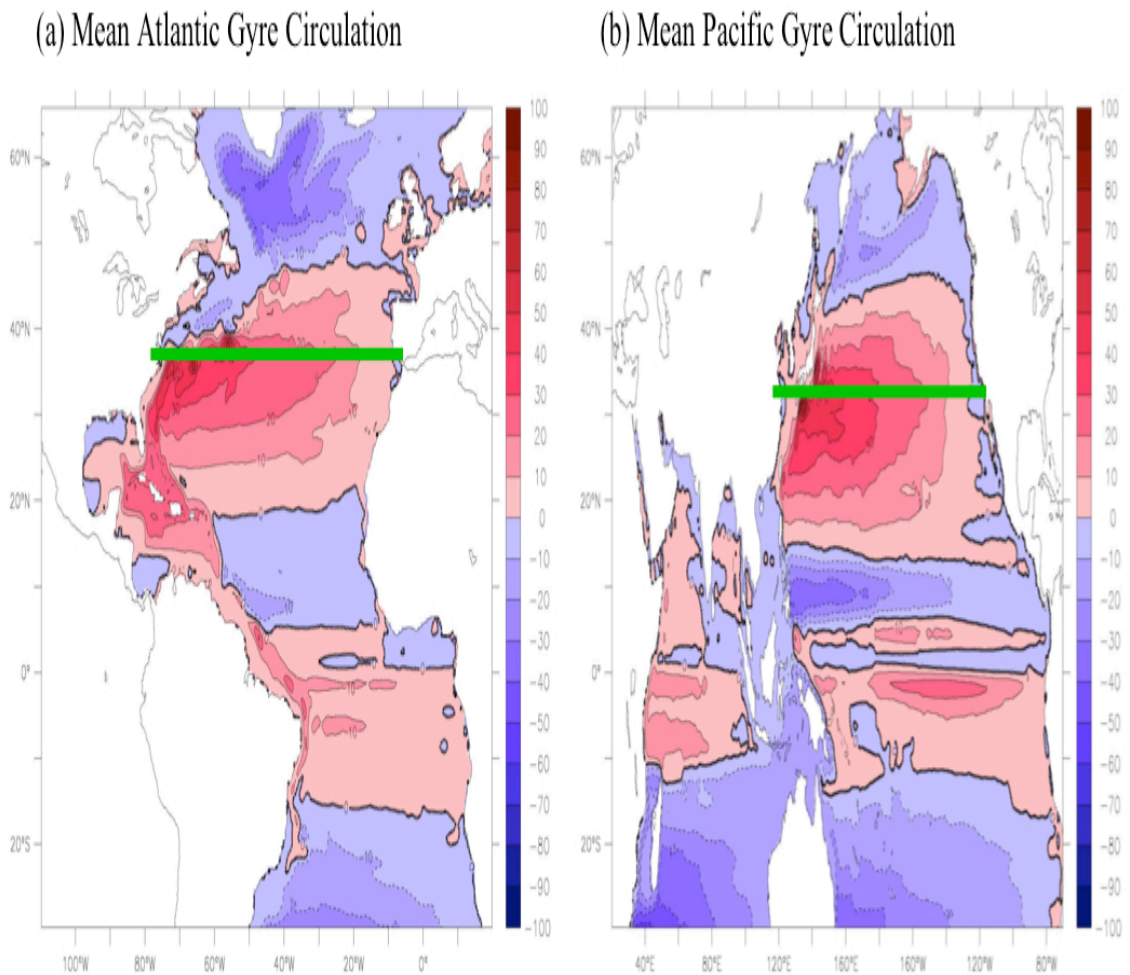


Fig. 5.3 Mean gyre circulations in Sv of the (a) Atlantic and (b) Pacific Oceans and mean meridional overturning circulations of the (c) Atlantic and (d) Pacific Oceans.

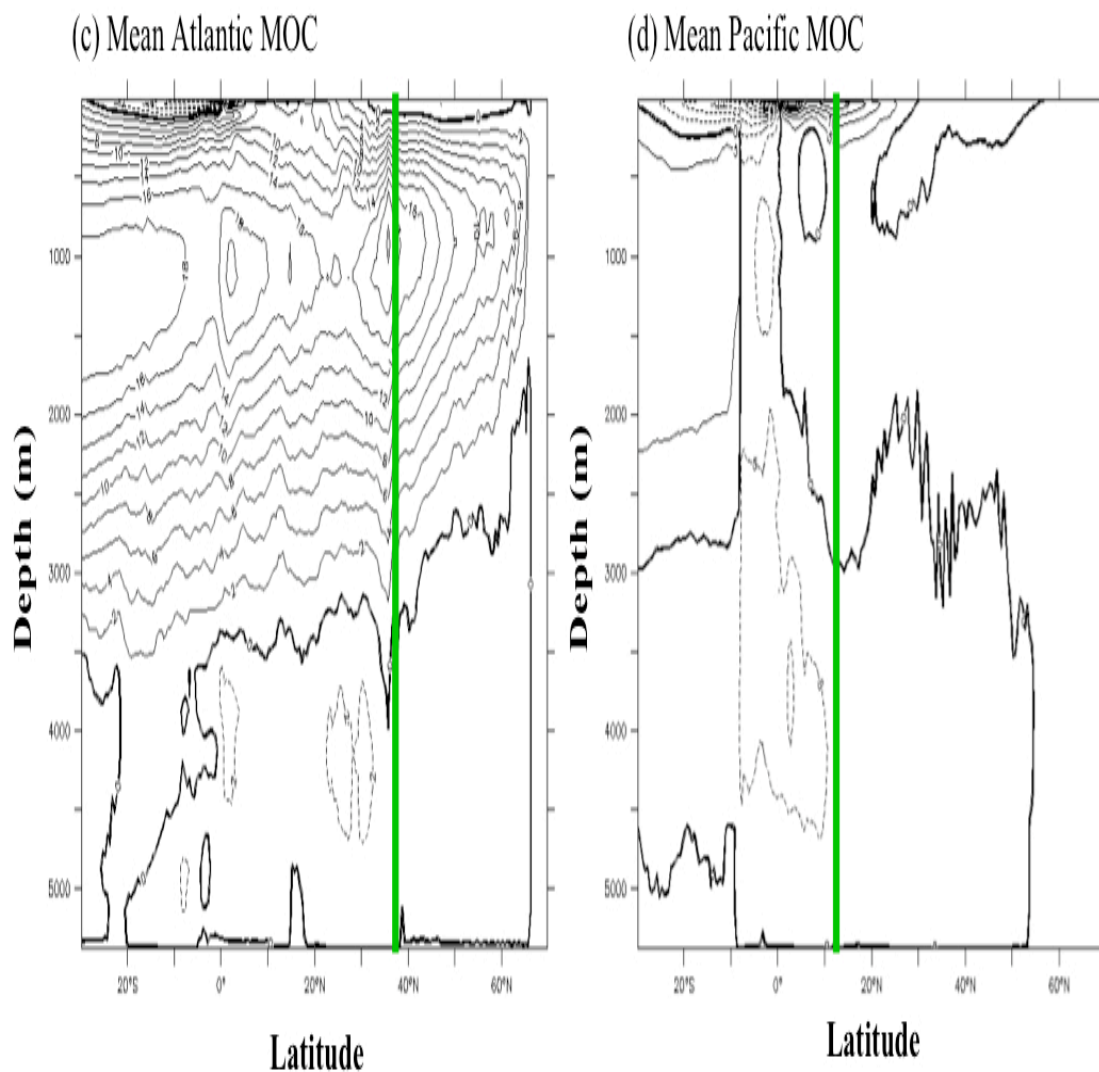


Fig. 5.3 (Continued)

subtropical and subpolar gyres are clearly identified in the Atlantic and Pacific Oceans. The subtropical gyres in the Atlantic and Pacific Oceans both have a maximum volume transport of more than 40 Sv. The vertical streamfunction in the Atlantic shows that wind-driven shallow overturning cells overlay the density-driven intermediate

(500-2000m) and deep overturning cells associated with deep water formation. The maximum streamfunction value at $36^{\circ}N$ in the North Atlantic is about $20 Sv$, which is almost half of subtropical gyre circulation. The MOC in the Pacific is quite different from that of the Atlantic. The strongest meridional overturning cells in the Pacific are in the upper 400 meters with strength of more than $20 Sv$. The deep cells in the Pacific Ocean are very weak and irregular as compared to those of the Atlantic Ocean.

b. OHT Response to MOC and Gyre

We choose $36^{\circ}N$ as a location of both maximum mean meridional overturning streamfunction and horizontal streamfunction for the North Atlantic. Because the deep cell is weak in the Pacific, the latitude of maximum overturning is $14^{\circ}N$, whereas the latitude of maximum gyre circulation is $35^{\circ}N$. These locations are denoted by green lines in Fig. 5.3. The value of the maximum streamfunction for MOC and gyre circulations in the North Pacific and Atlantic Oceans are then obtained. An index derived from anomalies of these peak values is chosen to define the strength of anomalous ocean circulation. Anomalies of meridional heat transport in the Atlantic and Pacific Oceans are then linearly regressed onto the index. Each of the resulting slopes is called ocean heat transport response to the MOC or gyre circulation. The meridional ocean heat transport response to the Atlantic MOC/gyre and Pacific STC/gyre is shown in Fig. 5.4. The amplitude of response of heat transport to ocean circulation is calculated by regressing ocean heat transport on the strength of the ocean circulation. A regression

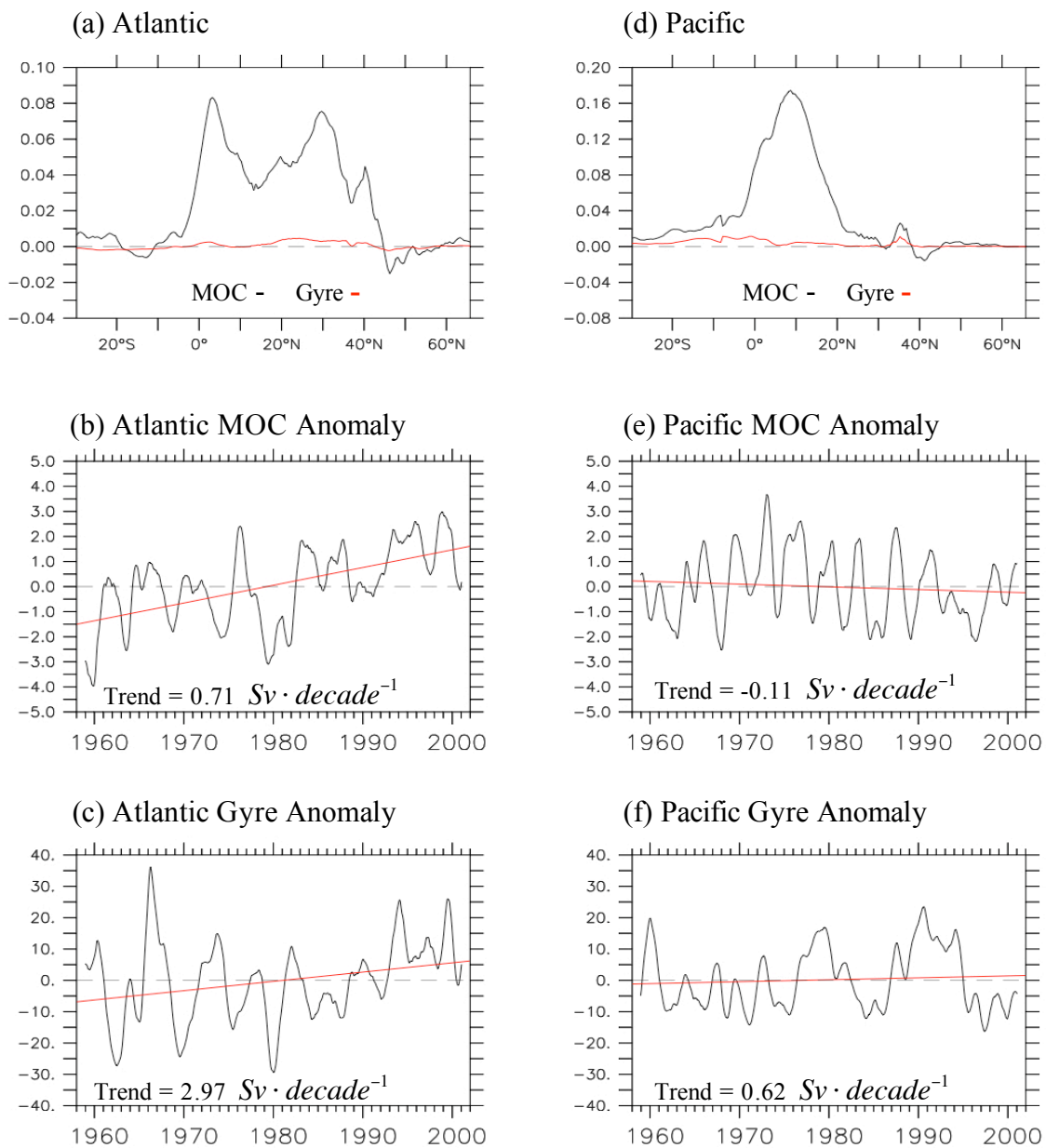


Fig. 5.4 Meridional heat transport response to strength of MOC and gyre circulation in the Atlantic and Pacific Oceans.

analysis is often useful for identifying a response between variables that have a physical connection. Variability of ocean heat transport is linked to changes in the ocean currents as described in section 3.1 of Chapter III. Apparently the ocean heat transport response to meridional circulation is much stronger than to gyre circulation both in the Atlantic and Pacific Oceans. This common feature implies that meridional heat transport in the oceans is primarily governed by ocean circulation in the meridional-vertical plane instead of the horizontal plane. The spatial patterns of response in the Atlantic and Pacific are different. In the Atlantic two peak values (one near equator and one near $30^{\circ}N$) in heat transport response to the Atlantic MOC is present. By contrast, in the Pacific there is only one peak value (near $8^{\circ}N$). In the Atlantic the response to MOC appears to be within a latitudinal band from 0 to $40^{\circ}N$, whereas in the Pacific the response is from $20^{\circ}S$ to $20^{\circ}N$. This structure of response in latitudinal bands is probably linked to the spatial features of meridional heat transport as shown in Fig. 3.8. Note that in the Atlantic Ocean there is a negative response of heat transport near $10^{\circ}S$ and $45^{\circ}N$, and a positive response near $60^{\circ}N$. One possible explanation for the negative response near $10^{\circ}S$ is variability of heat transport is closely linked to the change of STC. Negative response near $45^{\circ}N$ is probably because change in circulation is opposite to that described by the index. The dynamical cause of the different response patterns in the Atlantic and Pacific Oceans is still not fully understood, although it is probably associated with distinct meridional ocean circulations in the two basins. Interestingly, strong interannual variability of the wind-driven STC (Fig. 5.4e) can explain strong interannual variability of meridional heat transport in the tropical Pacific. Because the

linear trend in the STC of the Pacific Ocean ($-0.11 \text{ Sv} \cdot \text{decade}^{-1}$) is much smaller than its counterpart in the Atlantic Ocean ($0.71 \text{ Sv} \cdot \text{decade}^{-1}$), we focus next on the Atlantic Ocean.

c. Phase Relationship between OHT and MOC

In order to verify whether ocean heat transport is linked with MOC/STC strength, it is necessary to examine the phase relationship between meridional heat transport and strength of MOC/STC, and the gyre circulation. The phase relationships between meridional heat transport at $30^\circ N$ and local MOC/gyre circulation strength in the Atlantic Ocean are shown in Fig.5.5. The strength of the local MOC/gyre circulation is defined to be the maximum mass transport across $30^\circ N$ in the Atlantic Ocean. Clearly, meridional heat transport in the Atlantic is closely associated with local MOC rather than with the gyre circulation strength, since a zero-lag correlation with local MOC is 0.90, while a zero-lag correlation with local gyre circulation strength is only 0.32.

d. Evolution of the Atlantic MOC and OHT

An interesting question arises: Is the relationship between Atlantic MOC and OHT as described in section 2.1c valid for all latitudes? To address this question, we compare the temporal and spatial patterns of the Atlantic MOC and OHT. Fig. 5.6 exhibits the

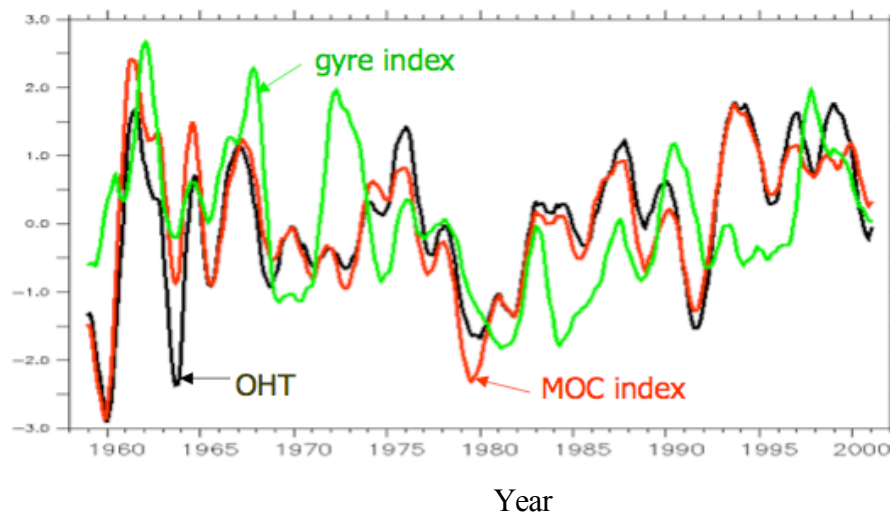


Fig. 5.5 Normalized ocean heat transport (black), local MOC (red) and gyre circulation (green) strength at $30^{\circ}N$ in the Atlantic Ocean. Normalized values are obtained using the anomalies divided by their standard deviation.

evolution of anomalous Atlantic MOC streamfunction which represents the change in strength of the MOC and the meridional heat transport for the period 1958 through 2004. At low to mid latitudes, anomalous meridional heat transport is synchronous with the strength of the Atlantic MOC on interannual to decadal timescales, such that positive anomalies of meridional heat transport is synchronous with the enhanced MOC and vice versa. At high latitude, this relationship is less pronounced. The difference of ocean heat transport in response to strength of MOC at low and high latitude reflects the relative importance of the roles of ocean currents and temperature fields in heat transport at different latitudes. The different responses are illustrated in Fig. 3.11 whereby in the region south of $50^{\circ}N$ the change in currents dominates heat transport variability, and in

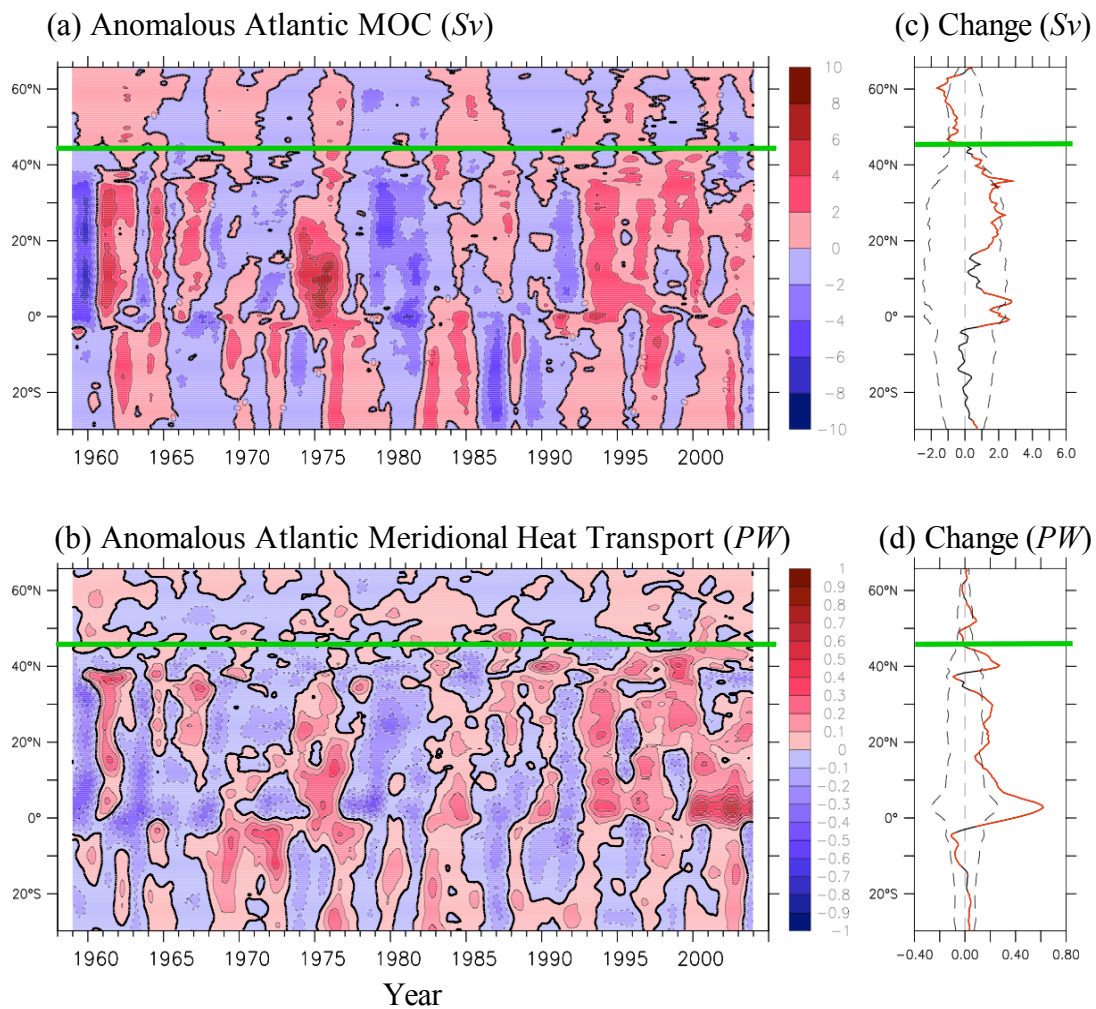


Fig. 5.6 Temporal evolution of anomalous strength of (a) the Atlantic MOC and (b) meridional heat transport in PW for the period 1958-2004.

regions higher than $50^{\circ}N$ the importance of temperature grows and so it is a mixture of change in currents and temperature fields that describes the response of heat transport. This sensitivity of heat transport to temperature at high latitude in the Atlantic Ocean provides a different scenario in that weakening of MOC does not necessarily mean a

decrease in meridional heat transport in the northern North Atlantic Ocean.

Linear changes in the strength of MOC and in ocean heat transport as a function of latitude are shown by a solid curve in Figs. 5.6c, 5.6d. Shown by a red solid line is the change at a 95% significance level using a student t-test specified by red solid curves. One standard deviation of MOC and ocean heat transport is denoted by a dashed curve. There is a significant change in heat transport at most latitudes while change in MOC is significant except in the South Atlantic Ocean. An interesting feature of the Atlantic MOC is that it tends to weaken in the Northern North Atlantic Ocean and tends to strengthen in the region south of $40^{\circ}N$. This bidirectional signal in the strength of the Atlantic MOC implies a convergence of water in the region between $40^{\circ}N$ and $50^{\circ}N$. It also implies that change of MOC strength estimated at a few latitudes using observations may not represent the change of the basin-scale MOC. Another intriguing feature of the relationship between ocean heat transport and MOC change is apparent at high latitude. Although the MOC tends to weaken in the northern North Atlantic Ocean, there is a slight increase in ocean heat transport for the period 1958-2004.

Before the late-1960s the primary temperature profiling instrument was the Mechanical Bathythermograph, which was limited to depths shallower than 285m and therefore did not sample the main thermocline in many parts of the ocean. With the exception of the International Geophysical Year (1957-58) the total number of observations reaching a depth of 300m was less than 5000 per year. The estimate of ocean heat transport depends on the spatial and temporal temperature distribution of observations. Scarcity of temperature observations before the late-1960s in our

assimilation model may lead to a poor representation of the real ocean state. Therefore we also examine the trend of ocean heat transport and MOC strength starting in 1970. The results are shown in Fig. 5.7. The fundamental features of ocean heat transport and MOC are the same as for the entire period, however. There is a decrease in ocean heat transport in the south tropical Atlantic Ocean and an increase in MOC strength (up to 1 Sv) in the north tropical Atlantic Ocean between $20^{\circ}N$ and $40^{\circ}N$.

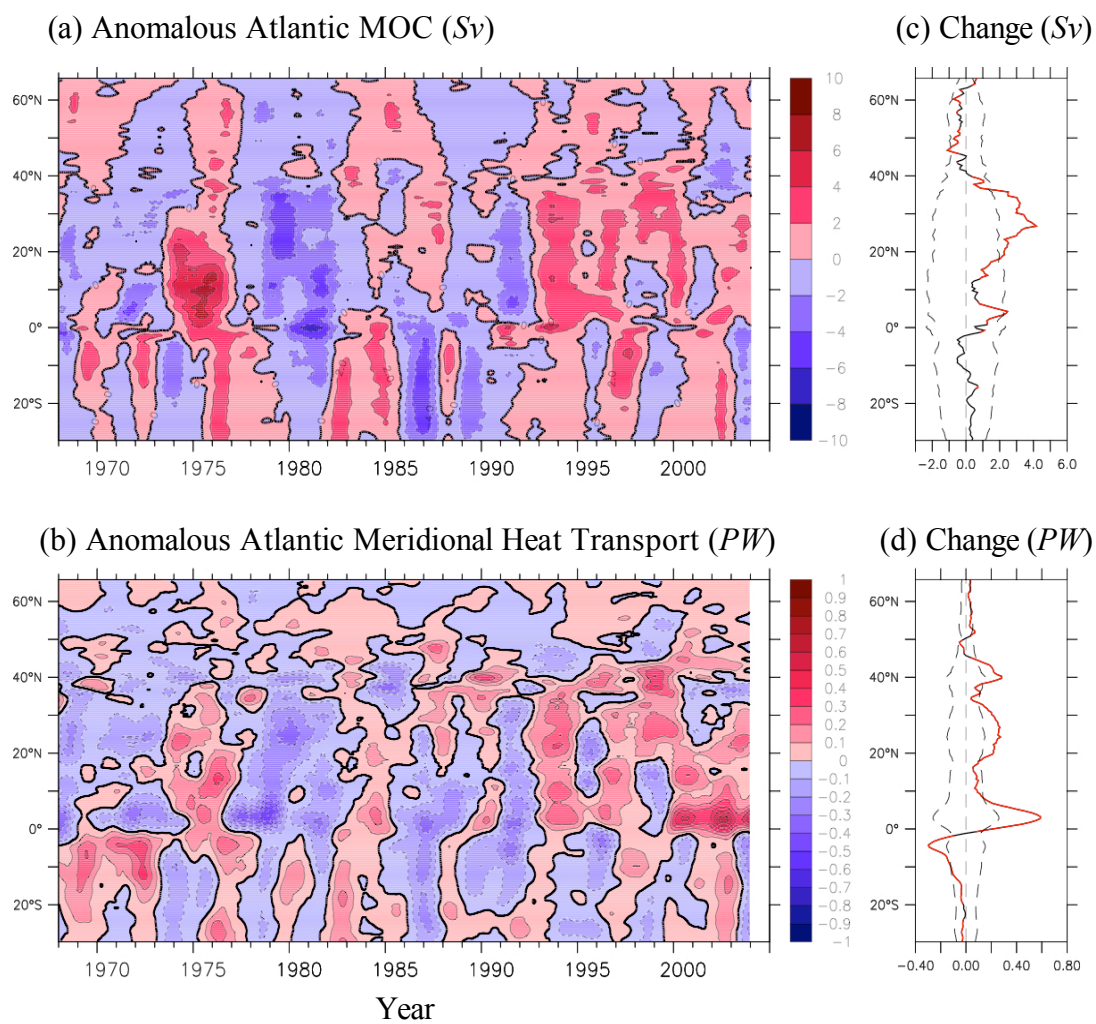


Fig. 5.7 Same as Fig. 5.6 except for the period 1968-2004.

e. Pseudo-heat Function

Recently, Boccaletti et al. (2005) investigate the roles of different Atlantic MOC components in meridional OHT by defining a heat. They posit that it is the shallow surface (0-500m) intensified circulation that dominates the poleward heat transport. The calculation of heat function requires the condition of steady state and determination of temperature diffusivity κ , an important quantity that is able to affect heat transport. Abyssal mixing is not important in affecting heat transport as argued by Boccaletti et al. (2005) and Scott and Marotzke (2002), however mixing in the thermocline is able to influence the total heat transport. Thus a constant diapycnal mixing coefficient in the thermocline is a potential contamination in estimating heat transport.

Using the method of Bryden and Imawaki (2001) to diagnose the vertical feature of ocean heat transport, we introduce a quantity Π called the pseudo-heat function

$$H = -\frac{\partial \Pi}{\partial z} \quad (5.1)$$

where $H = \int_{west}^{east} \rho C_p V T dx$. This quantity can be used to identify where the accumulated heat (or enthalpy) transport has large variability. The mean pseudo-heat function for the Atlantic MOC is presented in Fig. 5.8a. The largest mean enthalpy transport occurs in the upper 1000 m, and the rapid increase of enthalpy transport also appears in the layer 0-1000 meter. In contrast to the sharp rise in the upper 1000m, the heat transport gradually falls to a depth of 2500m. No discernible change in heat transport deeper than 4000m is found. The vertical structure of interannual to decadal variability of meridional

heat transport is shown by the standard deviation of pseudo-heat function in Fig. 5.8b. The location of peak variability of heat transport is collocated with the maximum mean value. The center of largest variability is found at 500m near $4^{\circ} N$, other peak values fall within a 500-1000m layer. The fact that depth of peak variability in heat transport falls within 500-1000m layer for all latitudes indicates that wind-driven shallow overturning circulation (0-500m) combined with density driven intermediate overturning cells (500-1000m) may play an important role in generating the mean and interannual-decadal variability of meridional

(a) Mean Atlantic MOC Pseudo-heat Function

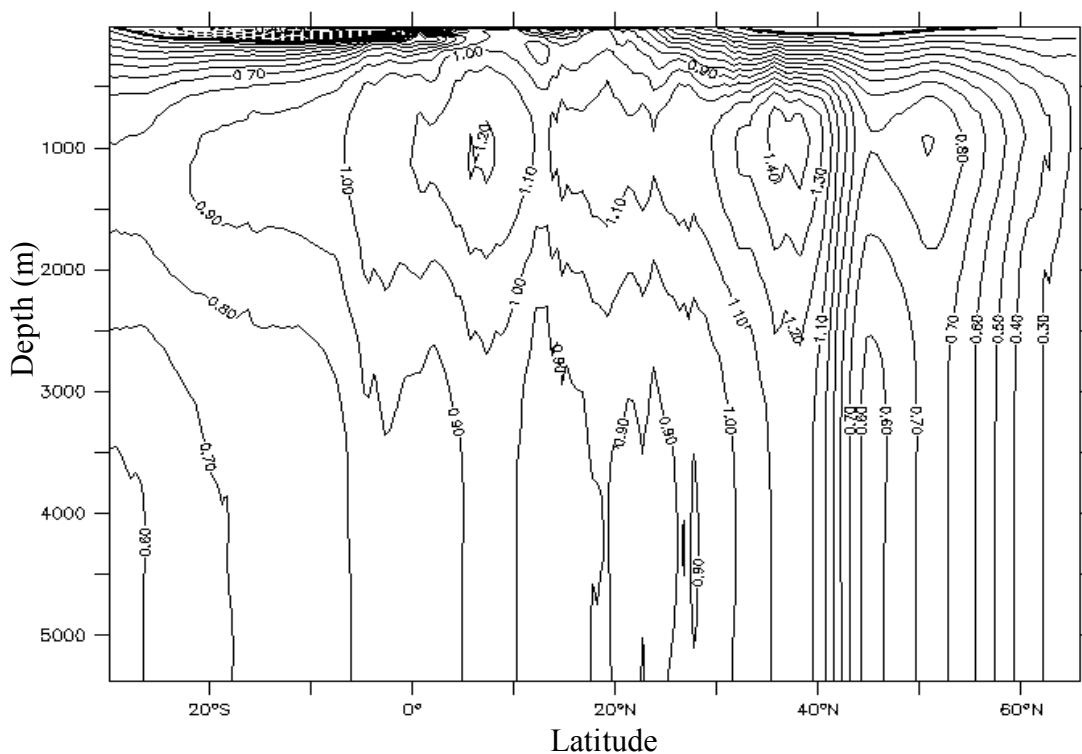


Fig. 5.8 Mean (a) and standard deviation (b) in PW of the Atlantic MOC pseudo-heat function.

(b) Standard Deviation of Atlantic MOC Pseudo-heat Function

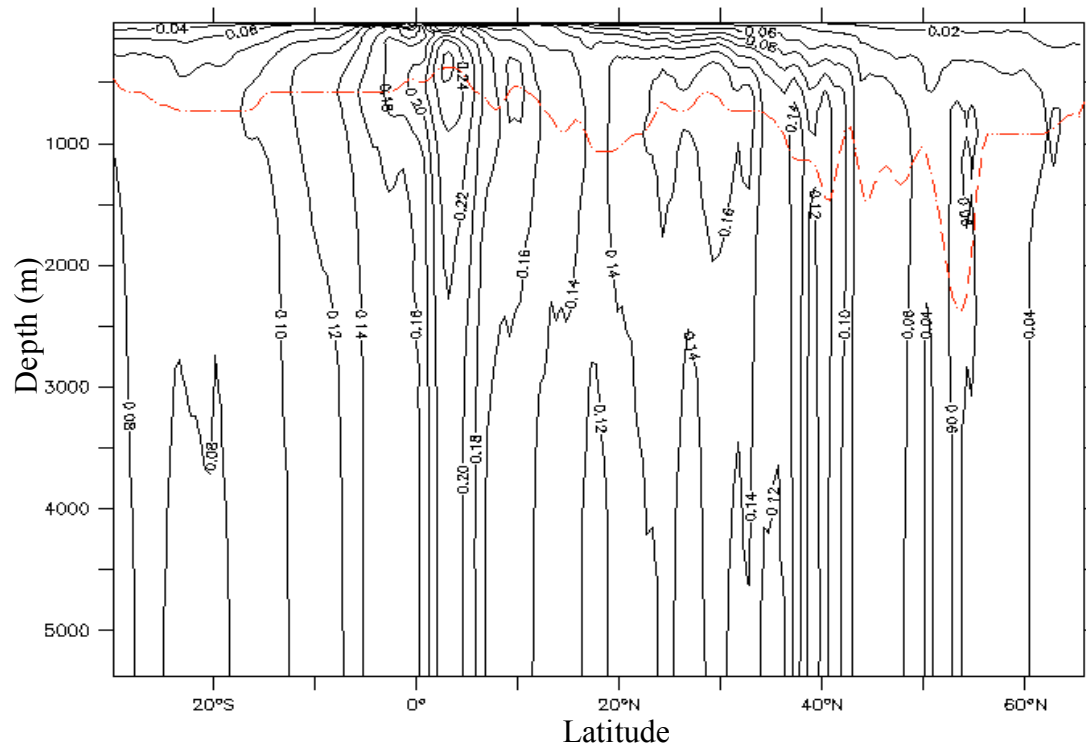


Fig. 5.8 (Continued)

heat transport. At high latitudes, the influence of the density-driven component of MOC in heat transport rises. Although the low branch of the Atlantic MOC is associated with deep water formation, this does not make a significant contribution to the change in meridional heat transport. Significant change in deep water formation may give rise to a noticeable change in the heat transport if it accelerates the northward movement of the upper branch in order to observe mass conservation in a closed ocean.

Fig. 5.9 shows the mean and standard deviation of the pseudo-heat function for the Indo-Pacific MOC. The vertical structure of mean heat transport in the Indo-Pacific Ocean is also similar to the vertical pattern of its mean ocean circulation. The MOC in the Pacific Ocean is very shallow (see Fig. 5.3d) compared to the MOC in the Atlantic Ocean (Fig. 5.3c), the large mean transport of heat in the very shallow layer as indicated in Fig. 5.9a, particularly in the upper 500m. Similar to Fig. 5.8b, the variability of pseudo-heat function in the Indo-Pacific Ocean as a function of depth, shown in Fig. 5.9b, has largest temporal change in mean heat transport above 1000m. The depth of the largest variability of mean heat transport varies with latitudes. Interestingly, in the equatorial region the location of peak variability is particularly shallow compared to the Atlantic Ocean, and it resides in a layer that is tens to hundreds of meters deep. The maximum gets as deep as 1000m at high latitudes, associated with the deepening of zonal-mean thermocline in the oceans. This implies that the processes within and adjacent to the thermocline may be important to the variability of heat transport in the Indo-Pacific Oceans.

(a) Mean Indo-Pacific MOC Pseudo-heat Function

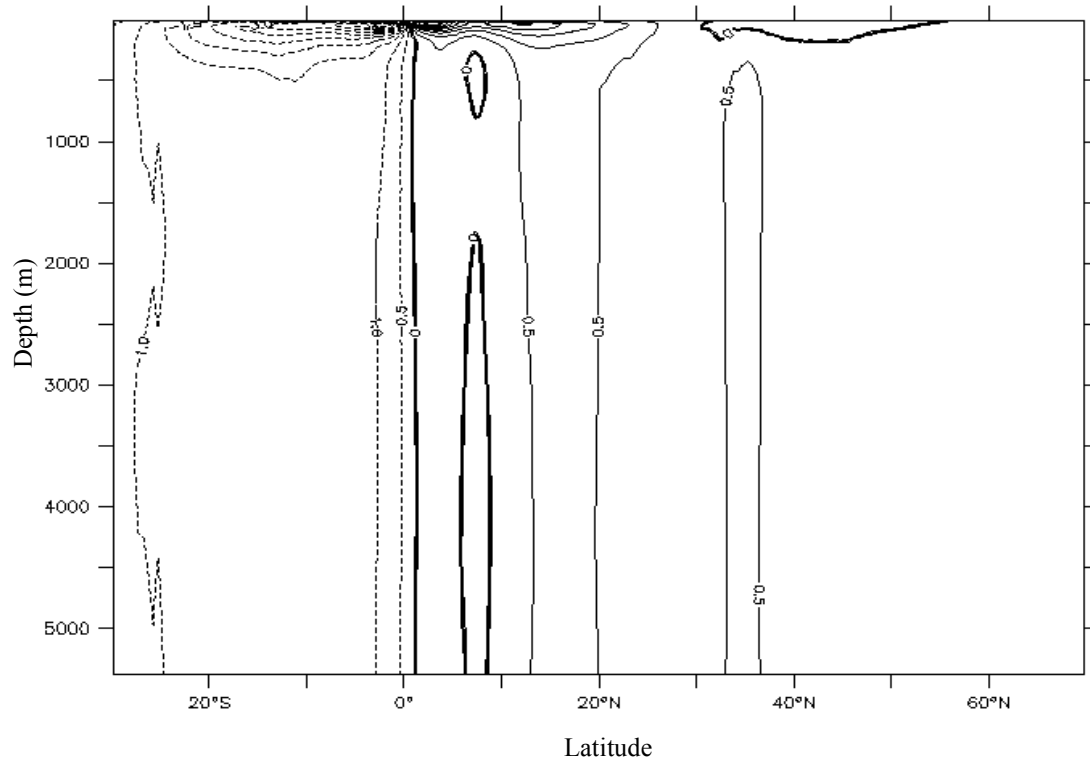


Fig. 5.9 Same as Fig. 5.8 except for the Indo-Pacific Ocean.

(b) Standard Deviation of Indo-Pacific MOC Pseudo-heat Function

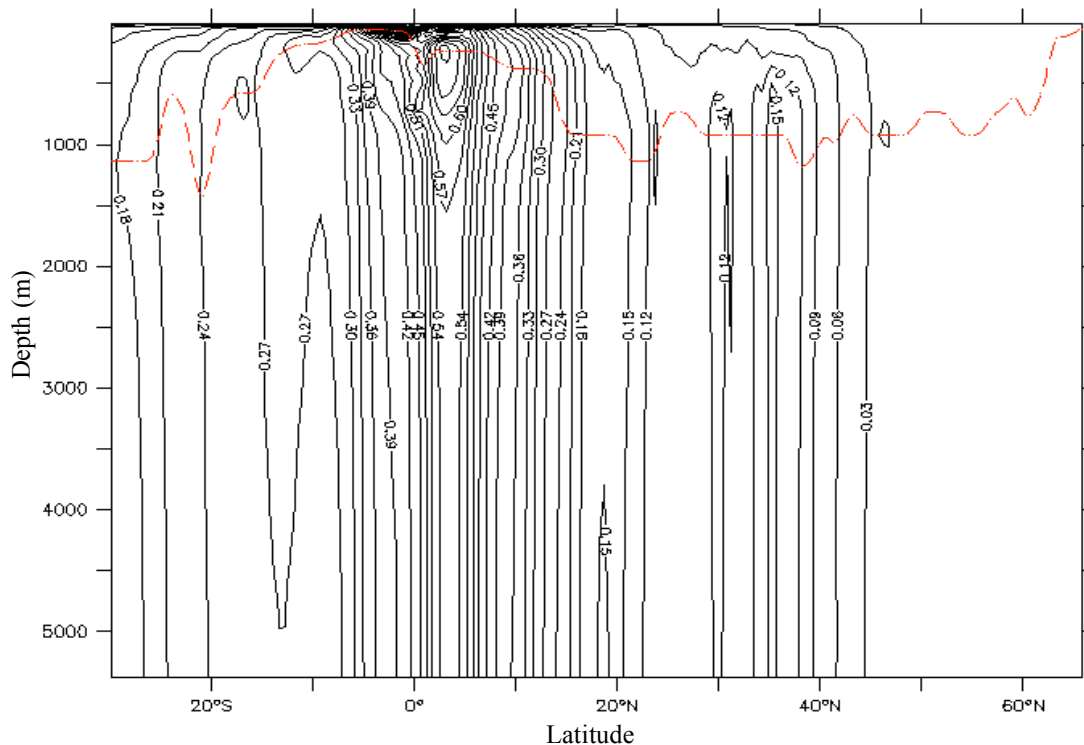


Fig. 5.9 (Continued)

5.2.2 NAO and SST in the North Atlantic Ocean

Recent changes in the Atlantic MOC might be associated with the overlying atmospheric circulation (e.g., Eden and Willebrand, 2001). Therefore ocean heat transport could be affected by wind stress change due to changing atmospheric circulation. One of the important measures of change in the atmosphere is the NAO, which affects the subpolar zone of the North Atlantic Ocean. The subpolar gyre of the

North Atlantic circulates cyclonically between $50^{\circ}N$ and $66^{\circ}N$ and contains strong boundary currents. It is a region of intense interaction between the ocean and the atmosphere. Cold winds in winter remove heat at rates of several hundred $W \cdot m^{-2}$, giving rise to deep convection in the ocean reaching as deep as 2500 meters below the sea surface. Subpolar waters combine with dense Nordic Sills overflows to provide the origins of North Atlantic Deep Water (NADW). Marshall et al. (2001) argue that the NAO and MOC are intimately connected on a wide range of timescales and should therefore be considered together. In the mid-latitude Atlantic, shifts in wind stress patterns and air-sea heat fluxes resulting from the NAO can lead to anomalous wind-driven gyres, thermohaline circulation and associated heat transport.

The NAO is defined by an index of normalized, time-averaged surface air pressure difference between stations representing its two centers of action, such as the Azores and Iceland (Rogers 1984; Hurrell 1995a). Although there is no surface air pressure in SODA, the NAO index can be approximately defined as the difference of the normalized mean wind stress between $50^{\circ}N - 66^{\circ}N$ and $30^{\circ}N - 40^{\circ}N$ of the Atlantic sector. The NAO index based on our definition and the normalized SST averaged over the region $50^{\circ}N - 66^{\circ}N$ in the Atlantic sector is shown in Fig. 5.10. The NAO index defined here is similar to Hurrell's NAO index shown in Fig. 1 of Marshall et al. (2001) which was derived from sea level pressure data of the NCEP-NCAR reanalysis. It is clear that SST in the North Atlantic is out of phase with the NAO index on decadal timescales. Positive anomalies in SST at this region start to occur in 1995 and persist through 2003. This sustained warming parallels the weakening subpolar gyre of the 1990s as argued by

Hakkinen et al. (2004). The reason we are concerned with the atmospheric forcing (i.e., wind stress) in our study is that there are two effects that wind stress has on ocean heat transport, particularly in the northern North Atlantic Ocean. One is a dynamical factor that influences ocean circulation and salt transport, and another is a thermal factor that controls surface temperature. Thus either vertical processes via seawater density change, or direct participation in heat transport via heat content change can make a contribution to the change of Atlantic Ocean heat transport. The possible effects on ocean heat transport and the strength of MOC will be further examined and discussed in the subsequent section.

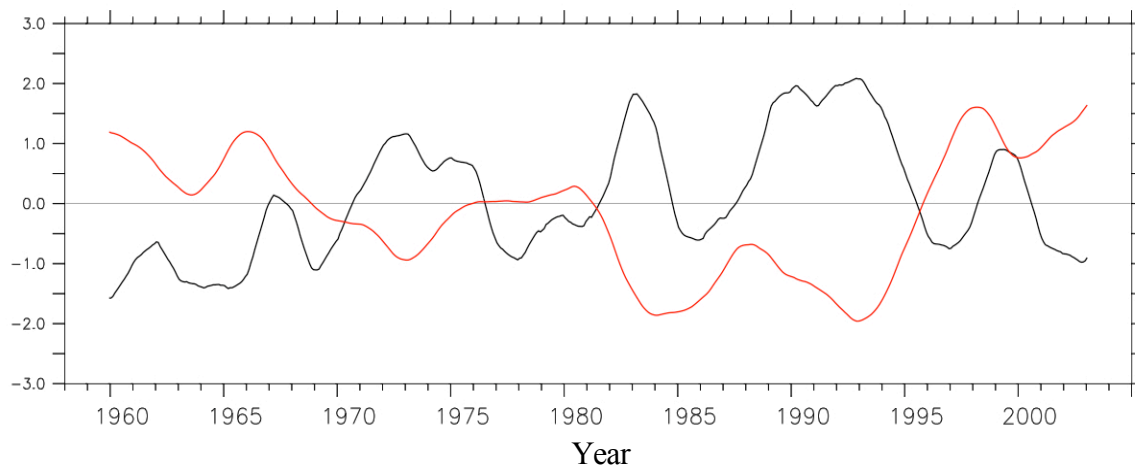


Fig. 5.10 Time series of the NAO index (black) and the normalized SST (red) averaged over ($50^{\circ}N - 66^{\circ}N$) in the northern North Atlantic for the period 1958-2004.

5.3 Possible Causes of the Atlantic MOC Changes

As we demonstrate in section 2, the variability and change of ocean heat transport is closely linked to the variability and change of the Atlantic MOC. There are two possible scenarios that describe the change of the Atlantic MOC. One possibility is that MOC at high latitude in the North Atlantic Ocean becomes weaker. Alternatively it could be strengthened in low latitude. This prompts the questions: (1) what processes are important to changes of the MOC? (2) Why is the change in the MOC different between high latitude and low latitude?

Fig. 5.11 exhibits the mean Atlantic MOC based on the period 1958-2001 and the difference between the periods (1958-1980) and (1981-2001). Since there is no apparent shift of the Atlantic MOC as shown in Figs. 5.6, 5.7, strengthening or weakening of the Atlantic MOC in a period can be detected in terms of the amplitude change of the MOC streamfunction by comparing two long-term averaged values. Interestingly, there are relatively large changes in the Atlantic MOC for three different latitude bands, a high latitude $55^{\circ}N - 62^{\circ}N$ band, a mid-latitude $20^{\circ}N - 45^{\circ}N$ band, and a low latitude $20^{\circ}S - 20^{\circ}N$ band. These changes in three bands are also apparent in Figs. 5.6 and 5.7. However, it may also result from freshening as found by many previous studies (e.g., Rahmstorf, 1996; Marotzke, 2000; Curry and Mauritzen, 2005), which occurs in the upper 1000 meters. In the mid-latitude band strengthening is significant because there is a sustained negative anomaly for the period from 1970 to 1980 and a persistent positive anomaly from the mid-1990s to 2004. Its core change occurs in the layer 500m-2000m.

In the region from $20^{\circ}S - 20^{\circ}N$, the largest change is at relatively shallow depth in the upper 1000m.

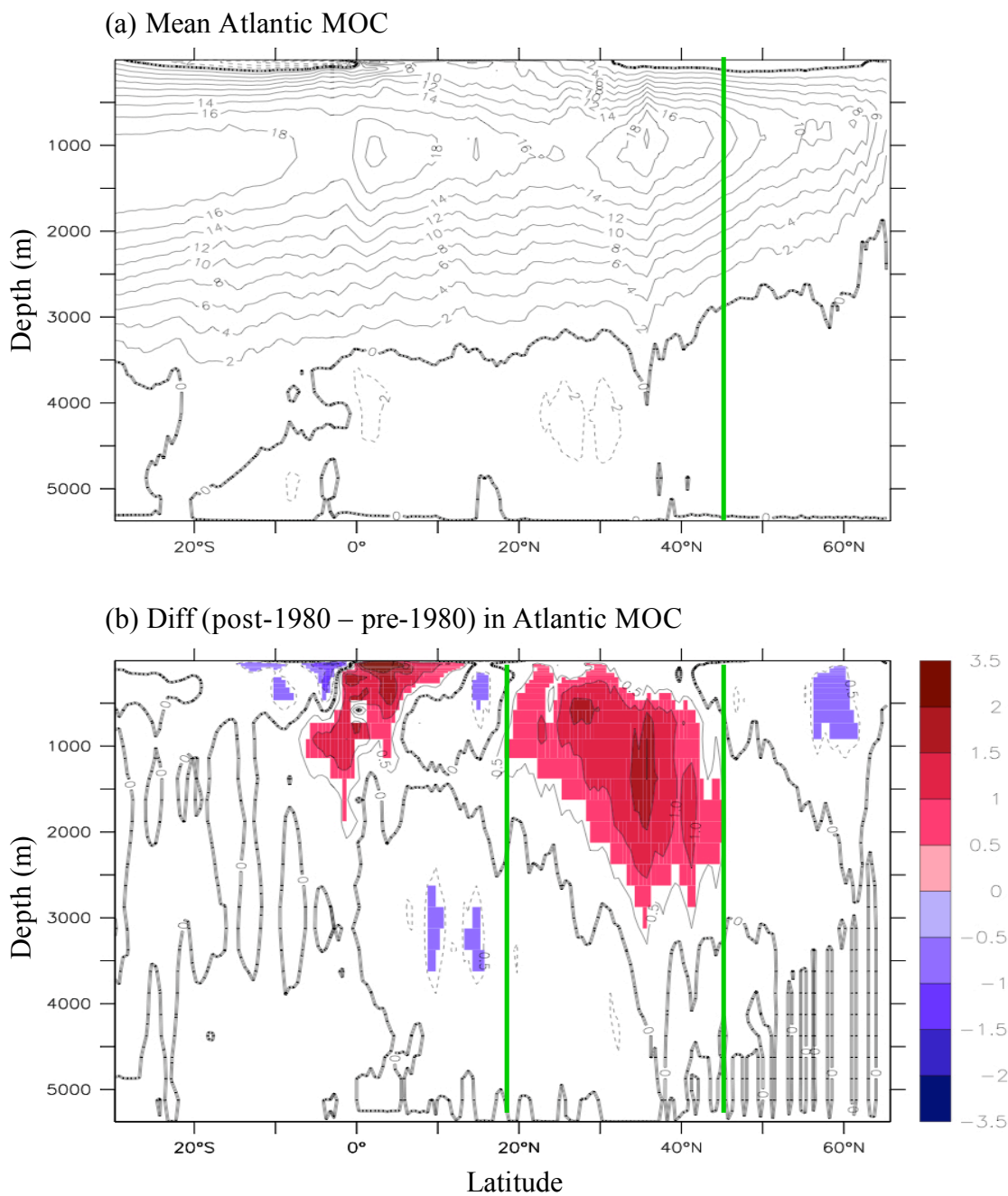


Fig. 5.11 (a) Mean and (b) difference of Atlantic MOC between (1981-2001) and (1958-1980).

5.3.1 Causes of Weakening Atlantic MOC

a. Spatial Pattern of Surface Properties

In order to understand the changes of water properties in the North Atlantic Ocean, we compute the linear change in zonal wind stress (τ_x in $\text{dynes}\cdot\text{cm}^{-2}$), sea surface temperature (SST in $^{\circ}\text{C}$), surface density (ρ in $\text{kg}\cdot\text{m}^{-3}$) and salinity (in $\text{g}\cdot\text{kg}^{-1}$) of ocean water for the period 1958-2004. The spatial pattern of the linear changes for 47 years of τ_x , SST, ρ , and salinity in the region of the North Atlantic Ocean 40°N - 70°N are shown in Fig. 5.12. We first address the change in atmospheric zonal wind stress over the North Atlantic Ocean. The region of most enhanced τ_x is centered in the region between 50°N – 60°N , spreading from Labrador Sea to Irminger Sea and regions adjacent to Greenland.

There are several interesting features in the change of surface density. First, a small region of surface water is denser ($\sim +0.1\text{kg}\cdot\text{m}^{-3}$) in the North Atlantic between 52°N and 55°N and 40°W along a southwest-northeast line. However, A relatively large area of surface water in the Labrador Sea (between 48°N and 60°N , west of 50°W) is much lighter ($\sim -0.2\text{kg}\cdot\text{m}^{-3}$), particularly in the sinking region. The decrease in surface density there can be expected to slow down the sinking process, hence may be an important factor in affecting the strength of the Atlantic MOC. Apparently the spatial pattern of surface density with northeast-southwest tilt is related to the Gulf Stream, an important component of ocean circulation in the change of ocean surface properties. In

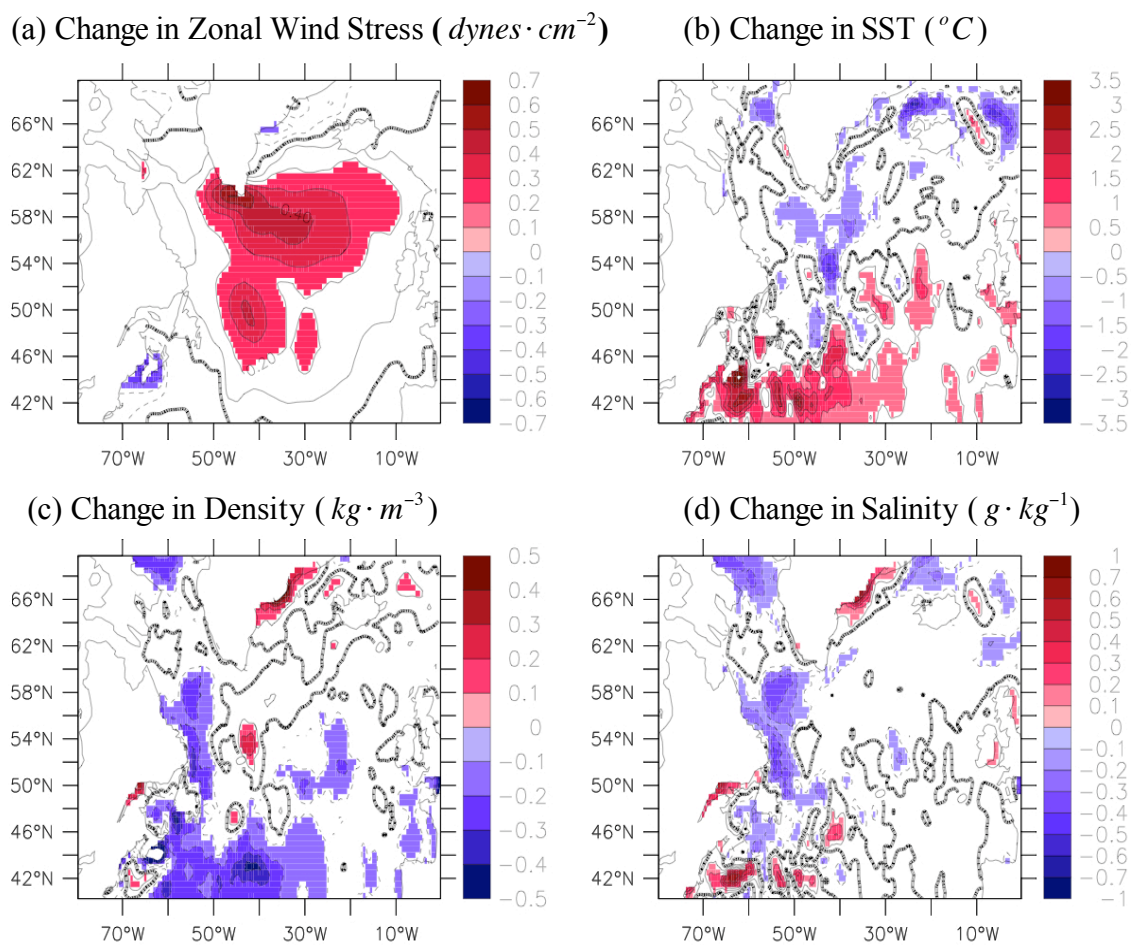


Fig. 5.12 Linear change in zonal wind stress, SST, surface density and surface salinity of the North Atlantic Ocean for the period 1958-2004.

the Subtropical regions the surface density is also decreased. The reduced surface density in the subtropical region prohibits local sinking. An enhanced τ_x can lead to local cooling, thus generating denser water. But why does the strengthening of wind stress cause such a slight increase in surface density? One explanation is that the salinity decrease due to weakened salt transport and freshening processes that counteract the cooling effect.

Density of seawater is primarily determined by temperature and salinity. Cold temperature and high salinity create dense water masses while warm fresh waters are relatively light. In the subtropical ocean, warm surface water counteracts the effect of high salinity due to strong evaporation, and so water is unable to sink. At high latitude in the North Atlantic Ocean, where water is cold, salinity rather than temperature, dominates the change of water density. Therefore a large discharge of fresh water into the region of the high latitude inhibits sinking, giving rise to a weak MOC. Changes of salinity at high latitude in the North Atlantic Ocean is crucial to the change of density, and hence the sinking rate. However, the influence of temperature on the density of seawater and sinking rate, particularly in the region where there is little fresh water available to offset the temperature effect, can not be ignored. SST, shown in Fig. 5.12, shows a decreasing trend in the North Atlantic Ocean north of $46^\circ N$. The tilt of $0^\circ C$ line is related to processes in the Gulf Stream and coldwater inflow through Labrador Current and East Greenland Current. A decrease in SST trend occurs in the region ($50^\circ W - 30^\circ W$, $45^\circ N - 60^\circ N$), which coincides with the region of increased density. The increase of water density induced by low SST is not large because of the

compensating effects from salinity. Otherwise, decreased SST would promote the sinking process. Freshwater discharge in the North Atlantic Ocean is primarily from the Arctic Ocean via the Labrador and East Greenland Currents and adjacent river runoff and precipitation. Cold water overflow from the Nordic seas into the North Atlantic Ocean across Greenland-Iceland-Scotland Ridge (i.e., Denmark Strait, Faroe Bank Channel) is also a fundamental component of the North Atlantic thermohaline circulation (Hansen et al., 2004). A salinity reduction is evident throughout the entire North Atlantic Ocean. The largest reduction ($\sim -0.4 \text{ g} \cdot \text{kg}^{-1}$) in salinity due to freshwater discharge occurs in the region west of 50°W where deep-water formation occurs. This is not the region of the slightly decreased SST that is to the east of 50°W . Hence the effect of salinity is depressed in the region of reduced SST, which explains the small increase of water density. This small increase of water density is not in the region where sinking is active, thus it may not be critical to the strength of the Atlantic MOC. The spatial distribution of changes in SST and salinity simplifies the partitioning of temperature and salinity effects on the change of seawater density. Since ice formation and enhanced wind stress occur during winter, sinking in the winter season is more active than at other times of the year. Therefore it is necessary to examine the changes in surface properties of the winter season. Fig. 5.12 is reproduced in Fig. 5.13 for the boreal winter season (December, January, and February). In general the change of surface properties is larger than those averaged over an entire year. The spatial pattern is similar in both cases, however magnitude of change for each field (right panel) is larger than those shown in Fig. 5.12. Both cases suggest the important influence of salinity on the surface density,

particularly in the Labrador Sea.

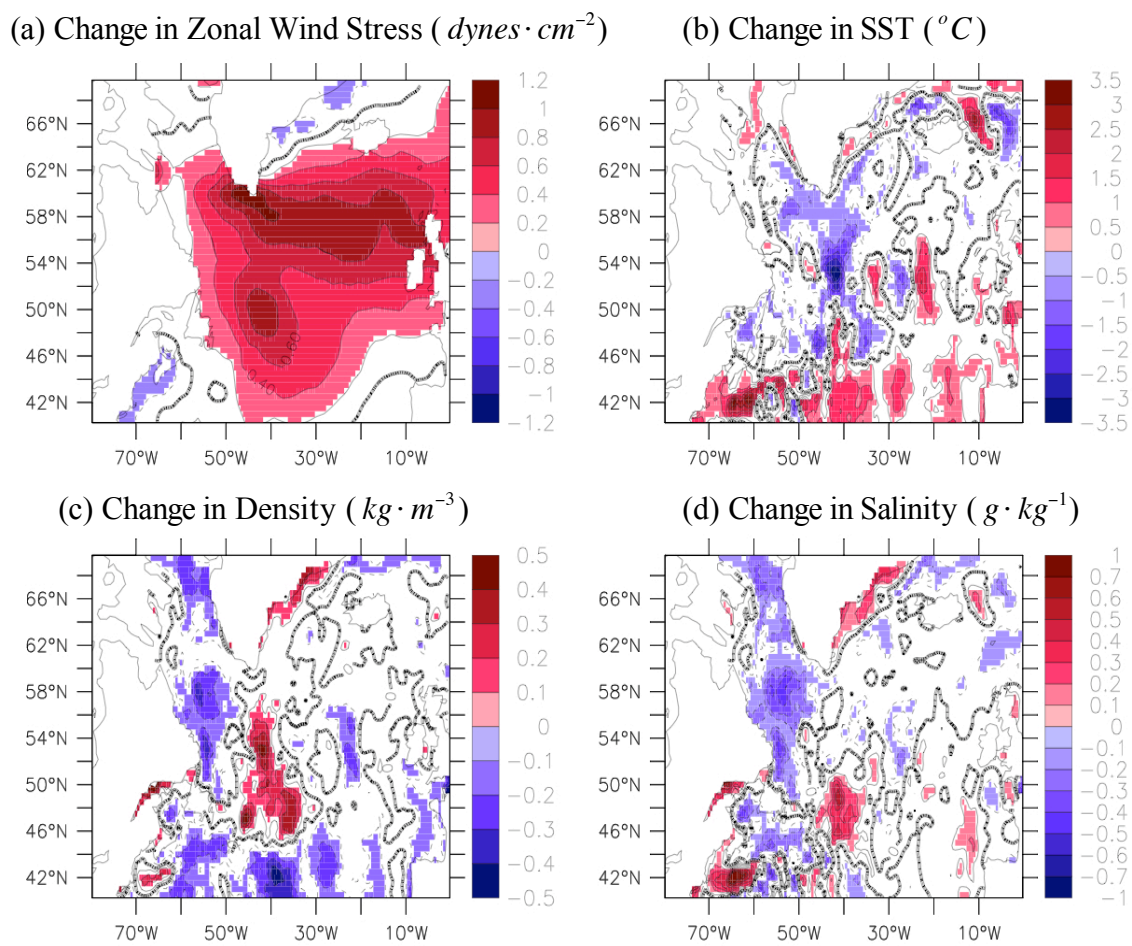


Fig. 5.13 Same as Fig. 5.12 except for boreal winter case.

b. Temporal Characteristics

It is important to examine the relationship between zonal wind stress τ_x and surface density of seawater since it may be crucial to understanding of the Atlantic MOC change with any change in τ_x . The largest changes in zonal wind stress, SST, surface density of seawater and salinity occur in the band from $50^\circ N - 62^\circ N$ of the North Atlantic Ocean (see Figs. 5.12, 5.13). The time series of $50^\circ N - 62^\circ N$ averaged zonal wind stress, SST, surface density of seawater, and salinity is shown in Fig. 5.14 as a function of longitude. The seasonal cycle has been removed. There is an enhanced zonal wind stress in the period from 1960-1995 and a weakening in the period from 1995-2004. As a result of strengthening zonal wind stress, negative anomalies of SST appear until the year 1995 when τ_x becomes negative. The variation of SST is correlated with the strength of the zonal wind stress, with positive anomalies of zonal wind stress correspond to negative anomalies of SST. Feedback can be used to explain the wind-SST negative correlation. Strengthening of zonal wind stress gives rise to enhanced evaporation, reducing SST. Alternatively, positive anomalies of SST in the North Atlantic Ocean may lead to a weak meridional gradient of SST between the lower latitude and higher latitude (right panel in Figs. 5.12, 5.13), which produces a weak atmospheric circulation overlying the ocean surface, hence a weak wind stress is formed. Since surface density of ocean is determined by SST and salinity variation, wind stress can affect the change in surface density through the change of SST and transport of salt.

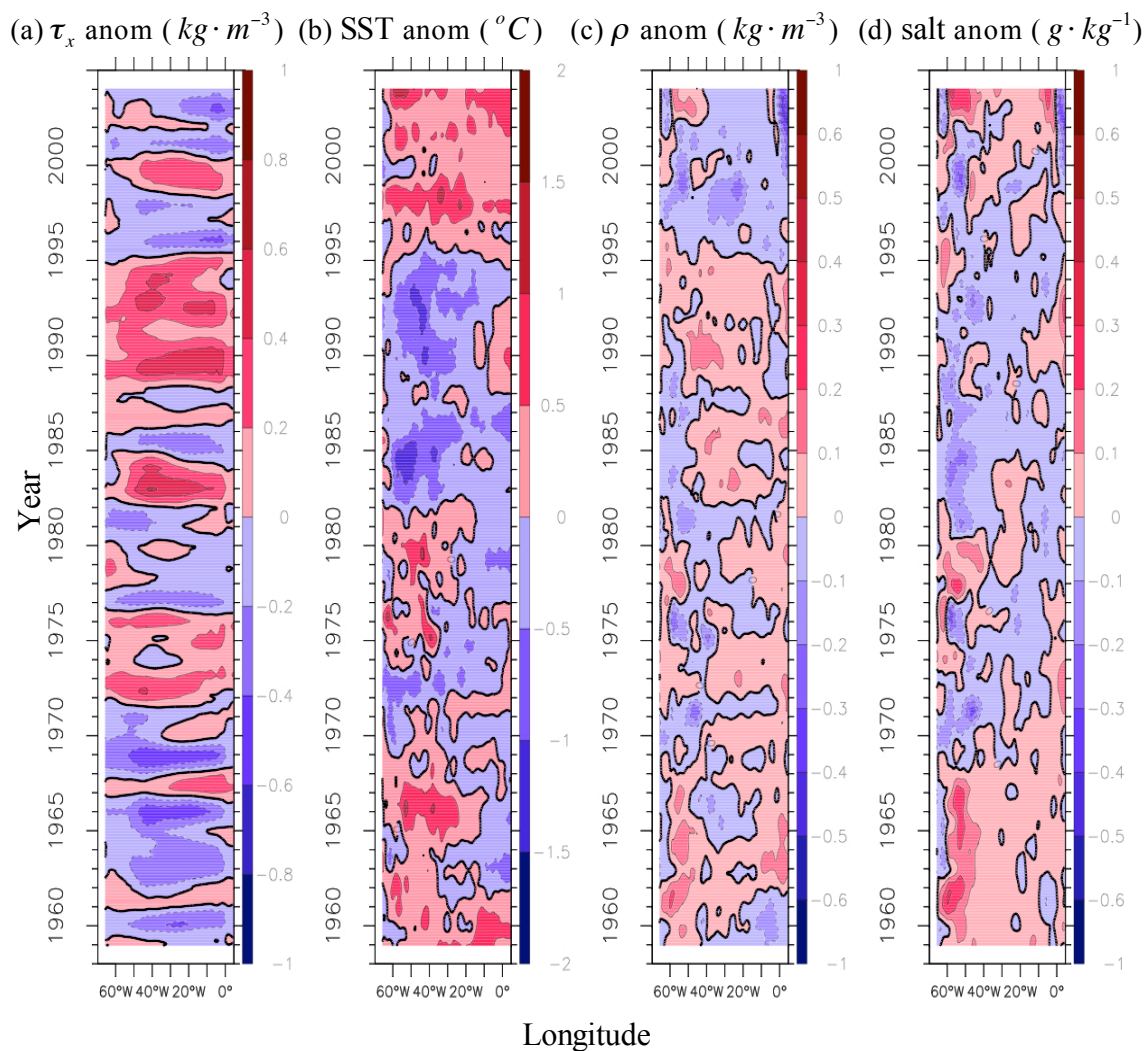


Fig. 5.14 Evolution of anomalous zonal wind stress τ_x in $dynes \cdot cm^{-2}$, SST in $^{\circ}C$, surface density ρ in $kg \cdot m^{-3}$ and surface salinity (in $g \cdot kg^{-1}$) of the North Atlantic Ocean for the period 1958-2004 averaged from $50^{\circ}N - 62^{\circ}N$.

The region of the North Atlantic Ocean between $50^{\circ}N - 62^{\circ}N$ the ocean water generally tends to become fresher (see Fig. 5.14), especially after the 1970s. Its largest

salinity anomaly apparently occurs in the region west of $50^{\circ}W$ from $+0.4 \text{ g} \cdot \text{kg}^{-1}$ in 1961 to $-0.4 \text{ g} \cdot \text{kg}^{-1}$ in 2000. The large change in salinity in the region west of $50^{\circ}W$ is linked to processes of freshwater transport in the Labrador Sea, which connects the Arctic Ocean with its considerable sea ice to the North Atlantic Ocean. Interestingly, in the region east of $50^{\circ}W$ the decrease of salinity is much smaller than that west of $50^{\circ}W$. As a result, surface density in the region west of $50^{\circ}W$ is primarily controlled by salinity variability rather than by SST variability. In contrast, in the region east of $50^{\circ}W$, density is largely determined by SST variability rather than by salinity variability. The difference in change of salinity may represent different mechanisms of freshwater transport such as surface ocean circulation and sources of fresh and salty water. In the region west of $50^{\circ}W$, salinity variability is fundamentally governed by the fresh water transport from the Arctic Ocean via the Labrador and East Greenland Currents. Melting glaciers and increased precipitation, both associated with greenhouse warming, have enhanced continental runoff into the Arctic and sub-Arctic seas. This region is less affected by salt transport via the Gulf Stream from the subtropical ocean. In contrast, in the region east of $50^{\circ}W$, salinity variability is determined by salt transport from the Gulf Stream and by the southward freshwater transport in the southward component of the subpolar gyre in the subpolar basin. Therefore, in the region of the Irminger and Iceland Basins, freshening of water is smaller than in the region west of $50^{\circ}W$ because these two processes have opposing effects on salinity. The different mechanisms that control density variability in these two regions are more pronounced in boreal winter as indicated in Fig. 5.15. One striking feature of salinity variability is that

after the year 2000, a positive anomaly of salinity is found. This high salinity in the North Atlantic inflow to the Nordic seas and the Arctic Ocean has been described by Hátún et al. (2005). This increase salt anomaly may counteract the long-term increase in freshwater supply to the Nordic seas and the Arctic Ocean and stabilize North Atlantic THC.

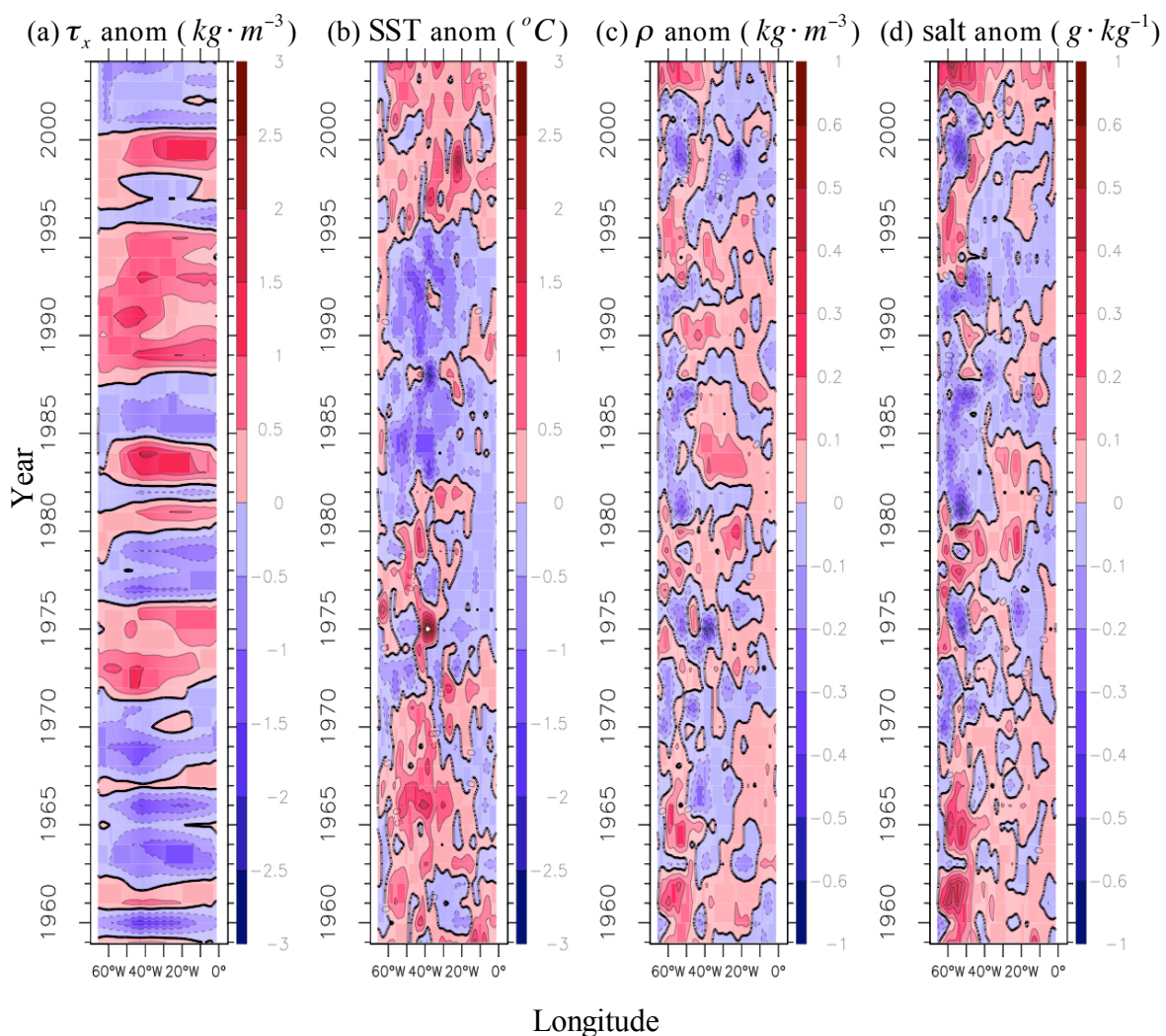


Fig. 5.15 Same as in Fig. 5.14 except for boreal winter case.

In order to partition the effect of salinity and temperature on the surface density change, we calculated density in two different ways. First, we use modeled salt data but use the climatology of SST in the calculation of density. In the second way, we use modeled SST data but use the climatology of salt. The difference between the two calculations is shown in Fig. 5.16. Fig. 5.16 also shows density calculated with modeled SST and salt. In the region west of $50^{\circ}W$ the change in density due to salinity variations is much greater than that due to the SST variations, so that salinity change dominates the density change (left panel). Conversely, in the region east of $50^{\circ}W$, cooling gives rise to a density increase and SST change dominates in density variability (right panel). The combined effects of salinity and temperature create lighter water in the region west of $50^{\circ}W$ and heavier water in the region east of $50^{\circ}W$. After 1995, there is lighter water throughout both regions. However, the linear change of surface density in the region west of $50^{\circ}W$ is more important than that east of $50^{\circ}W$, as shown in Figs. 5.12 and 5.13. The tendency of change in surface density of ocean water could weaken MOC. There is another important source of density forcing that can affect sinking process, which is the overflow of cold water from the Nordic seas into the northern North Atlantic Ocean. This source is believed to be largely responsible for the formation of North Atlantic Deep Water (NADW), whose change is critically important to the MOC's strength at high latitudes.

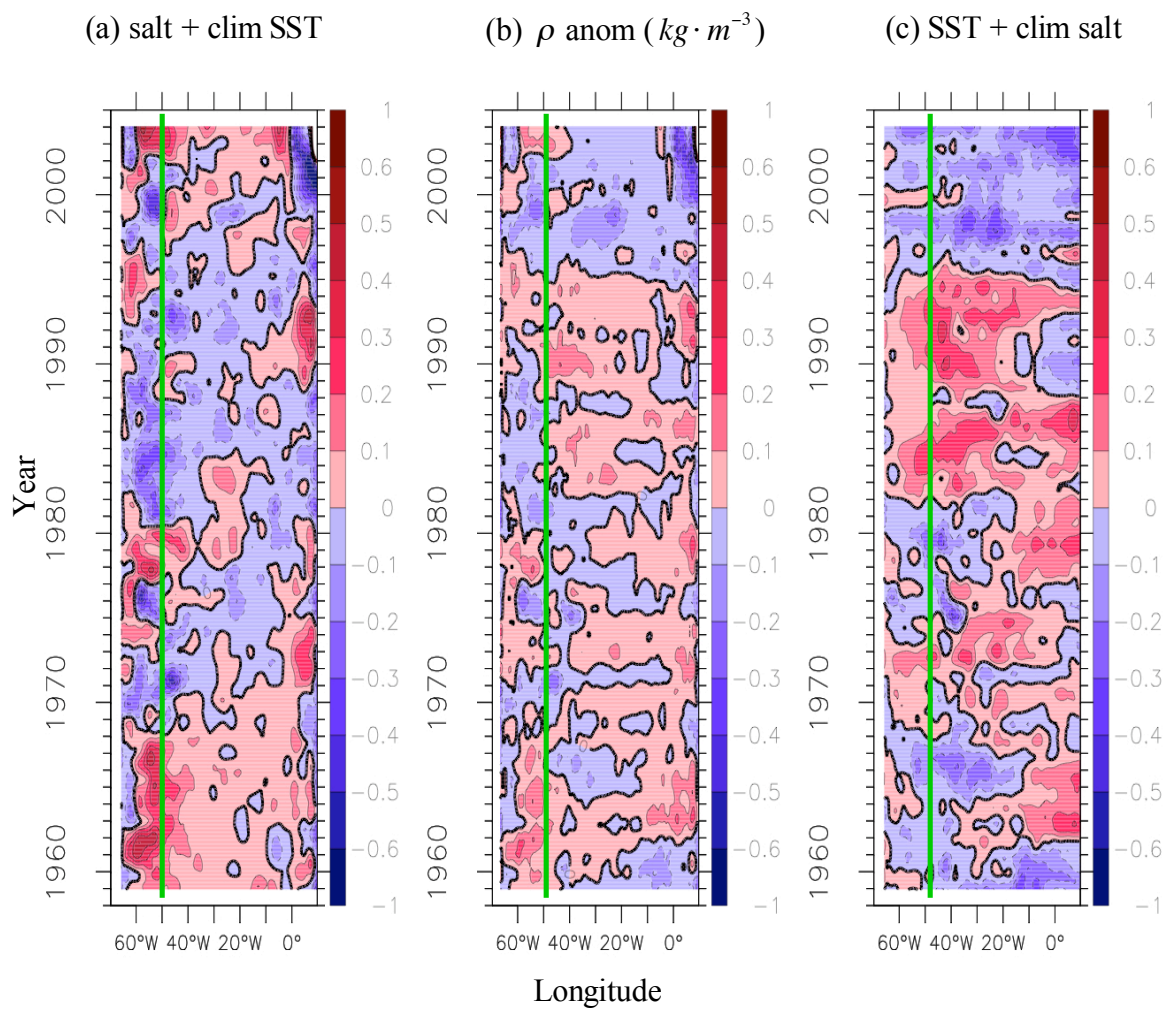


Fig. 5.16 Temporal evolution of anomalous density averaged from $50^{\circ}N - 62^{\circ}N$ of the North Atlantic Ocean is calculated three ways. The left hand panel uses climatological SST and the right hand panel uses climatological salinity. The central panel uses time dependence (actual) temperature and salinity.

c. *The Roles of the Overflows*

The Nordic Seas and the Arctic have been regarded as a reservoir whose exchanges with the rest of the world oceans are mainly governed by hydraulics since shallow convective processes keep the waters at the sill depth “topped up” (Bacon, 1998). The overflow and descent of cold, dense water in the Nordic seas from the sills of the Denmark Strait and the Faroe Bank Channel into the North Atlantic Ocean is essential to the formation of NADW, a driving source for the Atlantic thermohaline circulation. Very cold water at the Denmark Strait sill depth of about 600m forms that is estimated to be $3.0 \pm 0.2 Sv$, at Faroe-Bank Channel, forms $3.5 \pm 0.1 Sv$ (Curry et al. 2005). Both of which combine to form NADW. The two main overflows across the Greenland-Scotland Ridge and their spreading pathways to the Labrador Sea are schematically shown in Fig. 5.17. The overflows also help drive the inflow of warm, saline surface water into the Nordic seas. These two major flows (one through Denmark Strait and another through Faroe-Bank Channel) combine along the East Greenland shelf to form the deep and bottom waters below the convectively formed mode water (i.e., Labrador Sea Water, LSW) in the intermediate layer of Labrador Basin that drive the abyssal limb of the Atlantic MOC. Observational studies (Dickson et al. 2002; Curry and Mauritzen 2005) indicate the considerable freshening of the deep North Atlantic Ocean over the past four decades. Furthermore, in the Atlantic Ocean systematic freshening at both poleward ends is contrasted with large increases of salinity in the upper water column at low latitudes (Curry et al., 2003). The overflow from the Nordic seas into the Atlantic Ocean through

the Faroe Bank Channel is found to have decreased by at least 20% relative to 1950 (Hansen et al. 2001). However this 20% reduction in overflow strength was not persistent, as argued by Curry et al. (2005). Furthermore, no sustained long-term trend in the Denmark Strait overflow has been reported. This observational evidence suggests that transport of the overflows may be weakening. This could lead to a slowdown of the abyssal limb of the Atlantic MOC. The long-term strength of the overflow is dependent on the compensating inflow of saline water that could give rise to surface density change in the Nordic Seas. Latif et al. (2006) argue that the change in the MOC ($\sim 1 Sv$) due to the dilution and simultaneous cooling is well within the range of the variability ($\pm 1.5 - 3.0 Sv$) associated with the NAO-driven changes in LSW formation during the last century in their model results.

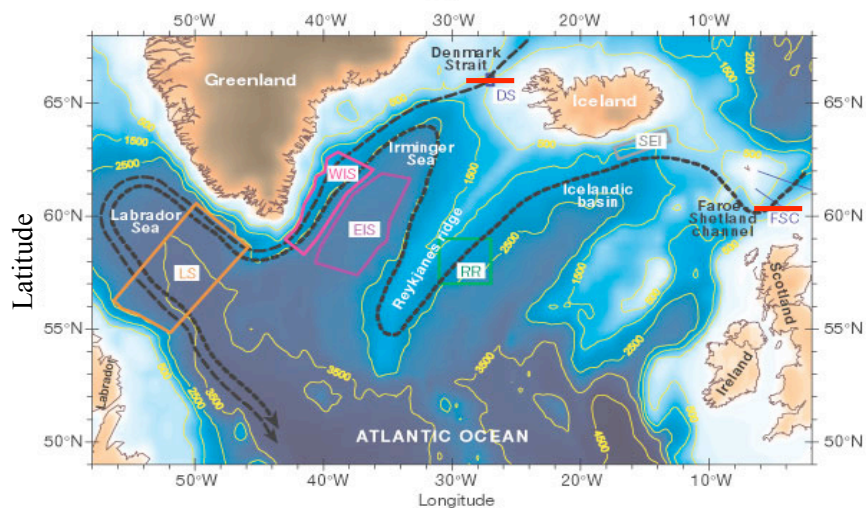


Fig. 5.17 Two main overflows across the Greenland-Scotland Ridge and their spreading pathways to the Labrador Sea (heavy dashed lines). (From Dickson et al., 2002)

The mean meridional currents and temperature across the Denmark Strait at $66.25^{\circ}N$ and the Faroe Bank Channel at $60.75^{\circ}N$ are shown in Fig. 5.18 for the period 1958-2004. The reanalysis has a strong southward transport of cold water pass across the sills. The volume flux of the overflows through Denmark Strait and the Faroe Bank Channel is shown in Fig. 5.19. Also shown is the sum of the two. The overflow is defined here as water colder than $3.0^{\circ}C$ with densities $\sigma_t (= \rho_t - 1000)$ in excess of 27.9. We also compute the flux of water that is colder than $0.3^{\circ}C$ in these two major sills which is shown as a dashed curve. This mode water is thought to account for about two-thirds of the total overflow flux (Hansen et al. 2001). However, in our reanalysis, this fraction is about 50% (see Table 2). There is a sustained reduction of about 0.4 Sv in the southward transport of overflow across the Denmark Strait giving a rate of $-0.087 Sv \cdot decade^{-1}$ during the last four decades. By contrast, the transport of the overflow in the Faroe Bank Channel increases slightly by 0.09 Sv for the period 1958-2004 at a rate of $0.019 Sv \cdot decade^{-1}$. This is in contrast with previous studies, which do not have sustained changes in the overflow rate in the Denmark Strait (Dickson and Brown 1994; Curry and Mauritzen, 2005), though the overflow rate in the Faroe Bank Channel was found to have decreased by about 20% from 1950 to 2000 (Hansen et al. 2001). Note that the surface density in the North Atlantic Ocean east of $50^{\circ}W$ does not change much (Figs. 5.12, and 5.13), except it does decrease in the last 15 years (Fig. 5.14). This implies that the entrainment rate over this region may not change significantly and the production rate of the NADW in the northern North Atlantic due to entrainment process may not alter sufficiently to affect the strength of the North Atlantic THC.

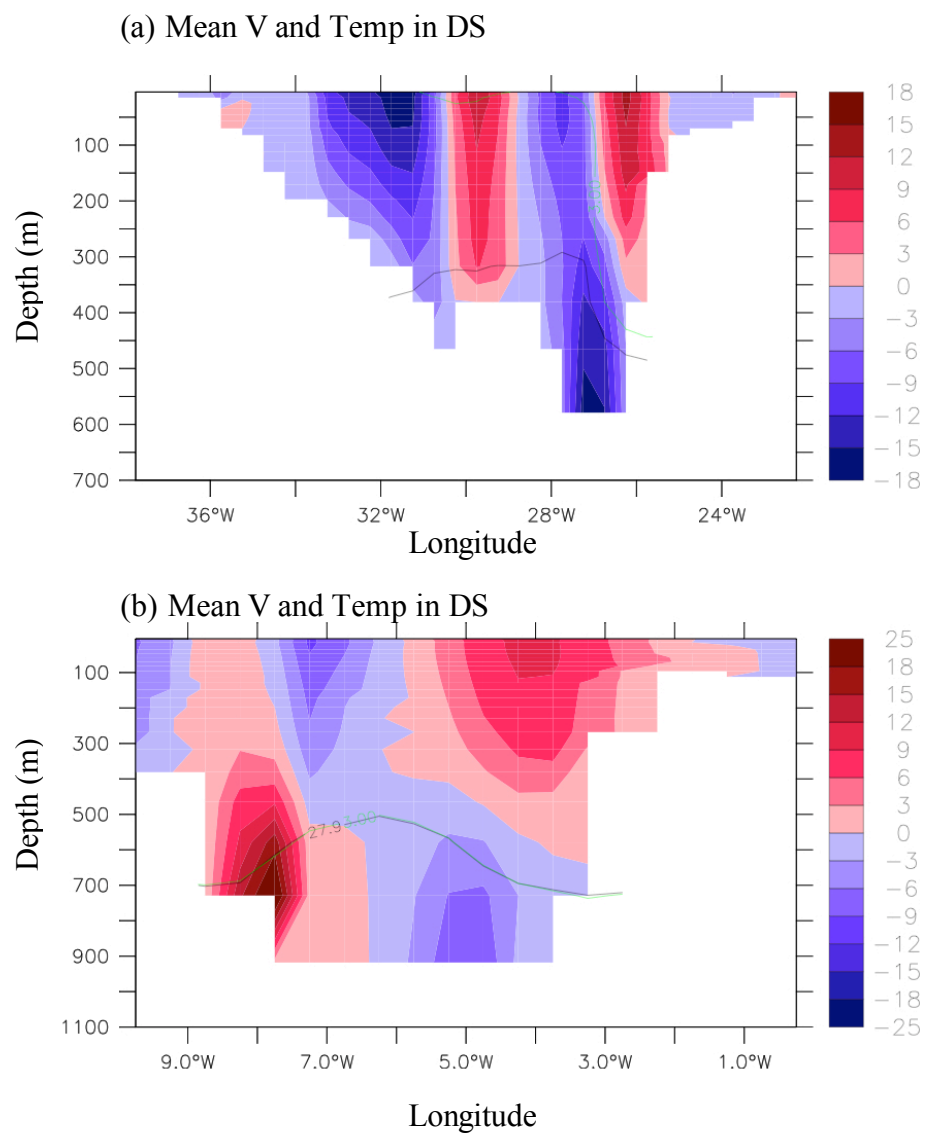


Fig. 5.18 Meridional current and temperature across the Denmark Strait at $66.25^{\circ}N$ (a) and Faroe Bank Channel at $60.75^{\circ}N$ (b) for the period 1958-2004.

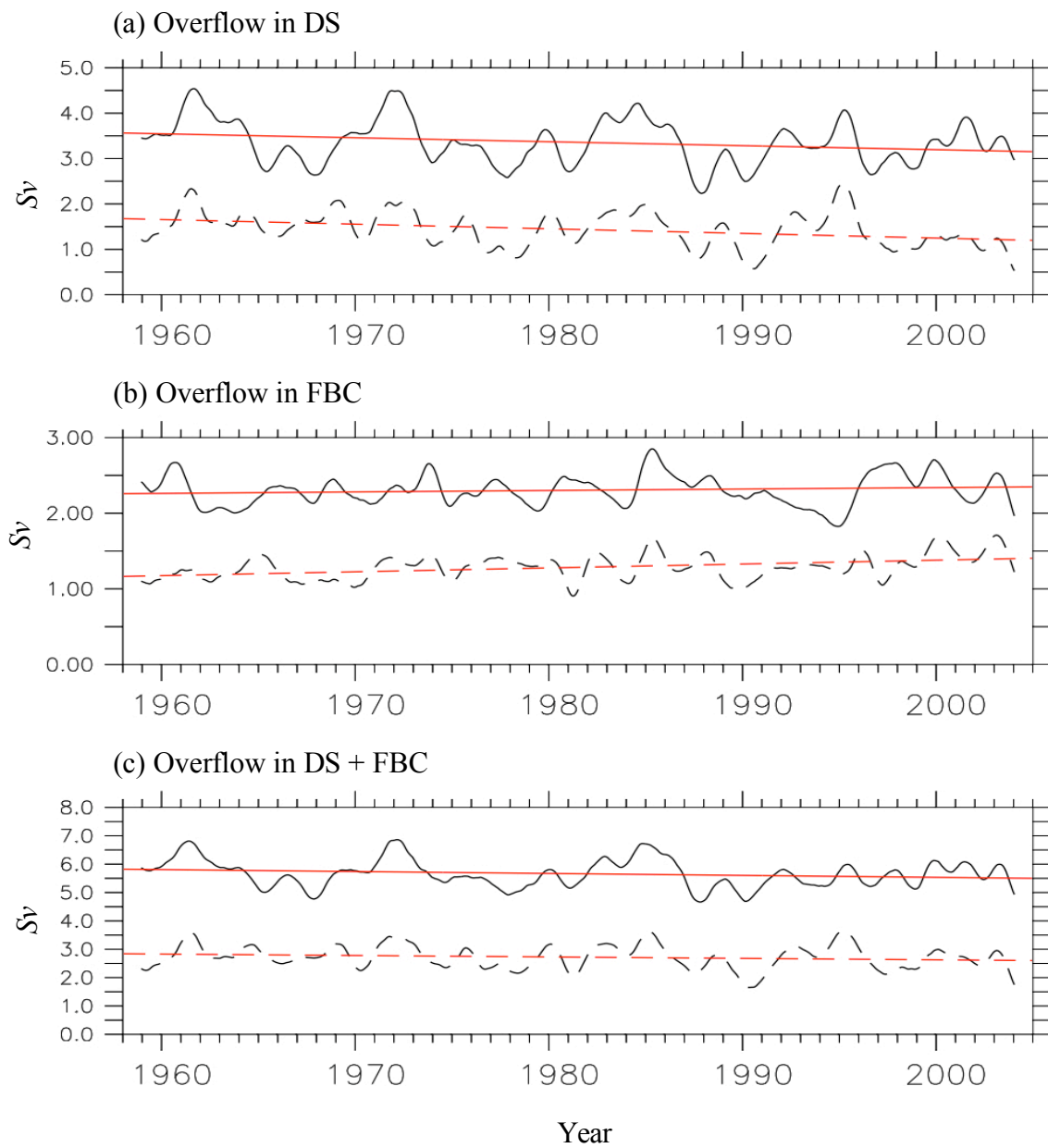


Fig. 5.19 Volume flux of overflow through DS (a), the FBC (b), and sum of DS and FBC (c).

Thus the flux of the NADW in the northern North Atlantic Ocean for the period 1958-2004 is largely determined by the change of the overflows. Note that the sum of the Faroe Bank Channel overflow ($\sim 2.30 Sv$) and the Denmark Strait overflow ($\sim 3.36 Sv$) which accounts for about one-third of the total NADW flux ($\sim 18 Sv$), decreases up to $0.32 Sv$ at an average rate of $-0.068 Sv \cdot decade^{-1}$. This represents a 5.8% reduction from 1958 to 2004 in the volume flux of the overflows across the Denmark Strait and Faroe Bank Channel sills. This trend is larger if applied to a mode water colder than $0.3^{\circ}C$. Thus there is a total reduction of $0.24 Sv$ in mode water which has a mean transport of $2.70 Sv$. This implies a 9.3% decrease of southward flux of overflow colder than $0.3^{\circ}C$ from 1958 to 2004. This reduction of overflow flux is consistent with the steadily declining salinity in the overflows (Curry and Mauritzen 2005). However, this decline of salinity in the Nordic Seas Overflows may reverse because of record-high salinities that have been observed in the Atlantic inflow to the Nordic Seas and the Arctic Ocean during the past decade (Hátún et al. 2005). This reversal is consistent with our results (Figs. 5.14, and 5.15). Hátún et al. (2005) further argue that the observed high salinity of the Atlantic inflow is attributable to dynamic changes of the North Atlantic subtropical and the subpolar gyres. Whether the change in the intensity of the overflows due to the density contrast across the ridge has an enduring impact on the Atlantic THC calls for climate models with high resolution and long-term observational systems to identify potential changes in our climate system. Generally, our reanalysis suggests that the change in the volume flux of the Nordic Seas Overflows appears to have decreased slightly from 1958 to 2004, which is summarized in Table 5.1.

Table 5.1 Volume flux of the overflow across the Denmark Strait and the Faroe Bank Channel.

Location	Definition	Mean*(Sv)	Trend#(Sv · decade ⁻¹)	Change (1958-2004)(Sv)
DS	T < 3.0°C	+3.36	-0.087	-0.41
	T < 0.3°C	+1.42	-0.102	-0.48
FBC	T < 3.0°C	+2.30	+0.019	+0.09
	T < 0.3°C	+1.28	+0.051	+0.24
DS+FBC	T < 3.0°C	+5.66	-0.068	-0.32
	T < 0.3°C	+2.70	-0.051	-0.24

*: Southward transport is positive.

#: “+” denotes positive trend of southward flux.

5.3.2 Causes of Strengthening MOC at Low – mid Latitudes

The linear trend of Atlantic MOC strength shown in Figs. 5.6 and 5.7 demonstrates that at low-mid latitudes, the MOC becomes enhanced, which is the opposite sign of what happens at high latitudes. Surface water in the mid latitude Atlantic generally becomes lighter (see Figs. 5.12 and 5.13) due to the warming effects even though salinity increases. Strong stratification in the subtropical regions prevents water in the surface layer from sinking into the layers below.

Fig. 5.20 shows the long-term mean and difference between two-decade periods in surface wind stress, curl of wind stress and gyre circulation. Between 20°N and 45°N, the atmospheric circulation changes are shown by the wind stress vector and its curl. In

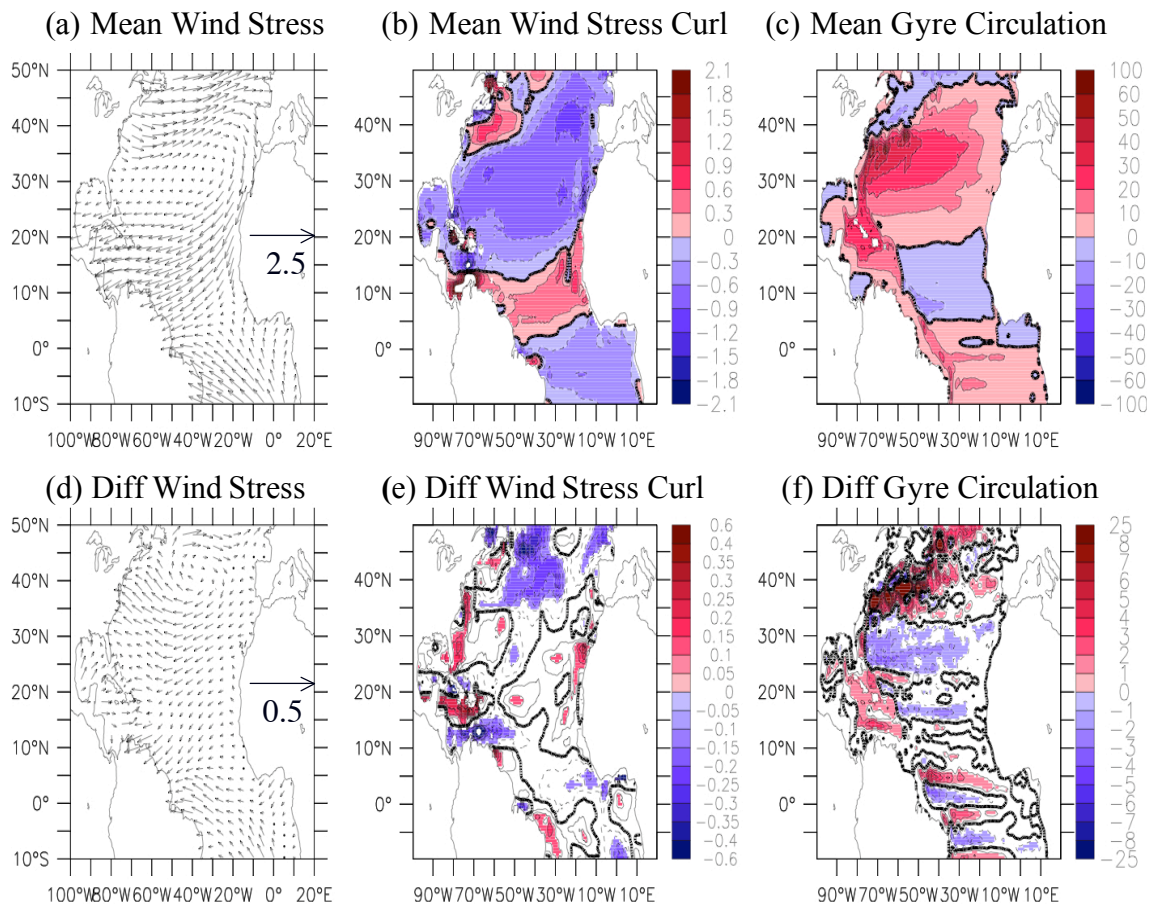


Fig. 5.20 Mean and difference of the Atlantic surface wind stress, curl of wind stress, and gyre strength for the period 1958-2001.

this region the atmospheric circulation becomes strengthened, particularly between $35^{\circ}N$ and $45^{\circ}N$ (see Figs. 5.20d and 5.20e). As a consequence, there is a considerable convergence of flow due to change in the curl of wind stress. The resulting convergence of flow can push water down to two thousand meters, where it connects with the NADW

and moves southward. In addition there is a recirculation in the layer from the surface to 2000m, which is intensified by wind forcing and increases meridional heat transport. This recirculation may speed up due to the wind effect. Hence this speeding recirculation exerts an influence on the rate of meridional heat transport. In the tropical region, the change in curl is not of the wind stress is not as large as at middle latitudes and because the thermocline in the tropics is shallow, enhanced easterlies in both hemispheres produce persistent strong Ekman divergence of flow and strong upwelling near the equatorial region (Fig. 5.20d). This gives rise to a stronger STC that affects the upper layer to a depth of 1000 meters.

What causes the change in atmospheric circulation? One possibility is that the atmospheric circulation pattern over shifted northward the North Atlantic Ocean. Fig. 5.21 displays the mean state and its change of wind stress between two-decade periods in the wind stress (Figs. 5.21a and 5.21b). The change between the two-decade periods in the zonal averaged τ_x as a function of latitude is also illustrated to provide evidence that there is a northward shift in the atmospheric circulation over the North Atlantic Ocean. This northward shift of the atmospheric circulation causes wind stress anomalies particularly over the region between $30^\circ N$ and $40^\circ N$, which is shown in blue in Fig. 5.21c. The resulting shift in atmospheric circulation is 1.6° from 1958 to 2001 at a linear rate of $0.4^\circ \cdot decade^{-1}$. The amplitude change from such a shift may be important in generating wind stress anomalies, particularly at the high latitudes. However, the assessment in the fractional influence on the wind stress change due to northward shift and local amplitude change is beyond the present study.

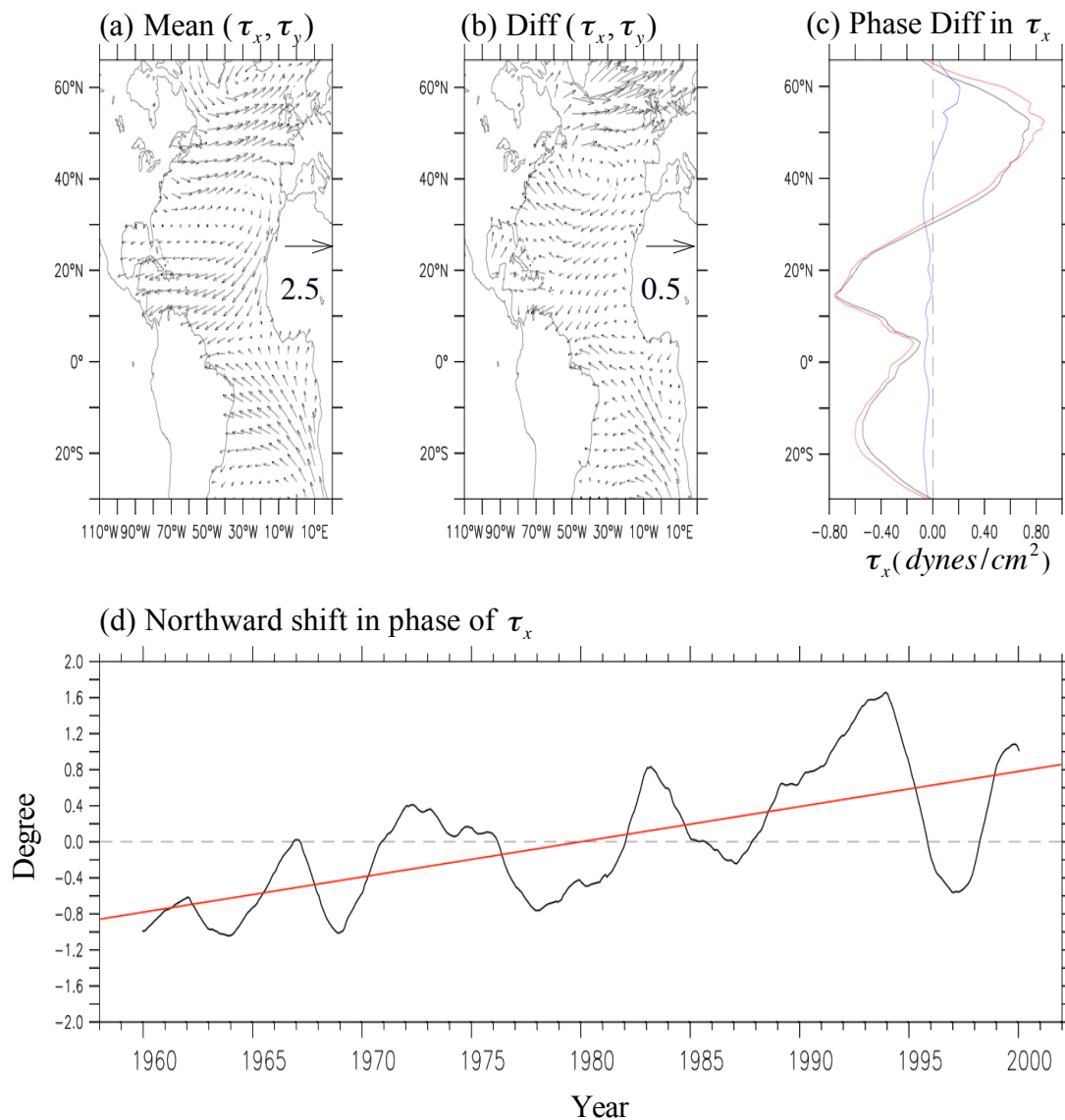


Fig. 5.21 Mean (a) and difference (b) in the wind stress over the Atlantic Ocean for the period 1958-2001. The difference between the period 1981-2001 and 1958-1980 is shown in (c). The implied meridional shift (in degree) is displayed in (d) along with its linear trend in red. There is a linear northward shift of $0.39^\circ \cdot \text{decade}^{-1}$, so there is a total northward shift of 1.56° for the period 1958-2001.

5.4 Discussion

The Atlantic MOC is usually described by the streamfunction, although the strength of the Atlantic MOC can also be defined by the peak seawater volume transport (Fig. 5.3). The definition used in this study is the peak value of streamfunction at $36^{\circ}N$. The average strength of the Atlantic MOC in the SODA reanalysis is about 18-20 Sv, consistent with other studies (Schmitz, 1995; Sun and Bleck, 2001). Results from our reanalysis reveal a trend in strength of $0.71 \text{ Sv} \cdot \text{decade}^{-1}$ of the Atlantic MOC for the recent four decades (Fig. 5.4). The Role of MOC in the heat transport is compared with that of the gyre circulation, particularly for the Pacific and Atlantic Oceans. Heat transport in the different MOC components is analyzed using pseudo-heat function. Our reanalysis suggests that meridional heat transport in the ocean is primarily in response to the MOC as opposed to that by changes in the horizontal gyre circulation (Fig. 5.4). The change in meridional ocean heat transport in the Atlantic Ocean is synchronous with local strength of the Atlantic MOC at low-mid latitudes, however at high latitude the situation is different. At high latitude there is a slight increase in meridional heat transport despite the fact that there is a weakening MOC. This oddity reflects the complex processes that control meridional heat transport at high latitudes. Since warming in the northern North Atlantic Ocean occurs in the post-1995 is synchronous with the more northward heat transport, the slight increase of heat transport (Figs. 5.6 and 5.7) is likely a consequence of warming during the previous decade (i.e., post-1995) (Figs. 5.14 and 5.15) even though MOC at high latitudes weakens.

It is surprising that MOC at high latitudes weakens while MOC at low-mid latitudes strengthens. Changes in the vertical structure of the Atlantic MOC may help explain this phenomenon (Fig. 5.11). There are four different aspects of changes of the Atlantic MOC streamfunction. The first is a weakening at high latitude centered at $58^{\circ}N$. The second is enhanced Atlantic MOC between $20^{\circ}N$ and $44^{\circ}N$ from the surface to a depth of 2500m. The third is relevant to a strengthening STC in the upper 500m between $20^{\circ}S$ and $20^{\circ}N$. Last is a feature that is likely associated with the Antarctic intermediate water which affects the layer from 500-1500m in the equatorial region.

Three possible mechanisms may explain the slight weakening MOC at high latitudes: (i) Changes in the local air-sea flux of fresh water [evaporation minus precipitation (E-P)]; (ii) Warming or cooling of the northern North Atlantic Ocean; (iii) Changes in the volume flux of the Nordic Seas Overflow into the North Atlantic Ocean through Green-Scotland Ridge, particularly across the sills of Denmark Strait and the Faroe Bank Channel. The change in surface properties in the northern North Atlantic Ocean is an important element for detecting change of the Atlantic MOC. From the reanalysis there is an evident change in the properties of northern Atlantic Ocean surface water during the recent decades. SST decreases by $1^{\circ}C$ in the northern North Atlantic Ocean (Figs. 5.12 and 5.13). Thus cooling in the North Atlantic Ocean is closely linked to strengthening of wind stress (Figs. 5.12, 5.13, 5.14, and 5.15). Cooling may arise from heat loss into the atmosphere and the southward movement of cold water from the Arctic Ocean into the Labrador Sea due to the strengthening subpolar gyre circulation. Large regions in the North Atlantic Ocean have been getting fresher since the early 1970s

(Figs. 5.12, 5.13, 5.14, and 5.15), particularly in the vicinity of the Labrador Sea. The change in salinity may be associated with greenhouse warming that melts glaciers and causes increased precipitation, and freshwater transport by ocean circulation. As a result, the surface density changes. There is an intriguing spatial feature in the change of surface density in the northern North Atlantic Ocean during the recent four decades. A greatly reduced density in the Labrador Sea (i.e., in the region west of $50^{\circ}W$) is found. This reduction in density is primarily determined by large scale freshening. In contrast, a very small increase of surface density around the Irminger Sea and Iceland Sea (i.e., in the region east of $50^{\circ}W$) is clearly seen which is associated with both freshening process and surface cooling, in which the latter probably is a local response to enhanced wind stress. The reduction in surface density in the region west of $50^{\circ}W$ is primarily controlled by salinity reduction, and the slight increase in surface density in the region east of $50^{\circ}W$ is principally determined by surface cooling (Fig. 5.16). Therefore, in the northern North Atlantic Ocean, the production rate of NADW due to ventilation and entrainment processes does not increase. On the other hand, the formation rate of LSW may slow down due to freshening in the Labrador Sea. The overflow from the Nordic Seas into the North Atlantic Ocean is one of the key components in the formation of NADW. The reanalysis suggests that there is a slowdown of the overflow across the Denmark Strait and a slight increase across the Faroe Bank Channel into the North Atlantic Ocean (Fig. 5.19 and Table 2). The overall influence of these three mechanisms leads to a slight weakening MOC in the northern North Atlantic Ocean.

Strengthened MOC in the mid-latitude Atlantic Ocean appears to be associated with

a northward shift of the atmospheric circulation (Fig. 5.21). This northward shift of surface atmospheric circulation induces an anomalous anti-cyclonic wind circulation centered at $40^{\circ}N$ over the North Atlantic (Figs. 5.20e and 5.21b) and stronger subtropical gyre (Fig. 5.20f). A similar air-sea interaction has been reported by Giese and Carton (1999) for the Pacific Ocean. As a result, an anomalous convergence of flow in the subtropical ocean is expected. This convergence of flow due to the northward shift of atmospheric circulation provokes anomalous downward motion and intensifies the vertical circulation cell below $40^{\circ}N$. Therefore the zonally integrated northward flow in the upper layer ($\sim 1000\text{m}$) in the subtropical Atlantic Ocean accelerates. At low latitudes ($20^{\circ}S$ - $20^{\circ}N$), the Atlantic STC intensifies due to strong persistent Ekman divergence by surface wind stress (Figs. 5.20d, 5.21b, and 5.21c) which induces more poleward transport of warm water in the upper layer from the equator, particularly in the north tropical Atlantic Ocean. Therefore northward heat transport is reinforced in the north tropical Atlantic Ocean and is mitigated in the south tropical Atlantic Ocean.

The mechanisms of change in the meridional ocean heat transport in the Atlantic Ocean associated with the Atlantic MOC are summarized in Fig. 5.22. The reanalysis suggests that the responsible processes for the variability and the trend of ocean heat transport in the Atlantic Ocean vary in the different regions.

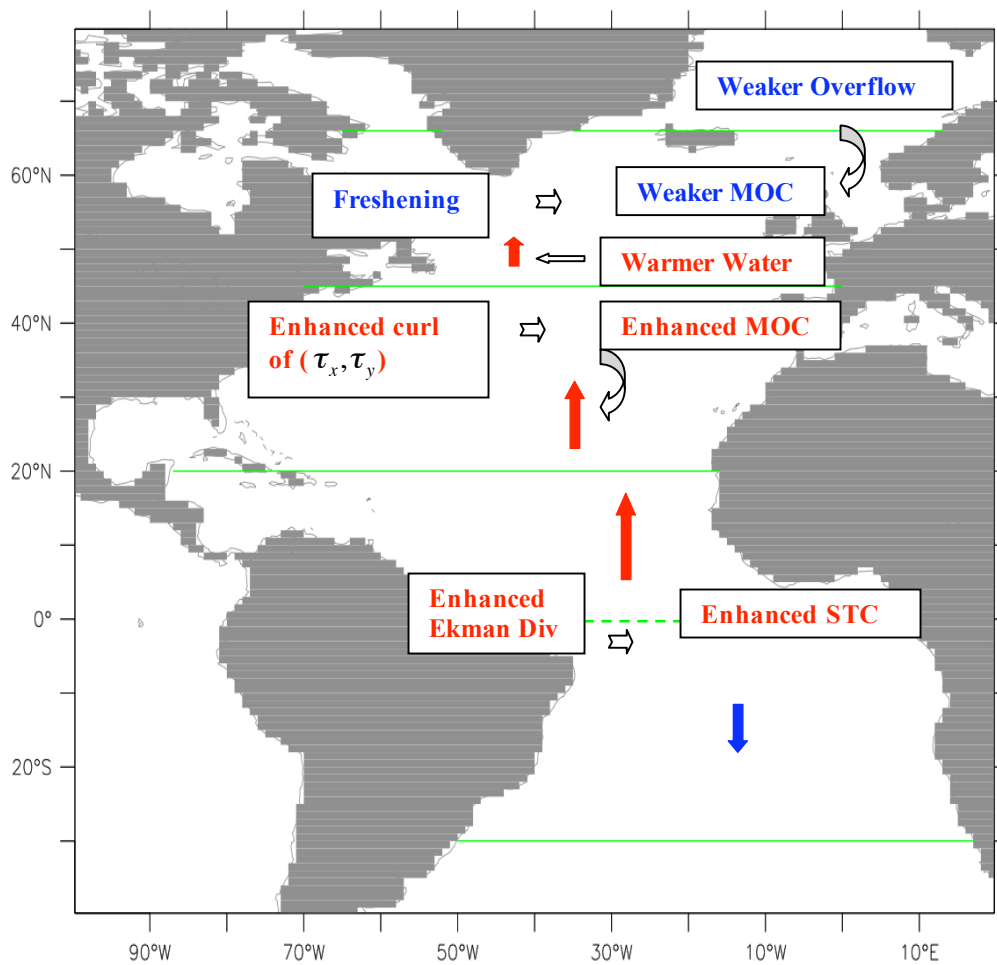


Fig. 5.22 Schematic map of mechanisms of change in the meridional transport of heat in the Atlantic Ocean for the period 1958-2004. Red (blue) arrows denote the increase (decrease) of meridional heat transport with respect to its prevalent mean transport.

CHAPTER VI

SUMMARY AND DISCUSSION

6.1 Summary

A recently completed ocean reanalysis called SODA is used to examine the global ocean heat transport for the period 1958-2004. Heat transport is described by exploring its mean, its trend, and its interannual to decadal variability. A simple heat decomposition method is used to explore the sources of heat transport variability. There are three major conclusions that result from this study.

First, robust interannual to decadal variability of ocean heat transport is found in the global ocean (Fig. 3.8), particularly in the Atlantic Ocean. A simple heat decomposition analysis indicates that it is ocean dynamics (the $\bar{v}'\bar{T}$ process) that dominates the fluctuation of ocean heat transport in the oceans. However, at high latitudes in the Pacific and Atlantic Oceans, thermal effects (the $\bar{v}\bar{T}'$ process) in ocean heat transport become important. Especially in the northern North Atlantic Ocean, fluctuation of temperature (the $\bar{v}\bar{T}'$ process) is more important than that of ocean currents. In the Gulf Stream and its extension region of the Atlantic Ocean and the Kuroshio and Kuroshio extension region of the Pacific Ocean, eddies become important in ocean heat transport. In contrast with the mid-latitude oceans, the change in temperature (the $\bar{v}\bar{T}'$ process) appears to be slightly more important than change in currents in the zonal transport of

heat in the Southern Ocean (Fig. 3.11). A study of the vertical structure of ocean heat transport shows that interannual to decadal variability of ocean heat transport in the upper 1000m exhibits a good representation of ocean heat transport over the entire depth of the oceans (Figs. 5.8 and 5.9). More interestingly, in the Atlantic Ocean southward movement of water in the deep layer due to the deep water formation yields a southward transport of heat of $0.2PW$ that is relatively large compared to that in the Pacific and Indian Oceans (Fig. 3.4). Analysis of ocean heat transport on density layers suggests that transport of heat in the mixed and shallow layers ($\sim 1000m$) is crucially important to interannual to decadal variability and its trend (Fig. 3.4). Ocean heat transport in the mixed and shallow layers generally reflects the important roles of Ekman and geostrophic currents in ocean heat transport, particularly in the tropical oceans (Figs. 3.4, 3.5, 3.6, 3.7, 3.13, and 3.14). Overall the mean heat transport by Ekman currents is largely compensated by the mean transport of heat induced by geostrophic currents (Figs. 3.5 and 3.13). At high latitudes in the Northern Hemisphere, processes other than Ekman currents and geostrophic currents become more important (Figs. 3.13 and 3.14).

Second, the reanalysis provides an estimate of change in the world ocean heat content which is similar to a previous study by Levitus et al. (Fig. 4.1). However, change in the heat storage rate is not important when compared with the divergence of heat transport. Results from a simple heat budget analysis of the North Atlantic Ocean indicate that the change in the convergence of heat transport by ocean currents is much larger than that in heat storage rate (Fig. 4.5), with the former ($1.4 W \cdot m^{-2} \cdot decade^{-1}$) almost three times larger than the latter ($0.5 W \cdot m^{-2} \cdot decade^{-1}$). As a result, in the North

Atlantic there is an increasing heat loss into the overlying atmosphere at a rate of $0.9 W \cdot m^{-2} \cdot decade^{-1}$. Therefore, it is the change in the convergence/divergence of heat transport by ocean currents that dominates the long-term change in the surface heat flux between ocean and atmosphere. However, at interannual to decadal scales, variability of surface heat flux is synchronous with that of heat storage rate (Fig. 4.5).

Third, climate mechanisms for the change in ocean heat transport of the Atlantic Ocean in the past four decades are examined. Ocean heat transport is found to be closely associated with the vertical MOC rather than the horizontal gyre circulation (Figs. 5.4 and 5.5). The reanalysis suggests that change in meridional heat transport in the Atlantic Ocean is closely linked to the change in the strength of the Atlantic MOC (Figs. 5.6 and 5.7). A small increase in meridional heat transport north of $50^{\circ}N$ seems to be at odds with the slightly weakening MOC over there. This oddity reflects the complex processes that control the change of heat transport at high latitude. At high latitude the effect of recent warming in the ocean heat transport grows and becomes comparable to the impact induced by the reduced MOC (Fig. 3.11a). The slight weakening of MOC in the northern North Atlantic Ocean results from freshening in the Labrador Sea (Figs. 5.12 and 5.13) and the slightly reduced production of NOSW (Fig. 5.19, Table 2). In the mid-latitude ocean, an increased northward heat transport is found which is related to the simultaneous increase of the Atlantic MOC (Figs. 5.5, 5.6 and 5.7). The increase in the strength of the Atlantic MOC appears to be strongly associated with the northward shift of the atmospheric circulation (Fig. 5.21) which produces a strong convergence flow in the ocean (Fig. 5.20), reinforcing the circulation cells to a depth of 3000m (Fig. 5.11). A

reduced northward heat transport in the south tropical Atlantic Ocean and an increased northward heat transport in the north tropical Atlantic Ocean (Figs. 5.6 and 5.7) are most likely induced by a strengthened STC (Fig. 5.11). The enhanced STC is primarily driven by stronger Ekman upwelling in the equatorial region, which is closely associated with intensified easterlies (Fig. 5.21b).

6.2 Discussion

The reanalysis suggests that variability and the trend of meridional ocean heat transport are primarily determined by the MOC. It is true that the strength of the Atlantic MOC at each latitude varies, so an interesting question arises: Is there a good variable (index) representing a uniform change in the Atlantic MOC? Some studies (e.g., Latif et al., 2006) take advantage of the inter-hemispheric SST anomaly pattern in the Atlantic and use the difference of SST between the North and South Atlantic. Other studies (e.g., Boning et al., 2006; Drijfhout and Hazeleger, 2006) do not use a uniform index to describe the Atlantic MOC but select the deviations from the time-mean MOC at each latitude as an indicator of the strength of the Atlantic MOC. In this study, we choose anomalies of the maximum Atlantic MOC streamfunction at $36^{\circ}N$ is used as an index to describe the change of the Atlantic MOC (Fig. 5.3c). This selection is based on the assumption that there is no significant shift in the Atlantic MOC, therefore the sign of anomalies at this location is the same at other latitudes. This assumption is supported (Fig. 5.6a) for most of the ocean except at high latitudes. Hence the assessment of ocean

heat transport in response to the Atlantic MOC in Fig. 5.4 is good except at high latitudes. The reanalysis also indicates a slight weakening of MOC in the northern North Atlantic Ocean. The result that the strength of the Atlantic MOC at high latitudes and low latitudes does not occur synchronously may reflect somewhat independent driving forces. For example, a slight weakening MOC in high latitudes stems partly from the freshwater discharge in the Labrador Sea (Figs. 5.12 and 5.13) and partly from the slowdown of overflow from the Nordics Seas (Fig. 5.19, Table 2). In contrast, strengthening of the Atlantic MOC at low-mid latitudes primarily results from response to anomalous atmospheric circulation (Figs. 5.20 and 5.21).

The different responses of meridional ocean heat transport to the Atlantic MOC at high and low-mid latitudes (Figs. 5.6 and 5.7) indicate that a weakening MOC at high latitude does not necessarily mean a weak northward heat transport there. Variability of temperature also becomes important for the northward heat transport in the northern North Atlantic Ocean (Fig. 3.11a). Therefore, as we examine the transport in the northern North Atlantic Ocean, we may have to pay attention to the change of temperature.

One important caveat in the present study is that the number of observations of salinity in the ocean in the data assimilation is much fewer than those of temperature. However, dilution of the northern North Atlantic Ocean in the recent decades is dominated in observational studies and may result from greenhouse effects. Another caveat in this study is concerning heat budget. Since an assimilation model is used in this study, sink or source of heat can not avoid being added into ocean system in order to

constrain the model forecast by observations. Inclusion of sink or source of heat may contaminate surface heat flux if sink or source is huge. Therefore we advise with caution evaluate our conclusion. We will have a new run that will keep the sink and source terms in the model output. Finally, that trend of heat transport in the world ocean in this study is calculated based on reanalysis datasets of relatively short duration (1958-2004). Therefore the question of whether the resulting trend of oceanic heat transport is caused by a secular trend in the Atlantic MOC or is due to decadal variability of ocean climate still remains.

REFERENCES

- Adler, R. F., G. J. Huffman, A. Chang, R. Ferraro, P.-P. Xie, J. Janowiak, B. Rudolf, U. Svhneider, S. Curtis, D. Bolvin, A. Gruber, J. Susskind, P. Arkin, and E. Nelkin, 2003: The Version-2 Global Precipitation Climatology Project (GPCP) Monthly precipitation analysis (1979-present). *J. Hydrometeorol.*, **4**, 1147-1167.
- Bacon, S., 1998: Decadal variability in the outflow from the Nordic Seas to the deep Atlantic Ocean. *Nature*, **394**, 871-874.
- Barnett, T. P., D. W. Pierce, and R. Schnur, 2001: Detection of anthropogenic climate change in the world's oceans. *Science*, **292**, 270-274.
- , —, K. M. AchutaRao, P. J. Gleckler, B. D. Santer, J. M. Gregory, and W. M. Washington, 2005: Penetration of human-induced warming into the world's oceans. *Science*, **309**, 284-287.
- Bingham, F. M., S. D. Howden, and C. J. Koblinsky, 2002: Sea surface salinity measurements in the historical database, *J. Geophys. Res.*, **107**, 8019, doi: 10.1029/2000JC000767.
- Boccaletti, G., R. Ferrari, A. Adcroft, D. Ferreira, and J. Marshall, 2005: The vertical structure of ocean heat transport. *Geophys. Res. Lett.*, **32**, L10603, doi: 10.1029/2005GL022474.
- Boyer, T. P., C. Stephens, J. I. Antonov, M. E. Conkright, L. A. Locarnini, T. D. O'Brien, and H. E. Garcia, 2002: World Ocean Atlas 2001, Volume 2: Salinity. S. Levitus, Ed., NOAA Atlas NESDIS 49, U.S. Government Printing Office, Washington DC, 165pp.
- Bryan, K. 1962: Measurements of meridional heat transport by ocean currents. *J. Geophys. Res.*, **67**, 3403-3414.
- Bryden, H. L., D. H. Roemmich and J. A. Church, 1991: Ocean heat transport across $25^{\circ}N$ in the Pacific. *Deep-Sea Res.*, **38**, 297-324.
- , and E. C. Brady, 1989: Eddy momentum and heat fluxes and their effect on the circulation of the equatorial Pacific. *J. Mar. Res.*, **47**, 55-79.
- , and M. M. Hall, 1980: Heat transport by ocean currents across $25^{\circ}N$ latitude in the Atlantic Ocean. *Science*, **207**, 884-886.
- , and S. Imawaki, 2001: Ocean heat transport, in *Ocean Circulation and Climate*, edited by G. Siedler, J. Church, and J. Gould, pp. 474-495, Elsevier, New York.

- , H. R. Longworth, and S. A. Cunningham, 2005: Slowing of the Atlantic meridional overturning circulation at 25N. *Nature*, **438**, 655-657.
- Carissimo, B. C., A. H. Oort, and T. H. Vonder Haar, 1985: Estimating the meridional energy transport in the atmosphere and ocean. *J. Phys. Oceanogr.*, **15**, 82-91.
- Carton, J. A., G. A. Chepurin, X. Cao, and B. S. Giese, 2000a: A Simple Ocean Data Assimilation analysis of the global upper ocean 1950-1995, Part I: methodology. *J. Phys. Oceanogr.*, **30**, 294-309.
- , —, —, 2000b: A Simple Ocean Data Assimilation analysis of the global upper ocean 1950-1995, Part II: results. *J. Phys. Oceanogr.*, **30**, 311-326.
- , B. S. Giese, and S. A. Grodsky, 2005: Sea level rise and the warming of the oceans in the Simple Ocean Data Assimilation (SODA) ocean reanalysis. *J. Geophys. Res.*, **110**, C09006, doi: 10.1029/2004JC002817.
- , and —, 2007: SODA: a reanalysis of ocean climate. *J. Geophys. Res.*, (in review).
- Chang, P., L. Ji, and H. Li, 1997: A decadal climate variation in the tropical Atlantic Ocean from thermodynamic air-sea interactions. *Nature*, **385**, 516-518.
- , —, and R. Saravanan, 2001: A hybrid coupled model study of tropical Atlantic variability. *J. Climate*, **14**, 361-390.
- Chepurin, G. A., J. A. Carton, and D. Dee, 2005: Forecast model bias correction in ocean data assimilation, *Mon. Wea. Rev.*, **133**, 1328-1342.
- Chirokova G., and P. J. Webster, 2006: Interannual variability of Indian Ocean heat transport. *J. Climate*, **19**, 1013-1031.
- CLIVAR, *CLIVAR Science Plan*, World Climate Research Program, WCRP-89 (WMO/TD NO. 690), 1995.
- Covey, C, and S. L. Thompson, 1989: Testing the effects of ocean heat transport on climate. *Palaeogeogr., Palaeoclimatol., Palaeoecol.*, **75**, 331-341.
- Curry, R., B. Dickson, and I. Yashayaev, 2003: A change in the freshwater balance of the Atlantic Ocean over the past four decades. *Nature*, **426**, 826-829.
- , and C. Mauritzen, 2005: Dilution of the northern North Atlantic Ocean in recent decades. *Science*, **308**, 1772-1774.

- Curry, R. G., and M. S. McCartney, 2001: Ocean gyre circulation changes associated with the North Atlantic Oscillation. *J. Phys. Oceanogr.*, **25**, 666-678.
- Dickson, R. R., and J. Brown, 1994: The production of north Atlantic deep water: sources, rates and pathways. *J. Geophys. Res.*, **99**, 12319-12341.
- , J. Lazier, J. Meincke, P. Rhines and J. Swift, 1996: Long-term coordinated changes in the convectivity of the North Atlantic. *Prog. In Oceanog.*, **38**, 214-295.
- Dickson, B., I. Yashayaev, J. Melncke, B. Threll, S. Dye, and J. Holfort, 2002: Rapid freshening of the deep North Atlantic Ocean over the past four decades. *Nature*, **416**, 832-837.
- Dong, B., and R. T. Sutton, 2001: The dominant mechanisms of variability in Atlantic ocean heat transport in a coupled ocean-atmosphere GCM. *Geophys. Res. Lett.*, **28**, 2445-2448.
- , and —, 2003: Variability of Atlantic Ocean heat transport and its effects on the atmosphere. *Annals of Geophysics*, **46**, 87-97.
- Drijfhout, S. S., and W. Hazeleger, 2006: Changes in MOC and gyre-induced Atlantic Ocean heat transport. *Geophys. Res. Lett.*, **33**, L07707, doi: 10.1029/2006GL025807.
- Eden, C., and J. Willebrand, 2001: Mechanism of interannual to decadal variability of the North Atlantic circulation. *J. Climate*, **14**, 2266-2280.
- Fillenbaum, E. R., T. L. Lee, W. E. Johns, and R. Zantopp, 1997: Meridional heat transport variability at 26.5°N in the North Atlantic. *J. Phys. Oceanogr.*, **27**, 153-174.
- Friedrichs, M. A. M., and M. M. Hall, 1993: Deep circulation in the tropical North Atlantic. *J. Mar. Res.*, **51**, 697-736.
- Ganachaud, A., 1999: Large scale oceanic circulation and fluxes of freshwater, heat, nutrients and oxygen. Ph.D. dissertation, Mass. Inst. of Technol./Woods Hole Oceanogr. Inst. Joint Program, Cambridge, MA.
- , and C. Wunsch, 2000: Improved estimates of global ocean circulation, heat transport and mixing from hydrographic data. *Nature*, **408**, 453-457.
- , and —, 2003: Large-scale ocean heat and freshwater transports during the World Ocean Circulation Experiment. *J. Climate*, **16**, 696-705.
- Giese, B. S., and J. A. Carton, 1999: Interannual and decadal variability in the tropical and midlatitude Pacific Ocean. *J. Climate*, **12**, 3402-3418.

Gregory, J. M., H. T. Banks, P. A. Stott, J. A. Lowe, and M. D. Palmer, 2004: Simulated and observed decadal variability in ocean heat content. *Geophys. Res. Lett.*, **31**, L15312, doi: 10.1029/2004GL020258.

Gu, D., and Philander, S. G. H., 1997: Interdecadal climate fluctuations that depend on exchanges between the tropics and extratropics. *Science*, **275**, 805-807.

Hakkinen, S., 1999: Variability of the simulated meridional heat transport in the North Atlantic for the period 1951-1993. *J. Geophys. Res.*, **104**, 10 991-11 007.

—, and P. B. Rhines, 2004: Decline of subpolar North Atlantic circulation during the 1990s. *Science*, **304**, 555-559.

Hall, M. M., and H. L. Bryden, 1982: Direct estimates and mechanisms of ocean heat transport. *Deep-Sea Res.*, **29**, 339-359.

Hansen, B., and R. Kristiansen, 1999: Variation of the Faroe Bank Channel overflow. *Rit Fiskideildar*, **16**, 13-22.

—, W. R. Turrell, and S. Østerhus, 2001: Decreasing overflow from the Nordic seas into the Atlantic Ocean through the Faroe Bank Channel since 1950. *Nature*, **411**, 927-930.

—, S. Østerhus, Q. Detlef, and W. R. Turrell, 2004: Already the day after tomorrow? *Science*, **305**, 953-954.

Hansen, J. et al. 2005: Earth's energy imbalance: confirmation and implications. *Science*, **308**, 1431-1435.

Hastenrath, S., 1980: Heat budget of tropical ocean and atmosphere. *J. Phys. Oceanogr.*, **10**, 159-170.

—, 1982: On meridional heat transports in the world ocean. *J. Phys. Oceanogr.*, **12**, 922-927.

Hátún, H., A. B. Sandø, H. Drange, B. Hansen, and H. Valdimarsson, 2005: Influence of the Atlantic subpolar gyre on the thermohaline circulation. *Science*, **309**, 1841-1844.

Holfort, J., and G. Siedler, 2001: The meridional oceanic transports of heat and nutrients in the South Atlantic. *J. Phys. Oceanogr.*, **31**, 5-29.

Hsiung, J., 1985: Estimates of global oceanic meridional heat transport. *J. Phys. Oceanogr.*, **15**, 1405-1413.

- , R. E. Newell and T. Houghtby, 1987: Annual variation of heat transport in the Pacific and Indian Oceans. *Nature*, **325**, 518-520.
- Huang, R. X., and S. Russell, 1994: Ventilation of the subtropical North Pacific, *J. Phys. Oceanogr.*, **24**, 2589-2605.
- Hurrell, J. W., 1995a: Transient eddy forcing of the rotational flow during northern winter. *J. Atmos. Sci.*, **52**, 2286-2301.
- , 1995b: Decadal trends in the North Atlantic oscillation: regional temperatures and precipitation. *Science*, **269**, 676-679.
- Jayne, S. R., and Marotzke, J., 2001: The dynamics of ocean heat transport variability. *Rev. Geophys.*, **39**, 385-411.
- , and —, 2002: The oceanic eddy heat transport. *J. Phys. Oceanogr.* **32**, 3328-3345.
- Jones, P. W., 1999: First- and Second-Order Conservative Remapping Schemes for Grids in Spherical Coordinates. *Mon. Wea. Rev.*, **127**, 2204-2210.
- Josey, S.A., E. C. Kent, and P. K. Taylor, 1999: New insights into the ocean heat budget closure problem from analysis of the SOC air-sea flux climatology. *J. Climate*, **12**, 2685-2718.
- Joyce, M. T., C. Frankignoul, J. Yang, and H. E. Phillips, 2004: Ocean response and feedback to the SST dipole in the Tropical Atlantic. *J. Phys. Oceanogr.* **34**, 2525-2540.
- Keith, D. A., 1995: Meridional energy transport: uncertainty in zonal means. *Tellus*, **47A**, 30-44.
- Klinger, B. A., and J. Marotzke, 2000: Meridional heat transport by the subtropical cell. *J. Phys. Oceanogr.* **30**, 696-705.
- Lamb, P. J., 1981: Estimate of annual variation of Atlantic Ocean heat transport. *Nature*, **290**, 766-768.
- Latif, M., C. Boning, J. Willebrand, A. Biastoch, J. Dengg, N. Keenlyside, U. Schweckendiek, and G. Madec, 2006: Is the thermohaline circulation changing? *J. Climate*, **19**, 4631-4637.
- Lavin, A., H. L. Bryden, and G. Parilla, 1998: Meridional transport and heat flux variations in the subtropical North Atlantic. *Global Atmos. Ocean Syst.*, **6**, 231-241.
- Levitus, S., 1982: Climatological atlas of the world ocean, NOAA *Prof. Pap.* **13**, 173 pp.,

U. S. Govt. Print. Off., Washington DC.

—, J. I. Antonov, T. P. Boyer and C. Stephens, 2000: Warming of the world ocean. *Science*, **287**, 2225-2229.

—, —, J. Wang, T. L. Delworth, K.W. Dixon, and A. J. Broccoli, 2001: Anthropogenic warming of Earth's climate system. *Science*, **292**, 267-270.

—, —, and T. P. Boyer, 2005: Warming of the world ocean, 1955-2003. *Geophys. Res. Lett.*, **32**, L02604, doi: 10.1029/2004GL021592.

Macdonald, A. M., and C. Wunsch, 1996: An estimate of global ocean circulation and heat fluxes. *Nature*, **382**, 436-439.

—, 1998: The global ocean circulation: a hydrographic estimate and regional analysis. *Progress in Oceanography*, Vol. **41**, Pergamon, 281-382.

Manabe, S., and R. J. Stouffer, 1995: Simulation of abrupt climate change induced by freshwater input to the North Atlantic. *Nature*, **364**, 215-218.

Marotzke, J., 2000: Abrupt climate change and thermohaline circulation: mechanisms and predictability. *Proc. Natl. Acad. Sci., U.S.A.*, **97**, 1347-1350.

Marshall, J., Y. Kushnir, D. Battisti, P. Chang, A. Czaja, R. Dickson, J. Hurrell, M. McCartney, R. Saravanan, and M. Visbeck, 2001: Review: North Atlantic climate variability: phenomena, impacts and mechanisms. *Int. J. Climatol.*, **21**, 1863-1898.

Miller, J. R., 1976: The salinity effect in a mixed layer ocean model, *J. Phys. Oceanogr.*, **6**, 29-35.

Molinari, R. L., E. Johns, and J. F. Festa, 1990: The annual cycle of meridional heat flux in the Atlantic Ocean at 26.5°N. *J. Phys. Oceanogr.*, **20**, 476-482.

National Research Council, *Global Environmental Change: Research Pathways for the Next Decade* (National Academy Press, Washington, DC, 1999).

Newell, R. E., J. W. Kidson, D. G. Vincent, and G. J. Boer, 1974: *The general circulation of the tropical atmosphere and interactions with extratropical latitude*, Vol. **2** (MIT, Cambridge).

—, and L. S. Chiu, 1981: *Climatic Variations and Variability: Facts and Theories* (ed. Berger, A.). 21-61 (Reidel, Dordrecht).

- Oort, A. H., and T. H. Vonder Haar, 1976: On the observed annual cycle in the ocean-atmosphere heat balance over the Northern Hemisphere. *J. Phys. Oceanogr.*, **6**, 781-800.
- Peterson, B. J., J. McClelland, R. Curry, R. M. Holmes, J. E. Walsh, and K. Aagaard, 2006: Trajectory shifts in the Arctic and subarctic freshwater cycle. *Science*, **313**, 1061-1066.
- Rago, T. A., and H. T. Rossby, 1987: Heat transport into the North Atlantic Ocean north of $32^{\circ}N$ latitude. *J. Phys. Oceanogr.*, **17**, 854-871.
- Rahmstorf, S., 1995: Bifurcations of the Atlantic thermohaline circulation in response to changes in the hydrological cycle. *Nature*, **388**, 825-826.
- , 1996: On the freshwater forcing and transport of the Atlantic thermohaline circulation. *Clim. Dyn.*, **12**, 799-811.
- Reichert, B. K., R. Schnur, and L. Bengtsson, 2002: Global ocean warming tied to anthropogenic forcing, *Geophys. Res. Lett.*, **29(11)**, 1535, doi: 10.1029/2001GL013954.
- Riishojgaard, L. P., 1998: A direct way of specifying flow-dependent background error. *Tellus*, **50A**, 42-57.
- Rintoul, S., 1991: South Atlantic interbasin exchange. *J. Geophys. Res.*, **96**, 2675-2692.
- Robbins, P. E., and J. M. Toole, 1997: The dissolved silica budget as a constraint on the meridional overturning circulation of the Indian Ocean. *Deep-Sea Res.*, **44**, 879-906.
- Roemmich, D., 1980: Estimation of meridional heat-flux in the North-Atlantic by inverse methods. *J. Phys. Oceanogr.*, **10**, 1972-1983.
- , and J., Gilson, 2001: Eddy transport of heat and thermocline waters in the North Pacific: a key to interannual/decadal climate variability? *J. Phys. Oceanogr.*, **31**, 675-687.
- Rogers, J. C. 1984: The association between the North-Atlantic Oscillation and the Southern Oscillation in the Northern Hemisphere. *Mon. Wea. Rev.*, **112**, 1999-2015.
- Rossby, C. 1959: Current problems in meteorology, in *The Atmosphere and Sea in Motion*, pp. 9-50, Rockefeller Inst. Press, New York.
- Sato, O., and T. Rossby, 2000: Seasonal and low-frequency variability of the meridional heat flux at $36^{\circ}N$ in the North Atlantic. *J. Phys. Oceanogr.*, **30**, 606-621.

- Schmitz, W., 1995: On the interbasin-scale thermohaline circulation. *Rev. Geophys.*, **33**, 151-173.
- Schott, F. A., J. P. McCreary Jr, and G. C. Johnson, 2004: Shallow overturning circulations of the tropical-subtropical oceans. in: *Earth Climate: The Ocean-Atmosphere Interaction*, Geophysical Monograph Series 147, pp.261-304. doi: 10.1029/147GM15.
- Scott, J. R., and J. Marotzke, 2002: The location of diapycnal mixing and the meridional overturning circulation. *J. Phys. Oceanogr.*, **32**, 3578-3593.
- Seager, R., Y. Kushnir, P. Chang, N. Naik, J. Miller, and W. Hazeleger, 2001: Looking for the role of the ocean in tropical Atlantic decadal climate variability. *J. Climate*, **14**, 638-655.
- Shaffrey, L. and R. Sutton, 2004: The interannual variability of energy transports within and over the Atlantic Ocean in a coupled climate model. *J. Climate*, **17**, 1433-1448.
- Sloyan, B. M., and S. R. Rintoul, 2001a: The Southern Ocean limb of the global deep overturning circulation. *J. Phys. Oceanogr.*, **31**, 143-173.
- Smith, R. D., J. K. Dukowicz, and R. C. Malone, 1992: Parallel ocean general circulation modeling. *Physica D*, **60**, 38-61.
- Smith, W. H. F., and D. T. Sandwell, 1997: Global seafloor topography from satellite altimetry and ship depth soundings. *Science*, **277**, 1957-1962.
- Spall, M. A., 1991: A diagnostic study of the wind- and buoyancy-driven North Atlantic circulation. *J. Geophys. Res.*, **96**, 18509-18518.
- Stephens, C., J. I. Antonov, T. P. Boyer, M. E. Conkright, R. A. Locarnini, T. D. O'Brien, H. E. Garcia, 2002: World Ocean Atlas 2001, Volume 1: Temperature. S. Levitus, Ed., NOAA Atlas NESDIS 49, U.S. Government Printing Office, Washington D.C., 167pp., CD-ROMs.
- Stott, P. A., S.F. B. Tett, G. S. Jones, M. R. Allen, J. F. B. Mitchell, and G. J. Jenkins, 2000: External control of twentieth century temperature by natural and anthropogenic cause, *Science*, **290**, 2133-2137.
- Sun, S., and R. Bleck, 2001: Thermohaline circulation studies with an isopycnal coordinate ocean model. *J. Phys. Oceanogr.*, **31**, 2761-2782.
- Sverdrup, H. U., M. W. Johnson, and R. H. Fleming, 1942: *The Oceans*. Prentice-Hall, 1087pp.

- Talley, L. D., 1983: Meridional heat transport in the Pacific Ocean. *J. Phys. Oceanogr.*, **14**, 231-241.
- , 2003: Shallow, intermediate, and deep overturning components of the global heat budget. *J. Phys. Oceanogr.*, **33**, 530-560.
- Trenberth, K. E., and A. Solomon, 1994: The global heat balance: heat transports in the atmosphere and ocean. *Climate Dyn.*, **10**, 107-134.
- , and J. M. Caron, 2001: Estimates of meridional atmosphere and ocean heat transports. *J. Climate*, **14**, 3433-3443.
- Vazquez, J., A. Tran, R. Sumagaysay, E. A. Smith and M. Hamilton, NOAA/NASA AVHRR Oceans Pathfinder Sea Surface Temperature Data Set User's Guide Version 1.2, JPL Tech. Rep., 53pp., 1995.
- Vonder Haar, T. H., and A. H. Oort, 1973: New estimate of annual poleward energy transport by Northern Hemisphere oceans. *J. Phys. Oceanogr.*, **3**, 169-172.
- Walker, G. T., 1924: Correlations in seasonal variations of weather IX, *Mem. Ind. Meteor. Dept.*, **24**, 275-332.
- Wang, J. and J. A. Carton, 2002: Seasonal heat budgets of the North Pacific and North Atlantic Oceans. *J. Phys. Oceanogr.*, **32**, 3474-3489.
- Wang, W., and M. J. McPhaden, 1999: The surface-layer heat balance in the equatorial Pacific. Part I: mean seasonal cycle. *J. Phys. Oceanogr.*, **29**, 1812-1831.
- Warren, B. A., 1999: Approximating the energy transport across oceanic sections. *J. Geophys. Res.*, **104**, 7915-7920.
- Wijffels, S. E., J. M. Toole, H. L. Bryden, R. A. Fine, W. J. Jenkins, and J. L. Bullister, 1996: The water masses and circulation at 10°N in the Pacific. *Deep-Sea Res.*, **43**, 501-544.
- Wu, P., R. Wood, and P. Stott, 2004: Does the recent freshening trend in the North Atlantic indicate a weakening thermohaline circulation? *Geophys. Res. Lett.*, **31**, L02301, doi: 10.1029/2003GL018584, 2004..
- Wunsch, 1996: The Ocean Circulation Inverse Problem. Cambridge University Press. Cambridge, UK, 442p.
- , 2005: The total meridional heat flux and its oceanic and atmospheric partition. *J. Climate*, **18**, 4374-4380.

—, and P. Heimbach: Decadal changes in the North Atlantic and Pacific meridional overturning and heat flux. (in preparation)

VITA

Yangxing Zheng was born in Zhejiang Province, China. He received his B. S. degree in meteorology from Ocean University of China in 1997, and M. S. degree in Atmospheric Sciences at the Institute of Atmospheric Physics (IAP), Chinese Academy of Sciences (CAS) in 2000. He also received an M.S. degree at Stony Brook University in August, 2003. In the fall of 2003, he went to Texas A&M University to pursue his Ph.D. degree in Atmospheric and Oceanic Sciences. He received his Ph.D. degree in August, 2007.

His permanent address: #24 Qianwu Village, Maofan Town, Jiangshan City, Zhejiang Province, China, 324115.